A techno-economic approach to optimizing offshore off-grid wind-based hydrogen production

Merlijn Hunik

Delft University of Technology

A TECHNO-ECONOMIC APPROACH TO OPTIMIZING OFFSHORE OFF-GRID WIND-BASED HYDROGEN PRODUCTION

THESIS - AE4020

JULY 18, 2024

BY MERLIJN HUNIK

MASTER OF SCIENCE
IN AEROSPACE ENGINEERING
DELFT UNIVERSITY OF TECHNOLOGY

GRADUATION COMMITTEE:

DR. IR G. LA ROCCA	TU DELFT	CHAIR
PROF. DR. IR. D.A. VON TERZI	TU DELFT	DAILY SUPERVISOR
DR. IR M.B. ZAAYER	TU DELFT	EXAMINER
IR M. GOORDEN	ENECO	COMPANY SUPERVISOR

[1] Source cover image: https://www.ramboll.com/net-zero-explorers/offshore-hydrogen-at-scale

CONTENTS

List of Figures

List of Tables

NOMENCLATURE

List of Abbreviations

AWE	Alkaline Water Electrolyser
CAPEX	Capital Expenditure
CCUS	Carbon Capture, Utilisation and Storage
DEVEX	Development Expenditure
ED	Electro Dyalisis
EDI	Electrodeionization
HVAC	High Voltage Alternating Current
HVDC	High Voltage Direct Current
IRR	Internal Rate of Return
IRR	Internal Rate of Return
LCOE	Levelised Cost of Energy
LCOH	Levelised Cost of Hydrogen
LHV	Lower Heating Value
MR	Model Requirement
NPV	Net Present Value
NZE	Net Zero Emission
O&M	Operations & Maintenance
P2G	Power-to-Gas
PEMEC	Polymer Electrolyte Membrane Electrolysis Cell
PV	Photovoltaic
RO	Reverse Osmosis
RO	Reverse Osmosis
SOEC	Solid Oxide Electrolysis Cell
TR	Technical Requirement
WTG	Wind Turbine Generator
XDSM	eXtended Design Structure Matrix

List of Symbols

α_{anode}	Charge transfer coefficient anode
$\alpha_{cathode}$	Charge transfer coefficient cathode
ΔG	Gibbs free energy
Δh	Height difference
$\Delta H(T)$	Total amount of energy to split water molecules
$\Delta S(T)$	Heat in electrolysis reaction
$\dot{m}_{H_2O}$	Water mass flow
$\dot{m}_{H_2}$	Hydrogen mass flow
$\dot{m}_{h2}$	Hydrogen mass flow
η_V	Voltage efficieny
η_{compr}	Compressor efficiency
η_{el}	Electrical efficiency
η_{fc}	Fuel cell efficiency
η_{isen}	Isentropic efficiency
η_{stack}	Stack efficiency
ηaux	Auxiliery system efficiency
Π	Compression ratio
σ_{per}	Electrical conductivity in the desalination permeate
ξ_i	Activation ovepotential polynomial constant at order i
A_{cell}	Cell area
C_{O_2}	Concentration oxygen
D_{pipe}	Pipeline inner diameter
e	surface roughness hydrogen pipeline
E_{cell}	Cell voltage
$E_{el,in}$	Electrical energy in
F	Faraday's constant
f	Friction factor
G	Specific gas gravity
g	Gravitational acceleration
H_2	Molecular structure hydrogen
H_2O	Molecular structure water

HHV_{H_2} Higher heating value hydrogen

I Operating current

i Current density

I_L Limit current

k Power setting

k Ratio of specific heat

L_{cable} Electricity cable length

L_{pipe} Hydrogen pipeline length

L_{total} Distance wind farm to connection point

LHV_{H_2} Lower heating value hydrogen

m_{H_2} Mass hydrogen

n Number of electrons

n_stage Number of stages

O_2 Molecular structure oxygen

P_b Reference pressure

P_{compr} Compressor output pressure

p_{compr} Compressor output pressure

p_{O_2} Partial pressure oxygen

$p_{pipe,out}$ Pipeline output pressure

$P_{wf,nom}$ Nominal wind farm power

P_{wf} Wind farm power

Q Hydrogen mass flow rate per day

R Universal gas constant

r Discount rate

R_{con} Contact resistance

R_{ele} Electronic resistance

$R_{initial}$ Ohmic resistance at 0 ° C

R_{ion} Ionic resistance

Re Reynolds number

SEC_{edi} Specific energy consumption electrodeionization

T Temperature

T_b Reference temperature

T_{compr} Compressor output temperature

u_{limit} Hydrogen pipeline limit velocity

u_{pipe} Hydrogen pipeline velocity

v Hydrogen viscosity

V_{act} Activation overpotential

V_{app} Applied cell voltage

V_{app} Applied voltage

V_{cell} Cell operating voltage

V_{con} Concentration overpotential

V_{ohm} Ohmic overpotential

v_{ref} Hydrogen reference viscosity

V_{rev} Reversible voltage

V_{th} Thermo-neutral voltage

W_{compr,H_2O} Water compressor power

W^k_{copmpr} Compressor work required at power setting k

W_{elec} Electrolyser power

W^k_{elec} Electrolyser power required at power setting k

W_{pump} Water pump power

W^k_{water} Water treatment work required at power setting k

W_{wf} wind farm nominal power

x_{loc} Lateral Location Electrolyser

y_{loc} Longitudinal Location Electrolyser

Z Compressibility factor

PREFACE

Two years ago, I decided to switch my attention from the aviation industry towards renewable energy. Since then I have never doubted this choice. I started this transition with an interest in hydrogen courses. Next up was a really interesting internship in offshore wind system design. With this thesis, I combined both hydrogen and offshore wind in this thesis research. This thesis report is the result of a year of working on improving the knowledge of wind-based hydrogen production. Hopefully, the research will speed up the process of producing emission-free hydrogen in Europe in the near future.

I want to thank my daily supervisor Dominic for his help last year and also his patience when I was not doing so well. Thanks, Marjolijn for helping me on the hydrogen side. Your knowledge and expertise on hydrogen was really helpful and having an industry view on the problem was a good addition to the knowledge of Dominic. This thesis would not have been here without my partner Floor. Last year, when I had a mental breakdown she helped me through the deep valley and continued to support me all the way to the end. Lastly, I would like to thank friends and family for giving advice and support throughout the year.

ABSTRACT

The Paris Agreement, adopted during COP21, aims to limit global temperature increases to well below 2°C, ideally, 1.5°C, necessitating a significant rise in hydrogen production to 614 megatonnes annually by 2050. Hydrogen is expected to fulfill 12% of energy demand and reduce CO2 emissions by 10% in 2050, and has the potential for cost-effective production through offshore wind. However, real-time data on offshore hydrogen production using wind energy is scarce, and existing facilities are limited. The Dutch government's recent hydrogen tender for a 100 MW demonstration offshore hydrogen project followed by a 500 MW tender, reflects a commitment to large-scale offshore hydrogen production. This further emphasises the need for efficient design strategies and optimizing the layout.

For electrolysers technology PEM electrolysers promise to be more efficient and operate under a lower minimal load compared to AWE electrolysers, the main type of electrolyser currently used. PEM electrolysers require constant power at all times to prevent accelerated degradation. In previous research, the constant power requirement has been neglected and the assumption was made that the electrolyser can be turned off when wind energy is not available. When the PEM electrolyser is placed off-grid this will pose serious problems and would require frequent replacement of the electrolyser stacks. This highlights the critical need for implementing effective off-grid strategies to ensure the longevity and efficiency of PEM electrolysers in offshore applications.

This thesis employs Multidisciplinary Design Optimization (MDO) to enhance off-grid offshore hydrogen production using wind energy, focusing on reducing the Levelized Cost of Hydrogen (LCOH). The modelled system consists of an electrolyser, hydrogen compressor, pipeline, offshore platform, cable, fuel cell and water treatment subsystems. A novel approach to using a fuel cell for providing power stability to the electrolyser is proposed. By modelling the system from the electricity cable to the hydrogen pipeline, excluding the wind farm and distribution network, the research assesses design parameters influencing LCOH and optimizes system performance. The PEM electrolyser is modelled for performance under different temperatures, pressures, sizes and locations. A compressor subsystem and water desalination and pump are modelled to complement the electrolyser. This thesis integrates operational and capital expenditures, utilizing Python-based modules to simulate hydrogen production and costs.

The use of MDO has given the option to run the model for a range of variables in a fast matter. This made it possible to visualise the design space. It was found that the optimization problem contained several discontinuous regions that were infused by the stochastic nature of pipeline design and shortcomings in linearizing the whole system work required. On the other hand, using power settings proved useful in creating a more convex design space. The thesis has applied two optimization algorithms to find an optimal value of LCOH. A gradient-based Powell-Conjugate optimization and sequential differential evolution. Since the design space of the model used consisted of a non-convex regions especially related to the pipeline and compressor design, the gradient-based method proved only useful in finding local optima that would still considerably reduce the LCOH compared to the 15.50 €/kg baseline. The use of a sequential differential evolution optimization algorithm is shown to be effective in finding a global optimum in the non-convex and discontinuous design space. The readjustment of the mutation size of the design vector proved to overcome the non-convex region of the design space.

The baseline 15.50 €/kg LCOH was shown to be reduced to 13.83 €/kg at the optimum design vector. This value is considerably higher than earlier reported LCOH values of 4-8 €/kg. The main reason driving this increase in LCOH was found to be a doubling of LCOE of the wind farm in combination with having to reuse hydrogen for supplying the electrolyser with backup power. With the newly found LCOH figures, it will be hard to compete with grey hydrogen production as the LCOH for that method lies considerably lower at around 4 €/kg. The LCOH proved to be mainly influenced by the LCOE of the wind farm and the Capital Expenditure (CAPEX) of the PEM electrolyser. Only with significant reductions in LCOE and electrolyser CAPEX can off-

grid offshore hydrogen compete with other hydrogen sources. Lastly, the analysis also showed that placing the electrolyser offshore does seem to improve the LCOH compared to onshore hydrogen production. The reduction in electricity infrastructure expenditure does not outway the extra costs related to installing and maintaining the system in an offshore location.

1

INTRODUCTION

During the UN Climate Change Conference (COP21), 196 parties to the United Nations adopted the Paris Agreement. The main goal of the agreement was to keep the global temperature increase well below 2 C° above pre-industrial temperatures. In addition, efforts should be made to limit the increase to 1.5 C° [6]. To achieve this goal, hydrogen production will need to increase fivefold to 614 megatonnes of hydrogen per year [7]. Hydrogen is expected to meet 12% of energy demand. It will also reduce 10% of CO_2 emissions by 2050. In certain locations, renewable hydrogen production from offshore wind could be the cheapest option [3]. However, only one small green offshore hydrogen production facility is currently in operation [8].

Due to the lack of operational facilities, there is no real-time data on hydrogen production from wind energy at an offshore site. Instead, the technical and economic performance of offshore electrolysis needs to be modelled as best as possible in order to report on the effects of different design choices, such as the size of the electrolyser plant. In the absence of physical projects, the governments of several European countries, such as the Netherlands, Germany and Denmark, expect to produce significant amounts of offshore hydrogen by 2030. Both the fact that the announced plans are looking at electrolyser size ranges that are not yet commercially available, and the fact that research into electrolysers was limited until three years ago, shows that more research into this topic is needed [3].

Current research into the topic of offshore hydrogen production has focussed on the choice of producing hydrogen at the wind turbine (decentralized) or in a central location (centralized) [9, 10]. The choice of centralized offshore hydrogen production proved to be less complex and possibly cheaper. Furthermore, centralized hydrogen production can also later be installed at a wind farm without a complete overhaul of the wind farm design. The sizing of the electrolyser unit has also been looked into [11].

Currently, three different types of electrolysers are commercially available. The oldest and most common of the three, are the Alkaline Water electrolyser, the already commercially ready Proton Exchange Membrane (PEM) electrolyser and lastly the lesser technologically ready Solid Oxide Electrolyser. The PEM electrolyser proves to be the best option at this moment for offshore hydrogen production in this research. However, each electrolyser requires a minimum power when not producing hydrogen to keep gasses from permeating the membrane that keeps them separated [11].

The research that has worked on modelling and optimizing has not included backup power to prevent the permeation of gasses [11–14]. This will however be necessary to maintain the electrolyser system. In a current project off the British coast, called Dolphin, they are planning on using a fuel cell which will supply this electricity when there is no wind power. The fuel cell will use the hydrogen that was produced before and is still available in the hydrogen pipeline.

Furthermore, the problem of offshore hydrogen production has a lot of factors that influence the production or costs. Some of these factors also cross-influence with the other metrics such as the sizing of the electrolyser, when to turn on the electrolyser and where to place the electrolyser. A Monte Carlo simulation in this case would require a long computation time and the design will not always follow a linear relationship to the selected values. Therefore the need arises to use Multidisciplinary Design Optimization (MDO). This method divides the model up in different subsystems with fixed inputs and outputs. One module combines the different subsystems and calculates the objective function. This creates a framework which can be easily incorporated into existing optimizer algorithms.

This thesis report aims to show the effectiveness of applying MDO to the design problem of offshore hydrogen production while satisfying the constraint of minimum power availability at all times over the lifetime of the

project.

1.1. RESEARCH OBJECTIVE

The objective of this research is to optimize off-grid offshore hydrogen production using wind energy. A good metric to show the costs and market competitiveness of hydrogen production is the Levelized Cost of Hydrogen (LCOH). This metric is basically all costs related to the project divided by the total value of hydrogen production during the lifetime of the project. Therefore, this research plans on using this metric to evaluate the design. The focus of the research is to model the offshore off-grid hydrogen production: from the electricity cable to the hydrogen pipeline. The wind farm is not included in the modelling as well as the hydrogen network that needs to be constructed to bring the hydrogen to the off-takers.

1.1.1. RESEARCH QUESTION

The research question that is aimed to be answered in this research is the following:

To what extent can Multidisciplinary Design Analysis & Optimization reduce the Levelized-Cost-Of-Hydrogen of off-grid offshore hydrogen production using wind energy?

The subquestion that aid in answering this research question are:

- How is the off-grid offshore electrolyser system modelled?
- What system parameters drive the LCOH optimum?
- What MDAO method is best suitable for optimizing off-grid offshore hydrogen production?

1.2. METHODOLOGY

The research question is to be answered by creating a model in Python which aims at modelling the hydrogen production and cost of the project to find the Levelized-Cost-Of-Hydrogen (LCOH). This model is then optimized for a minimal LCOH.

To estimate the hydrogen production and costs firstly a literature study is performed on the different components and drivers related to efficiency losses. Subsequently, each of the components is modelled in a different module in Python which can be accessed separately. Each module has fixed inputs that include the design variables but also variables that are outputted by other modules. The modelled system is presented in an XDSM model.

The model includes an operational expenditure and capital expenditure estimation for each subsystem. These figures are then collected in a LCOH calculation model. The different cash flows will be calculated over the whole lifetime of the project and divided by the total hydrogen production.

After the model was constructed an differential evolution optimization algorithm was selected to optimize the 7-parameter design vector. A gradient based method is used to validate the use of genetic differential evolution algorithm. After inspection, this algorithm was altered to function better in the design problem that was caused due to non-convex design spaces. Since the model was constructed with different packages several visualisations of the design space were used to aid in finding the optimization limitations.

1.3. THESIS OUTLINE

The structure of this thesis report is as follows:

Chapter 2 discusses the current state of modelling and optimisation of offshore hydrogen production. This includes a discussion of the different layouts and the main design options being considered in industry and research. Finally, a small market survey of the current LCOH for different technologies is presented.

In Chapter 3, the current electrolyser technologies are reviewed and a design matrix is constructed to find the best electrolyser type for off-grid offshore hydrogen production using wind energy as a source. This type of electrolyser will form the basis of the model and the system constraints and requirements in the following chapters.

In Chapter 4 the modelling of the system is discussed in detail. Each of the different subsystem designs is discussed, including the outputs and inputs of each module corresponding to that subsystem. The last section of this chapter details the LCOH calculation which is the objective of the optimisation. The methods used to optimise the design problem are summarised and visualised in an XDSM diagram.

Chapter 5 presents the results of the baseline model scenario and the results of the optimisation. The chapter starts with an overview of all the different results produced by the model with the baseline scenario inputs. To aid the optimisation, several heat maps of critical parts of the design space in the optimisation problem are produced. Finally, the results of the optimisation are presented and compared with the baseline scenario.

In Chapter 6 the results presented in Chapter 4 are discussed and a critical point is made about the limitations of the model and the optimisation. Based on the limitations and the results, some recommendations for future research are presented.

2

Offshore Hydrogen Production

2.1. Decentralized and Centralized Layout

The first main choice in modelling offshore wind based hydrogen is the distinction between decentralized offshore, centralized offshore and onshore hydrogen production. Since this study explores offshore production onshore hydrogen production will not be discussed in detail.

2.1.1. Decentralized Hydrogen

Decentralized hydrogen is presented in figure Figure 2.1. The basic idea of this layout is that the electrolysers are placed at the location of the Wind Turbine Generators (WTG) . This requires more electrolysers to be placed since each WTG will include an electrolyser. However, the main benefit is that there is no need for a large platform with the accompanied high costs, and the mitigation of electricity lines to be placed between the substation and the WTG. Furthermore, the use of more electrolysers causes the whole system to be robust in case of failure. On the other hand, each of the turbines needs to be equipped with a desalination plant, and depending on the distance to the substation platform compression might be needed at each turbine. Current electrolysers are low scale and therefore using the decentralized layout could prove useful since MW-scale electrolysers are already available. Lastly, the brine rest product of desalination is already more spread out compared to centralized hydrogen production. The main problems, however, are the extra O&M related to having two different systems at each WTG location [15].

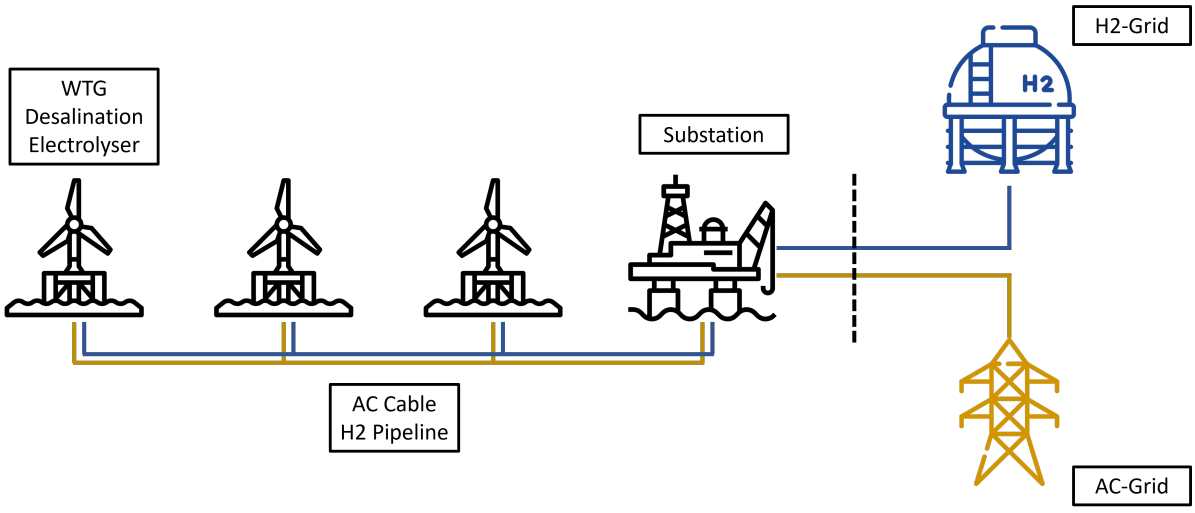

Figure 2.1: Decentralized layout

Decentralized hydrogen production will require platforms at each turbine. This makes the weight carried by the foundation higher and will increase the cost of the foundation. The farther the distance to shore is of the wind farm the more economically optimal decentralized hydrogen becomes if you look at LCOH [9]. However, if you look at the North Sea, water depths are rather shallow (<100m). Therefore, especially in the Netherlands and the North Sea decentralized hydrogen production is not optimal compared to centralized

hydrogen production [9]. This method would not only require more research into floating WTG but also the required maintenance at each WTG.

2.1.2. CENTRALIZED HYDROGEN

Centralized hydrogen is presented in figure Figure 2.2. The main intention of centralized hydrogen production is a central location where all hydrogen production takes place. This only requires a hydrogen pipeline from the offshore platform to the shore. In the offshore substation, all HVAC cables from several WTG come together. The power is then transmitted in a larger cable to shore. The choice of HVDC or HVAC for this cable depends on the length of the cable and the availability of HVDC cables at larger wind farm powers [16]. On this substation, the full capacity is placed as well as the desalination plant and potentially a hydrogen compressor. The main advantage of this layout is the centring of hydrogen infrastructure in one place. This results in a less complex method and can potentially be installed in existing offshore wind farms. The maintenance of the WTG will be less complex compared to centralized hydrogen. Disadvantages of this layout could be the effects of failure of the plant as well as the need for substations to be staffed permanently [15]. Both [15] and [9], propose the use of centralized hydrogen in locations with water depth below 100m and less than 100 km from the shore. In [10], it was estimated that with centralized hydrogen production, the lowest LCOH can be achieved at 2.4 €/kg. This number is only reached at an installed electrolyser capacity of 12 GW. This is a huge figure given that only 1 MW is installed offshore in 2023. At lower scales, the LCOH increases to more than 5 €/kg at 0.5 GW. This makes the LCOH of hydrogen offshore considerably less competitive with the LCOH of grey hydrogen between 2 and 6 €/kg

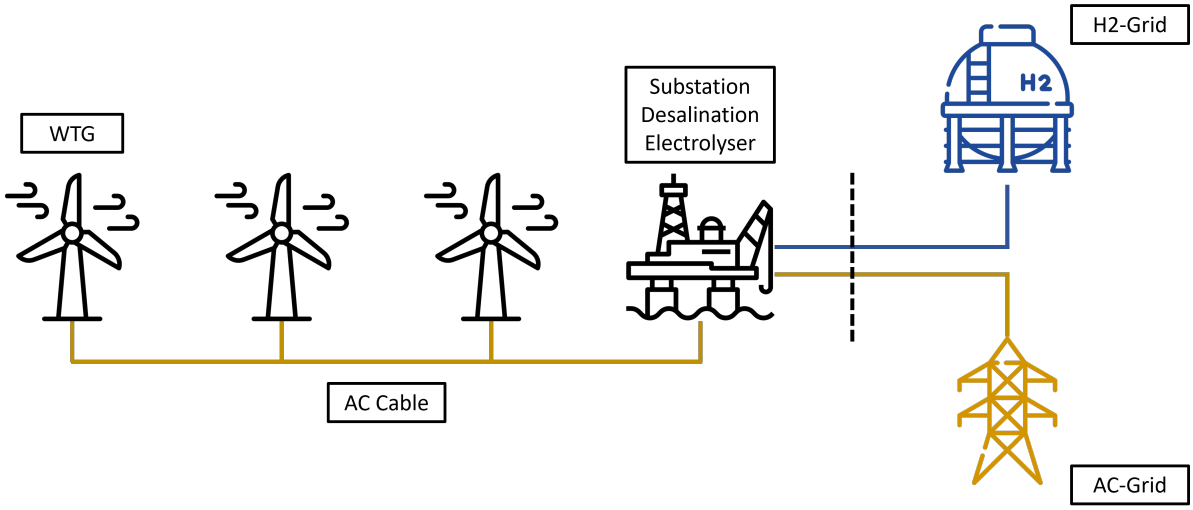

Figure 2.2: Centralised Layout

Each of these studies only consisted of building a model and selecting a few scenarios. In these scenarios, only a handful of parameters such as installed power, distance from shore, scale of operation and sea depth were varied in the sensitivity analysis. Neither of these studies used any optimization methods to systematically look for improvements in the design parameters. [9] mentions specifically in the recommendations that a proper optimization should be carried out for hydrogen storage for example in order to choose between hydrogen pipelines or transportation via tankers. Another recommendation is to further look into the use of fuel cells and optimize hydrogen/power production. Since an offshore hydrogen case study shows that fuel cells and storage systems could be useful in ensuring the minimum load of PEM electrolysers it seems unfit to not model these system parts into the model and still consider LCOH prices as low as 2.4 €/kg.

2.2. DESALINATION AND WATER TREATMENT

In order to minimise the degradation of the electrolyser water needs high purity. Offshore, the availability of fresh water is limited and thus the best option is to desalinate the seawater. Both SOEC and PEM can not operate with seawater. The use of a desalination plant impacts the production of hydrogen since it requires energy, adds weight and footprint to the offshore platform and needs a system to diversify the leftover brine. The important factors to model are the electricity use, water use and footprint of the system.

Research suggests that electrolysers require 9 L of water in order to produce 1 kg of hydrogen [15]. In other research, this figure reaches up to 15 L per kg of hydrogen [10]. In the electrolyser used in the operational Lhyfe project the water usage is stated to be 10.23 L per kg of hydrogen [17]. The electrolyser to be used in the Oyster project reports a tap water usage of 33.4 l/kg of hydrogen. This figure seems quite excessive and suggests water is also used for cooling at some stage. Since advancements can be made in the next few years, it is safe to use the lowest reported number of the Lhyfe project of 10.23 L per kg hydrogen.

Desalination can be done using different methods and energy sources. Since the only available energy source in this case is electrical the focus on choosing the best desalination option focuses on electrical systems. Over 300 million people in 150 depend on water desalination which makes desalination a more mature technology compared to electrolysers [18]. There are several methods for desalination of water. However, only a few are effective in using wind energy. This is due to the absence of heat in offshore locations. These two methods are Reverse Osmosis (RO) and Electro Dialysis (ED) [18] [19] [20]. These two systems make use of a membrane to filter the water and are both placed in the membrane desalination category. The other category is thermal desalination. Since this category makes use of heat to split the water from salt using evaporation this is less effective.

According to [19] RO uses about 3-10 kWh/m^3 of fresh water produced. However, this figure is taken from a paper published in 2009 [21]. More recent numbers on wind-based RO are 4.6 kWh/m^3 [20] and 3-7 kWh/m^3 [18], and 2-6 kWh/m^3 [22]. The 2 kWh/m^3 is the lowest of the three and is questionable. Especially [20] has a clear distinction between energy requirements for brackish desalination and seawater desalination where offshore desalination is dealing with. It is therefore unwise to not use any given energy usage numbers where no distinction is made between brackish desalination and seawater desalination. Another point to note is that hydrogen electrolysis typically requires far more energy than the desalination of the water used. For example with an overall efficiency of 56% [23] and an LHV of hydrogen of 33.3139 kWh/kg the rest of the value chain requires around 60 kWh/kg hydrogen. For one kilogram of hydrogen, you require at least 10.23 L of water. With a 4.6 kWh/m^3 the energy required for the water usage of 1 kg of hydrogen is about 0.05 kWh. This is less than 0.1% of the energy usage.

The cost appreciated with desalination could prove to be more significant. The desalination process requires more than just the RO plant. Included in recent modelling are for example a pre-desalination seawater treatment. After desalination, the waste product is called brine. This highly salinated water can not simply be returned to the North Sea for example. For a simulation of an offshore 111 MW electrolyser 1100 m^3 of is produced [24]. This requires site-specific discharge equipment in order to diffuse the brine. Little is mentioned about this in the research provided in this section. For a comprehensive model, it is therefore clear that excluding post- and pre-treatment facilities is questionable if costs are involved in the research. However, the extra energy required for desalination is negligible compared to the electrolyser power and due to large availability clear linear relations are available.

2.3. HYDROGEN STORAGE

Since the Dolphyn case study uses small hydrogen storage facilities and fuel cell to supply minimum power to the electrolyser. The question arises to what extent are these systems incorporated and what is the effect on the overall system efficiency in producing hydrogen and the Levelized Cost of Hydrogen. Hydrogen storage comes in many forms. It can be stored in high compression as a gas, cryogenic liquid, in liquid hydrogen carriers such as methanol and ammonia and in solids [25]. A last option is the use of salt caverns to store

hydrogen [26]. This is only possible in locations where these salt caverns are available.

Within research that models hybrid hydrogen production, the main storage method is a high-pressure storage tank [12] [27] [28]. The main reason for using steel tanks is their wide use in the industry making it a cost-effective method. The specific utilisation strategy for the tanks varies. From supplying the fuel cell in an offshore setting [12], or storing hydrogen for energy islands [27] to storing hydrogen without pipeline infrastructure [28].

From a modelling perspective, the hydrogen storage is kept simple. The storage system is modelled with a cost model with a CAPEX per kg storage and a percentage of OPEX cost on yearly basis. This was mostly done if the LCOH was the outcome of the research [12]. Other research that models in a time domain and focuses on the technical and economical aspects use a minimum and maximum storage tank without any efficiency losses [27] or with an efficiency factor to account for losses [29] [30]. Lastly, it should be noted that hydrogen tanks require a minimum capacity at all times. When optimizing the system the research constrained this quite varied from 5% to 30%.

In the case of using vessels to transport hydrogen to shore. The use of storage trailers was proposed in size optimization [28]. Many of the constraints used in this model were to guarantee storage space was always available as to not halt hydrogen production. Nothing is mentioned about any losses during storage in this paper. Since there is a loss of energy during storage this has an effect on the total amount of hydrogen produced or the amount of electricity required. Not modelling this, even in the case of a purely economical output, should be justified in some way.

2.4. BACKUP POWER

Both an AWE and PEM electrolyser require power input at all times to account for gas permeation. This shortcoming should be accounted for in modelling the system. Currently, PEM electrolysers require a minimum of 5% of maximum power to prevent rapid degradation [31]. Mentioned in the research is that by 2025 PEM electrolysers could reach a minimum load range of 0% [12] [32]. Both these statements can be backtracked to an NWO report from 2011 where no direct source is given, except for a small statement that experts were interviewed for the results [33].

In the Dolphyn case study, backup hydrogen storage in combination with a fuel cell is used to supply the PEM electrolyser with minimum power at all times. An offshore electrolyser would require constant monitoring and at this stage, it is unknown if the large electrolysers can be monitored remotely. This would require a constant supply of electricity as well. The question therefore is: can you neglect the constant power supply? This has all to do with what the goal is of the research. However, currently, the research seems to neglect the minimum load problem or finds a source that says in the future the minimum load constraint can be neglected.

Since there is hydrogen available in the pipeline at all times. This hydrogen could be used to power a fuel cell if reversed when there is no power available from the wind farm. In this thesis, a fuel cell will be used to supply backup power. The fuel cell was chosen as it can be made quite small and can continuously supply power with the hydrogen available. The other option would be a battery. However, the battery will have to be scaled to the maximum possible duration of no wind during the project's lifetime. It will therefore be larger and heavier than a fuel cell, while not having full certainty of power availability.

2.5. OFFSHORE HYDROGEN PIPELINE

The hydrogen produced offshore will require a means of transportation to the onshore grid. Several options exist including the use of vessels to transport the hydrogen in tanks to shore. The most commonly mentioned method is to use hydrogen pipelines to transport hydrogen to shore. Furthermore, Gasunie has announced to provide a hydrogen pipeline infrastructure in the North Sea by 2030 as shown in Figure 2.3 [1]. This would

create a backbone for hydrogen exportation to shore.

Another aspect to note is that in the Netherlands the exporting infrastructure is mostly operated by governing organisations such as TenneT. The operating company pays a fee to the network operator or the exporting is already included in the tender prices. In current case studies in the offshore hydrogen production in the Netherlands the research on possible pipeline corridors is done by TenneT for example [34].

Figure 2.3: Proposed Gasunie hydrogen pipeline infrastructure [1]

None of the scientific studies on modelling offshore hydrogen electrolysis has included the hydrogen pipeline specifically in the modelling. However, in an international consortium, called North2, the costs of the pipeline have been modelled [35]. The technical background for modelling the pipeline can be taken from [36]. This book is used for the majority of modelling of the different aspects included in laying offshore pipelines.

2.6. OPTIMIZATION

In prior sections, several aspects of offshore hydrogen electrolysis were discussed. In this section, the research on the optimization of offshore hydrogen modelling is discussed. From a commercial point of view optimizing the LCOH, Net Present Value (NPV) or the Internal Rate of Return (IRR) can be beneficial. From an engineering perspective optimizing the hydrogen production, value chain efficiency or possibly greenhouse gas emissions are possible design objectives or even frequency response [30]. Several studies have been published outlining optimization research on the topic. These are listed in Table 2.1. The list is, however, limited. This already shows that there could be potential for a more nuanced optimization.

Most papers have conducted a size optimization with the goal of finding a competitive LCOH or maximising the net present value of the project. As seen in earlier sections of this chapter the research has not been modelling all systems of the offshore electrolysis to a detailed level. Optimization for offshore hydrogen production has been focused on sizing without including backup power [12] [13] [11] [14]. These choices have been justified but the justification was questionable. Other research focused on wind-hydrogen hybrid energy islands [27] [37]. Since these islands are similar to the layout of an offshore substation it can be interesting to see if the research performed on energy islands could be applied in offshore hydrogen production. The research performed in the mentioned paper focused on optimizing the electrolyser and storage for a minimum price. The system again did not include a backup power supply to the electrolyser.

From an optimization perspective the papers focused on finding algorithms that would perform better in supplying energy in remote locations [28] [29] [37]. The optimization algorithms included particle swarm op-

timization, seagull, fertile farmland and lastly a hybrid genetic-simulated annealing algorithm. The inclusion of not only particle swarm algorithms but also genetic algorithms was shown to be effective in order to reach better sizing. For these algorithms to perform well a linearised design space was constructed in most of the research mentioned above. This created a more continuous design space. Factors such as the degradation of the electrolyser show nonlinear relationships but research has been performed on making linear approaches to the real degradation of the electrolyser.

Lastly, it should be noted that optimization would either optimize for a control strategy or sizing in order to reach a higher value to the project. In one case first the optimal sizing was established before optimizing the control operation of the electrolyser. It could be interesting to see what the effect is of optimizing the control operation of the electrolyser system at different sizes compared to rated wind power of the wind farm.

2.7. WIND BASED HYDROGEN CASE STUDIES

In the previous chapters, the green hydrogen production capabilities of electrolysers were discussed as well as the system components and optimization for offshore hydrogen production using electrolysis. In this chapter, the different case studies regarding wind-based hydrogen production are reviewed. Lastly, a small section is directed towards announced government projects for wind-based hydrogen production.

2.7.1. OFFSHORE HYDROGEN PROJECTS

In Table 2.2 an overview is given of currently announced or in development projects for offshore hydrogen production [15]. Most projects are in the phase of announcing the 'first offshore hydrogen electrolysis'. Since several of these projects mention this it is important to note that neither of these projects have gathered the technical and financial means to actually build and start operating the electrolyser. The only exception is the Lhyfe project with the Sealhyfe electrolyser unit. This electrolyser has been deployed in June 2023 [38]. The main takeaway of these projects is that an initial investment has been announced. On the other hand several of these projects have secured this backing and have a clear project pipeline with intended power and start of operation date. The Dolphyn project actually includes public information on decisions and the modelling approach. The second project that will be discussed in more detail is the AquaVentus project. This project has also included the design of the pipeline and the overall offshore platform into the project. The last project to be further investigated is the Lhyfe project as it is already producing hydrogen.

Table 2.2: List of offshore hydrogen production projects

Project Title	Reference	Generating Capacity [MW]	Expected Completion Year	Description of Project
Dolphyn	[39]	100	2032	ERM project for the production of large-scale green hydrogen from the offshore floating wind. The aim is to increase production scale step by step to GW-Scale in the early 2030s
AquaVentus	[40]	300	2031	The AquaVentus project has a goal of placing a 300 MW electrolyser to produce 20000 tons of hydrogen annually. The project is divided into production development, pipeline construction and decentralized hydrogen production.
Oyster	[41]	>1	2024	Project by consortium to develop and validate a marine electrolyser and prepare for large-scale development of marine electrolyser and export capabilities.
Salamander	[42]	5000	2030	A 100 MW floating wind energy project that has the plan to include the Dolphyn desalination module that is being developed.
Crosswind	[43]	2.5	2024	Joint venture between Shell and Eneco with 759 MW offshore wind park has ordered a 2.5 MW PEM. The project is planned to produce hydrogen when energy production is high
H2-Wind	[44]	5	2025	Sub-project of the H2-Mare project by the Fraunhofer Institute. It aims to develop a scientific and technological basis for offshore hydrogen production. At the end of the project, the aim is to have a 5 MW up and running.
PosHYdon	[45]	1	2025	Dutch project to place 1 MW of to produce 400 kg hydrogen per day. It includes a desalination plant and will be placed 13 km off the Dutch shore.
H2Res	[46]	2	2022	Danish energy company Ørsted plans to build an onshore 2 MW in Denmark by late 2022. Production should yield 1000 kg hydrogen per day and is funded with 4.6 million Euro by the Danish government.
Lhyfe	[8]	1	2023	First operational offshore hydrogen production of the French coast in June 2023. The 1 MW will produce up to 400 kg of hydrogen per day. The Sealhyfe platform has a 200 m^2 footprint.

2.7.2. DOLPHYN

The Dolphyn project is a well-documented project of designing and up-scaling offshore hydrogen platforms. The project started with 2 MW and will scale to 10 MW and 100 MW subsequently. From a technical point of view, the project is interesting since there is intensive documentation on the choices in the modelling and

some technical specifications. In Figure 2.4 [2] the schematic of the system is proposed. Imported takeaways from this figure are the inclusion of desalination equipment, the use of a PEM and a fuel cell. In order to run the on stand-by mode when the floating wind turbine is not in operation the fuel cell and a hydrogen storage tank are available to supply the electrolyser with enough electricity to reach the lowest operating range. In the report, nothing is mentioned about how long the fuel cell and hydrogen storage can keep the running. For example, if the wind turbine needs maintenance. There is a backup battery available for emergencies. This will be further researched and does not answer one of the more imminent design problems faced in offshore electrolysis.

The produced hydrogen is stored at around 30 bar and ambient temperature. The storage is meant to be used in standby mode for the fuel cell to supply the standby power. The hydrogen is transported to shore via a 16 km pipeline with a 3-inch inner diameter. For the 10 MW scale, the optimal pipeline diameter will need to be refined. With a lot of the design decisions, the report mentions that the sizing is not based on a detailed optimization and they highly recommend this to be performed in the future.

The aim of the project is to produce hydrogen at a maximum LCOH of 6.15£/kg. This number is set to be the target price of green hydrogen in the Aberdeen area. The plan is to bring this figure down to 1.50£/kg by 2040. It should be reached by scaling the plant and removing bespoke parts with industry standards. However, no data are given to back up the 2040 price in the documentation. The last remark that can be made on the project is the choice of location for the 10 MW. Since WTG's are already surpassing 10 MW only one WTG is needed for this scale-up. Furthermore, several factors including the soil material, place for the hydrogen pipeline, and proximity to shore are factors in the selection of the location [2].

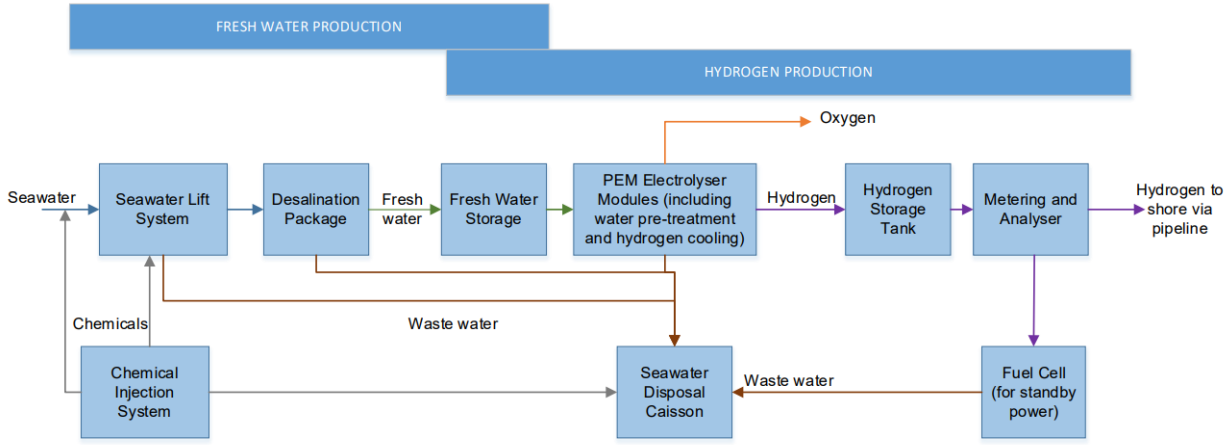

Figure 2.4: Dolphyn process schematic [2]

2.7.3. AQUAVENTUS

The AquaVentus project consists of three sub-projects. AquaDuctus is studying the infrastructure to transport hydrogen to shore. Secondly, AquaPrimus is working on decentralized hydrogen production. Lastly, the AquaSector project is aiming to build a large-scale offshore hydrogen production facility called AquaVentus. With these sub-projects the consortium of RWE, Gasunie and other partners wants to install 10 GW of hydrogen production by 2035. This is the aim of the German government. [40] However current production is zero and all the sub-projects are still in the feasibility stage. This shows again that projects are announced with the help of governments to reach green hydrogen production goals in the 2030s. However, any scientific backing is not provided.

The only information available about this project consists of studies performed by consultancy agencies about potential costs. [47] [48] These documents can be interesting for the modeling of offshore hydrogen. They outline quite a few essential costs of hydrogen production and compare the LCOH of hydrogen with

onshore production and PV electricity. In Figure 2.7 the assumed LCOH for the different production infrastructures is shown. These numbers are for a wind farm 100 km offshore. It is estimated that from 100 km onward it is favourable to use offshore electrolysis over onshore electrolysis.

Further useful conclusions from the document include that the cost of a hydrogen pipeline scales linearly with the diameter whereas the capacity increases more significantly with increasing diameter. This is one of the main drivers for relative LCOH with offshore electrolysis the further the wind farm is from shore. Estimates for the export via hydrogen pipelines are hard to come by. However, this project expects the pipelines to be cheaper. The cost of a methane or natural gas pipeline is 11 €/kW/100 km. The cost of electricity cables is 230 €/kW/100 km. Lastly the total value chain efficiency is estimated to be 63.18% [48]. This value is higher than what the literature suggests. In literature estimates for the chain efficiency for a cryogenic hydrogen at 100 km transport distance are 58% and 41% for liquid hydrogen. [49].

2.7.4. LHYFE

The Lhyfe project is the first offshore hydrogen project operational in the world. The unit that produces hydrogen is called SeaLhyfe. The SeaLhyfe unit has a power consumption of 1 MW and is coupled to a 2 MW floating wind turbine. Little technical information is published about the electrolyser and the systems that are used [8]. The only information that can be found is that the system makes use of a modified Plug EX-4250D electrolyser [17]. The electrolyser fact sheet states several important parameters such as the water requirements, output pressure but also the startup time of the electrolyser. With only 60 seconds from minimum to maximum, this is an important factor in reacting to varying electricity supply by the turbine. The electrolyser is stated to be able to produce 400 kg of hydrogen per day. For now, the electrolyser will be undergoing a series of tests. It is not intended to be supplied to the grid regularly.

2.8. ANNOUNCED OFFSHORE HYDROGEN TENDERS

2.8.1. NETHERLANDS

In the Netherlands, the minister of Climate announced a plan for DEMO I and DEMO II [34]. It was announced that for DEMO I a 100 MW electrolyser was to be coupled to an existing commissioned wind farm in the Hollandse Kust area as early as 2027. This would be a tryout for a bigger 500 MW electrolyser to be placed in the area Ten Noorden van de Waddeneileanden. The idea is that the first demonstration project will supply the industry with highly needed data and information on offshore hydrogen production. The exact location is still unknown and looked into. The hydrogen pipeline corridor is to be researched by the hydrogen network provider Gasunie.

For the second demonstration project an existing planned location for a wind farm was chosen. This location coincided with the proposed international hydrogen infrastructure. Alternatively, an existing natural gas pipeline could be used for hydrogen transportation.

2.8.2. GERMANY

The German government announced in their plan for 2030 that 1 GW of offshore hydrogen. The SEN 1 zone would exclusively produce hydrogen from wind energy. The produced hydrogen will be exported using hydrogen pipelines. The project for this pipeline is called AquaVentus. Already two companies have applied for funding for constructing the 400 km hydrogen pipeline to sea. By 2035 the hydrogen pipeline would need to be coupled to the international pipeline infrastructure for the hydrogen market [50].

2.8.3. DENMARK

The Danish government announced a hydrogen tender in April 2023 for an offshore electrolyser. No information is given on the size of the proposed electrolyser. Five companies have won the tender. The tender consisted of a budget for the development and construction of the facilities and then a budget for ensuring a market-competitive hydrogen price [51] [52]. The total electrolyser capacity for the 5 projects is 280 MW. This is to be constructed in the upcoming 4 years. The biggest electrolyser project consists of 150 MW [53].

2.9. LOW-EMISSION HYDROGEN MARKET

The demand for hydrogen is rising since it could be a sustainable alternative to fossil fuels in the industry and transportation, chemical feedstock for fertilizer or other CO_2 emission-free processes. In 2022 the demand for hydrogen was 95 Mt. This was 3% higher than in 2021. By 2030 this could increase to 115 Mt. All current government plans combined, the production of low-emission hydrogen should be 27-35 Mt in 2030. However, current efforts to increase demand for low-emission hydrogen only include 14 Mt of production in 2030. If all the announced projects for 2030 are realised the production of hydrogen could reach 38 Mt in 2030 worldwide. The demand for low-emission hydrogen is low since it is more expensive than hydrogen from fossil fuels with and without carbon capture methods [3].

The production of hydrogen is currently mostly composed of natural gas and coal-based technologies as can be seen in Figure 2.5 [3]. Only 0.1% of hydrogen is produced using electrolysis. Production using fossil fuels in combination with carbon capture, utilisation and storage consists (CCUS) of 0.6%. This means less than 1% of hydrogen production is low-emission. If the Net Zero Emission (NZE) scenario is to be satisfied in 2030 electrolysis production will need to increase to 28 Mt per year.

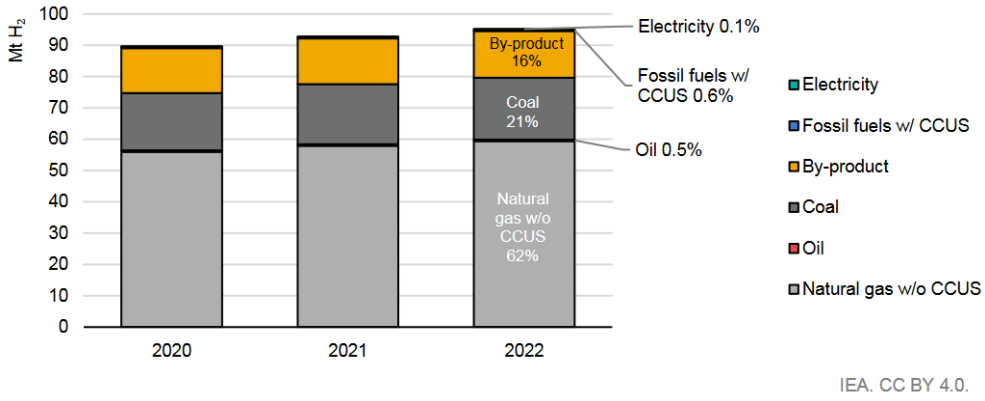

Figure 2.5: Hydrogen production per technology 2020-2022 [3]

In 2022, the 'global installed water electrolyser capacity is at 700 MW. In 2023 the expected production capacity will reach over 2 GW. This shows a big increase in electrolyser capacity installed. Most of this capacity is installed in China as can be seen in Figure 2.6 [3]. This figure also shows the target for installed electrolyser capacity in the NZE by 2030. If all the announced projects continue, 155 GW of electrolyser capacity will be installed each year by 2030.

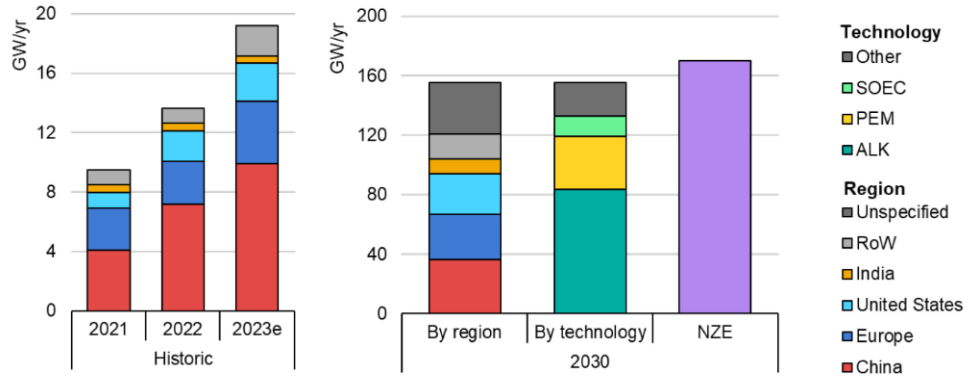

Figure 2.6: Electrolyser manufacturing capacity by region and technology according to announced projects and in the NZE by 2050 scenario [3]

An important factor in the feasibility of low-emission hydrogen production is the production cost or Levelized Cost of Hydrogen (LCOH). An overview of the LCOH for different technologies is shown in Figure 2.7 [3]. The current LCOH of wind-based hydrogen production is not competing with the LCOH of natural gas and coal technologies. Even with the reduction of cost in 2030 due to lower CAPEX and improvement of technologies by 2030, the price range is still higher than fossil fuel-based hydrogen. Without subsidies for low-emission hydrogen or higher taxes on fossil fuels the feasibility of wind-based hydrogen will stay low. The target for offshore hydrogen-based LCOH is between 2 and 7 USD/kg hydrogen. The current reached price is still lower. It will be an important factor in modelling and optimization to bring down the LCOH in order to be compatible with the market and make wind-based hydrogen production feasible before bigger projects can be made profitable. On the other hand, the hydrogen outlook shows that governments are willing to invest in low-emission hydrogen and the possibilities are increasing each year. This is also shown in the increase in announced electrolyser capacity.

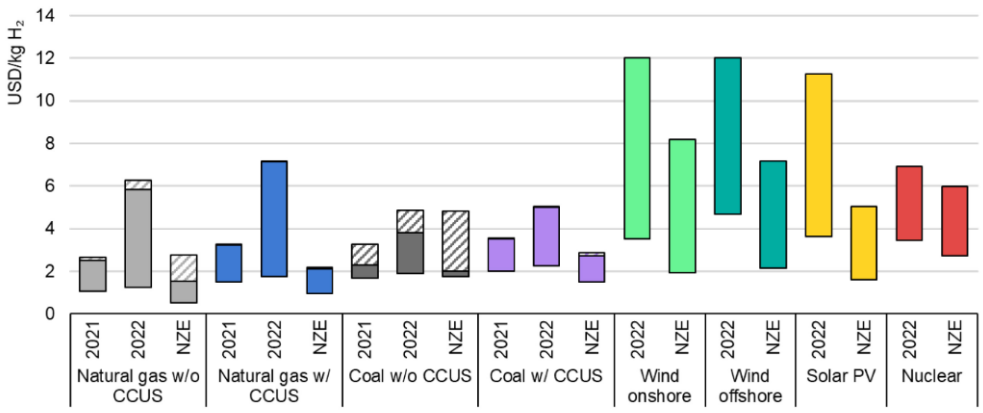

Figure 2.7: Levelised cost of hydrogen production by technology in 2021, 2022 and in the Net Zero Emissions by 2050 Scenario in 2030 [3]

Table 2.1: List of offshore electrolysis optimization research

Publication title	Reference	Publication Year	Design Objective [MW]
Optimizing hybrid offshore wind farms for cost-competitive hydrogen production in Germany	[12]	2022	Electrolyser size for optimal LCOH
Correlations between component size green hydrogen demand and breakeven price for energy islands	[27]	2023	Hydrogen tank sizing and WTG for optimal LCOH at zero NPV
Electrolysis plant size optimization and benefit analysis of a far offshore wind-hydrogen system based on information gap decision theory and chance constraints programming	[28]	2022	Size optimization for maximum NPV
Power generation cost minimization of the grid-connected hybrid renewable energy system through optimal sizing using the modified seagull optimization technique	[29]	2020	Optimizing for minimum power consumption of Onshore hydrid wind-solar-hydrogen production
Wind-farm and hydrogen-storage co-location system optimization for dynamic frequency response in the UK	[30]	2023	Optimizing dynamic freqeuncy response with component sizing for maximizing profit
Simulation of the optimal plant size to produce renewable hydrogen based on the available electricity	[13]	2023	Size optimization for optimal LCOH
Stand-Alone Offshore Wind Energy and Water Electrolysis: A Study on Optimal Electrolyser Sizing	[11]	2023	
Optimal sizing of a grid-assisted wind-hydrogen system	[14]	2018	Optimal electrolyser size for net zero annual power supply by the grid
Modeling and optimization of an energy generation island based on renewable technologies and hydrogen storage systems	[37]	2012	Optimizing an wind-hydrogen energy island for energy prizes

3

ELECTROLYSER

3.1. HYDROGEN PRODUCTION USING ELECTROLYSIS

Low-emission hydrogen is hydrogen produced via natural gas with carbon capture or electrolysis. Since wind-based hydrogen is produced using electricity the focus is diverted to electrolysis. Electrolysis is the process of producing hydrogen by splitting water into oxygen and hydrogen as shown in Equation 3.1[54]. In order for the splitting to occur a certain amount of energy, $\Delta H(T)$, needs to be supplied. This energy consists of the change in electrical Gibbs free energy, $\Delta G(T)$, and heat $T\Delta S(T)$ as shown in Equation 3.2 [54]

$$H_2O \rightarrow \frac{1}{2}O_2 + H_2 [54] \tag{3.1}$$

$$\Delta H(T) = \Delta G(T) + T\Delta S(T) [54] \tag{3.2}$$

In order for water to start splitting and create the reaction in Equation 3.1 a cell potential is needed. The minimum cell potential is called the reversible voltage V_{rev} which is calculated using the Gibbs free energy change of 237.22 KJ/mol , the number of electrons n and Faraday's constant F of 96387 C/mol, as in Equation 3.3. The reversible voltage for water splitting turns out to be 1.23 V [54].

$$V_{rev} = \frac{\Delta G}{nF} = 1.23 \text{ V} [54] \tag{3.3}$$

The reversible voltage is the physical limit at which water splitting will happen. However, to overcome the entropy increase of splitting the water heat is taken from the environment. This process is irreversible. If one includes the entropy change in the applied voltage the thermo-neutral voltage V_{th} is found using Equation 3.4.

$$V_{th} = \frac{\Delta H}{nF} = \frac{\Delta G}{nF} + \frac{T\Delta S}{nF} = 1.48 \text{ V} [54] \tag{3.4}$$

The operating voltage therefore has an effect on the thermodynamic behaviour of the electrolysis. At higher voltages than V_{th} the cell will start producing heat and has to be cooled for example. If the operating voltage E_{cell} is equal to V_{th} the heat consumption of the endothermic reaction is equalled by the heat input. Next to V_{th} and V_{rev} the operating voltage is defined by three losses that occur in the electrolyser cell. Firstly the ohmic resistances are overcome by the V_{ohm} overpotential. V_{ohm} is linearly dependent on the current density and has the potential of being the dominant factor at higher current densities. Secondly the V_{act} is the overpotential related to the losses at the anode and cathode due to limited electrode kinetics. This overvoltage has a logarithmic dependence on the current density and will be almost constant at higher current densities. The last loss is compensated by V_{con}. It is defined by concentration losses in the cell. The local concentration changes in the cell are caused by the transport issues with gaseous products. Combining the reversible voltage with all the overpotentials listed above in Equation 3.5 [54] the operating cell voltage is calculated.

$$V_{cell} = V_{\text{rev}} + V_{\text{act}} + V_{\text{ohm}} + V_{\text{conc}} \tag{3.5}$$

The efficiency of the electrolyser can be defined by Equation 3.6. Where HHV_{H_2} is the higher heating value in the case of liquid water being supplied to the electrolyser. m_{H_2} is the mass of hydrogen produced and lastly $E_{el,in}$ is the electrical energy used for making that amount of hydrogen.

$$\eta_{sys} = \frac{HHV_{H_2}\dot{m}_{H_2}}{E_{el,in}} \tag{3.6}$$

Another way of presenting the efficiency is by looking at a more detailed level where the electrical efficiency can be defined. This efficiency is close to the voltage efficiency. This efficiency is shown in Equation 3.7 [54]. Where the V_{app} is the applied voltage. This equation shows that increasing the overpotential decreases the efficiency of the electrolyser. Since the overpotentials discussed earlier depend on factors such as operating temperature the control regime of the electrolyser has an important effect on the efficiency.

$$\eta_{el} \approx \eta_V = \frac{V_{th}}{V_{app}} \tag{3.7}$$

There are several important characteristics of electrolysers that have an effect on the availability, costs and feasibility of using the technology for converting wind energy. Firstly, the current density has several effects on the process. A higher current density increases hydrogen production per cell area. This leads to a reduction in capital expenditure (CAPEX) per hydrogen production. The disadvantage of higher current density is a decrease in performance leading to an increase in operating expenditure (OPEX). The operating temperature of the electrolyser has an effect on the efficiency of the electrolyser. A higher temperature increases efficiency. However, at the same time, it is limited by the material properties of the electrolyser as well as the degradation issues of the cell [31]. Next to the temperature, each electrolyser has to operate above a low partial load in order to prevent drastic permeation of gasses. Diffusion of oxygen and hydrogen reforming water reduces the efficiency. Once this process is greater than the creation of hydrogen water will start to accumulate. Lastly, there is a large difference between electrolysers in minimum partial load and thus partial load range. [32].

In order to evaluate the effectiveness of possible electrolyser types several criteria are identified as well as their weights for a decision matrix. In Table 3.1 a list of the prior mentioned criteria is stated. Together the weights add up to 100. The weighted system is chosen since some factors are more influential on the performance of the electrolyser in a wind-based setting than others. The score of each category is calculated by taking the maximum of several review papers for each electrolyser type. Then using Equation 3.8 the score is calculated relative to the maximum in that category.

$$\text{Score}_{\text{i}} = \frac{\text{Maximum} - \text{Method}_{\text{iMaximum}}}{10} \tag{3.8}$$

Since the energy supply of wind energy is not consistent. Having a low minimum load factor is among the most important factors in choosing the type of electrolyser for wind-based hydrogen production. The other most important factor is the CAPEX of the electrolyser. Since wind-based hydrogen production needs to compete with low-priced blue and black hydrogen CAPEX is an important factor in the decision-making of the electrolyser type. [55] Therefore these two factors have been given the highest weight of 20. Next in line are the durability and efficiency of the electrolyser. Since an offshore wind farm will run for several decades the durability in running hours is a good indicator of the frequency at which the electrolyser needs to be replaced. The efficiency of the electrolyser will have an effect on the hydrogen price. Using less energy for production increases the hydrogen output at constant power. Both of these criteria have been given a weight of 15. This is slightly lower than the first two since they will greatly influence the pricing but are less important for the feasibility of the project. The last three categories, output pressure, current density and maturity of technology are given a weight of 10. Output pressure and current density will define the operating conditions and footprint of the whole installation. These will have a minor effect on the costs. Output pressure will dictate the amount of compression still needed for hydrogen after production. Lastly, the maturity of technology has been given a lower score. Since the use of electrolysers at the scale of offshore

wind parks is large and has not been used extensively the maturity of technology will be mostly influenced by how much the technologies can scale in the upcoming years until 2030.

In section 2.9 emphasis was placed on the LCOH to reach a feasible project and create demand for low-emission hydrogen. In the decision matrix, it was chosen to not simply incorporate the LCOH of hydrogen mentioned in the literature as one of the criteria. The reason for this is that the LCOH is dependent on the location at which it is produced as well as the hydrogen prices. For example, in one paper the numbers of 2 to 7 USD/kg hydrogen are given [56]. However, the lower limit is based on an electricity price of 0.03 USD/kWh. Current electricity prices in the USA are well above 0.10 USD/kWh. The uncertainty of electricity prices right now is too large to make a correct assumption on the scoring in the future. On the other hand, it could be important to look at the effect electricity pricing has on the scoring of the electrolysers in the future. A factor that is more important in an offshore location is the footprint and weight of the electrolyser equipment. Since it is hard to find any information on these variables this factor is not included as a weight in the decision matrix. The current density gives a small indication of the sizing of the system so it will be taken into account in that category.

Table 3.1: Weights per category of electrolyser

Criteria	Weight
Capital Expenditure (CAPEX)	20
Minimum Load Factor	20
Durability	15
Efficiency	15
Output Pressure	10
Current Density	10
maturity of technology	10
Total	100

3.2. ELECTROLYSER TYPES

There are three types of commercially available water electrolysers currently being researched and/or in use. The alkaline water electrolyser (AWE), the polymer electrolyte membrane electrolysis cell (PEMEC or PEM) and the solid oxide electrolysis cell (SOEC or SOE). The three named technologies have differentiating stages of development [31] [57]. The PEM and AWE have been commercially available for some time. Whereas the SOEC is still in development.

Alkaline Water Electrolyser (AWE) The AWE has been used in industrial applications since 1920 [58]. The main advantages of this electrolyser type are the low CAPEX and more mature components. The low CAPEX of this type of electrolyser is a result of not having to use noble expensive metals in the cathodes. The disadvantages of the AWE are the long start-up time and low performance at dynamic operation. High life cycles could result in a less efficient system and gas purity [54] [58]. Currently, the AWE is used industry-wide in producing hydrogen. It can operate for long times without a maintenance overhaul [54]. However, using this type of electrolyser in power-to-gas systems (P2G) proves to be problematic. With a fluctuating power output of wind and solar, it proves that the AWE produces lower hydrogen qualities, lower efficiency and reduced durability of the system. [54] [32]

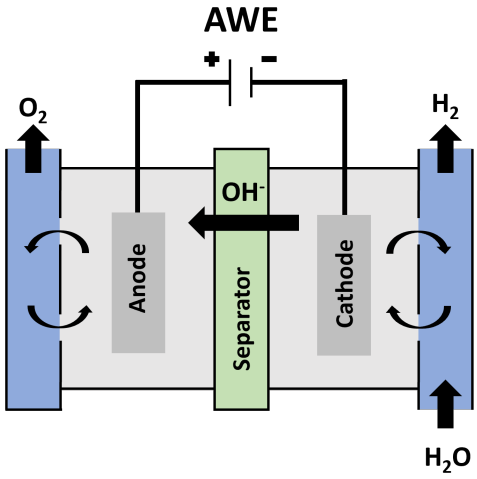

Figure 3.1: Alkaline Water Electrolyser

Proton Exchange Membrane (PEM) The PEM or proton exchange membrane is a newer technology than the AWE. It was introduced in the 1960s by General Electric [31]. A schematic layout of the PEM is shown in Figure 3.2. The anode and cathode are separated by a membrane that allows protons to move through. The membrane has a low gas crossover and can thus operate at higher pressures. Another advantage of the low gas crossover is that the cell can operate at a lower minimum power without having too much gas permeation. The main disadvantage is the high costs of the membrane, anode and cathode materials. The anode is constructed from noble catalysts like iridium and for the cathode platinum is used. The membrane is in most cases a $Nafion^{®}$. Since this is a trademarked product it also has high costs related to it [32].

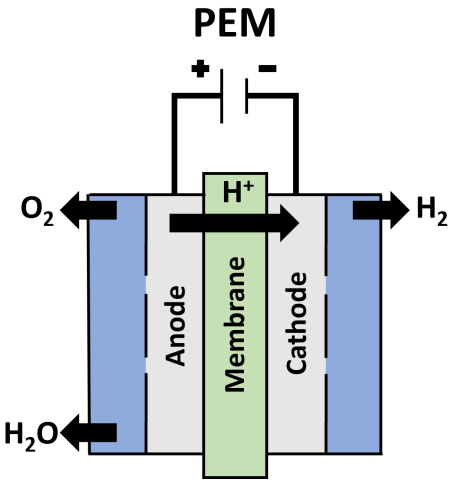

Figure 3.2: PEM electrolyser

Solid Oxide Electrolysis Cell (SOEC)
The third type of electrolyser discussed in this section is the Solid oxide electrolysis cell or SOEC in short. This type of electrolyser is still in a more early stage of development compared to the PEM and even more so the AWE electrolyser. Development of the SOEC started in the 1970's [59]. Nowadays the technology is in the demonstration phase and only a small amount of companies offer the technology [60] [61] [62]. A schematic of a SOEC electrolyser is shown in Figure 3.3. In an SOEC the membrane is gas-tight and is ion-conducting. Steam is entered at the anode side and oxygen ions are transported through the membrane to

the anode side. The main advantages of SOEC are high operating temperatures of 700-900 °C. This possibly results in higher efficiencies from improved kinetics, and thermodynamics favouring heat utilisation as well as dealing with the conversion of steam. Lastly, a SOEC is able to construct hydrogen from a combination of steam and CO_2. The use of CO_2 could result in better carbon neutral projects [31] [63]. In an offshore setting, CO_2 will not be available so this characteristic can not be taken advantage of. The main disadvantages of the SOEC technology are also related to the high operating temperatures. The material degradation in a SOEC is relatively high resulting in a lower lifetime. Furthermore, the high operating temperatures require steam to be supplied at around 1000 C° [64].

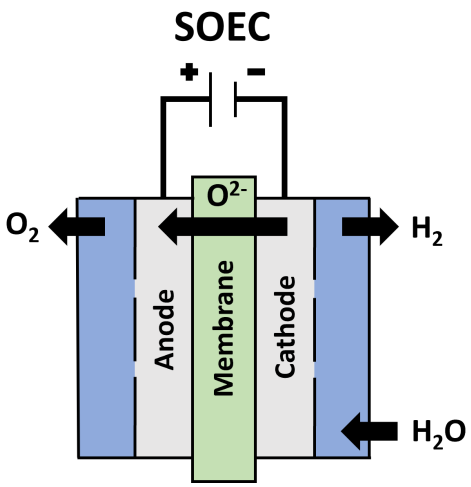

Figure 3.3: SOEC electrolyser

3.3. CHOICE OF ELECTROLYSER

In this section, the data from several publications on AWE, PEM and SOEC electrolysers was gathered. These data are shown in Table 3.2. Several of the publications mentioned in the table are slightly outdated. Therefore, the data were checked by comparing them with commercially viable systems listed in [31]. Since large infrastructure in the wind-based hydrogen production is planned for the future close to 2030 it could for future research be important to look for expected improvements in the parameters mentioned in the table. Several studies made use of experts giving their opinion on the improvements that can be made before 2030 [55] [65]. An important takeaway from the table is that there really is not a lot of data available about the SOEC electrolyser. In several categories, the parameter is not given as a range but more as a maximum or minimum. However, the studies mostly chose this way of presenting when only one data point was available. Another point to note is that experts expect the CAPEX of the PEM electrolyser to drop well below 1000 €/kW [55] in 2030. This shows that both the PEM and SOEC electrolyser could see some large improvements in overall performance and cost in the upcoming years.

Table 3.2: Summary of electrolyser parameters

Specifications	AWE	PEM	SOEC
Cathodic Reaction	$H_2O + 2e^- \rightarrow H_2 + O^{2-}$	$2H^+ + 2e^- \rightarrow H_2$	$2H_2O + 2e^- \rightarrow H_2 + 2OH^-$
Anodic Reaction	$O^{2-} \rightarrow 1/2O_2 + 2e^-$	$H_2O \rightarrow 2H^+ + 1/2O_2 + 2e^-$	$2OH^- \rightarrow H_2O + 1/2O_2 + 2e^-$
Operating Temperature [C°]	60-90	50-90	700-1000
Operating Pressure [bar]	2-30	15-50	<25
Cell Voltage [V]	1.8-2.4	1.8-2.2	0.7-1.5
Current Density [A/cm^2]	0.2-0.4	1.0-2.0	0.3-1
Voltage Efficiency	62-82	60-68	76-86
Load Range [%]	40-100	0-100	-100-100
CAPEX [€/kW]	800-1500	1400-2320	>2000
Technology Status	Mature	Commercial	Demonstration
Lifetime of Stack	60000 - 90000	30000-60000	<10000
Energy Consumption [kWh/Nm^3]	4.5-6.6	4.4-5.5	>3.7
Source:	[31] [55] [58] [66]	[31] [55] [58] [65] [66]	[31] [55] [58] [65] [66]

Using Equation 3.8 for each category and the type of electrolyser, the score is calculated and presented in Table 4.8. The maximum score in each category is 10 points. This is awarded to the best commercially available scoring electrolyser in this category. Each electrolyser then is than granted a score between 1 to 10 according to the average from Table 3.2. The method of taking the average is chosen since the maximum of each category is not a correct representation. Maximizing one category will not mean the other categories can be maximised. By taking the average of each electrolyser this co-dependence should be reduced.

The first takeaway from Table 4.8 is that the highest scoring electrolyser type is the PEM. It is closely followed by the AWE electrolyser. The gap of 25 points could be quite insignificant. The SOEC electrolyser scores more than 100 points lower. Although quite a lot of literature points it out as a potential new technology, it is not nearly scoring as high as the two more established technologies. Looking further into the category scores the PEM electrolyser scores decent in most categories. The drawbacks of more CAPEX and lower durability are compensated by a better minimum load factor, output pressure, current density and a decent maturity of technology. The AWE electrolyser scores high in maturity and technology, CAPEX and durability. However the minimum load factor is lower and the output pressure is also low compared to the PEM. The SOEC electrolyser scores very diverse. It has a high operating range due its reversible ability and also could reach higher efficiencies. However is scores low in all the other categories giving it a low score for the production of wind based hydrogen. It can be concluded that it can be wise to continue modeling with both the AWE and PEM in the future. Both electrolysers have their pros and cons and it is hard to distinguish both without any further calculations.

Table 3.3: Decision Matrix for three electrolyser types

Criteria	Weight	AWE	PEM	SOEC
Capital Expenditure (CAPEX)	20	7	4	3
Minimum Load Factor	20	6	9	10
Durability	15	6	4	2
Efficiency	15	7	6	8
Output Pressure	10	3	6	2
Current Density	10	2	8	4
Maturity of technology	10	10	8	4
Total	100	605	630	510

A last remark should be made on the decision matrix regarding future improvements. The matrix is build up using current numbers. However investment in electrolyser technologies is increasing rapidly as can be seen in figure Figure 3.4[3]. This rapid increase in development could lead to an improvement of the technologies. Especially the investment cost of the electrolysers is expected to decrease. For SOEC numbers of 200 USD/kW

are given [67] for estimates in 2050. This is considerably lower than the 750 USD/kW for PEM electrolyser. In research it could be interesting to look specifically at the sensitivity of the investment prices within models that are constructed. This also shows that ruling out the SOEC right away is not an option. Neither of the three electrolysers are already outperforming if you take into account the possible improvements that can be made.

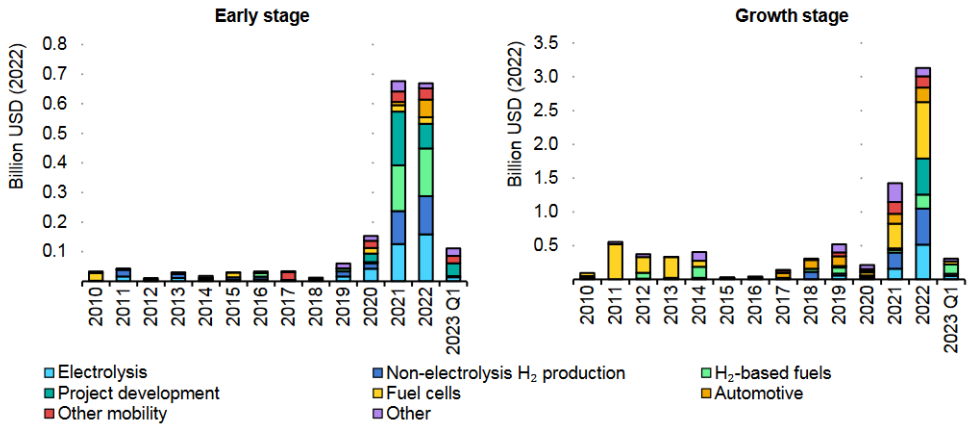

Figure 3.4: Venture capital investment in energy start-ups in hydrogen-related areas, for early-stage and growth-stage deals [3]

4

System Modelling

The previous chapter provided a comprehensive overview of the overall layout of offshore hydrogen production and electrolyser technology. From the outset, it was clear that a decentralised layout would be the best option, given the technical limitations of electrolyser technology. The research question will require that an offshore off-grid wind-based hydrogen production facility is modelled. It will have a strict selection of variables that will allow it to be optimised for the LCOH. This chapter will explain the model that has been constructed to answer the sub-questions and main research question. The chapter will begin with a clear visualisation of the system overview and an explanation of the requirements. The methods used to model the essential subsystems will be discussed in separate sections. In the final sections, the chosen methods to optimise the system will be explained. By the end of this chapter, you will understand how the research question will be answered.

4.1. Requirements

The off-grid offshore wind-based hydrogen system has several requirements. The requirements are listed as technical requirement (TR) and model requirement (MR) . The TR's are related to industry standards, limitations of the technology or safety standards. The MR's are needed to apply MDO to the model.

- TR1: The electrolyser will be placed offshore on an offshore platform.
- TR2: The hydrogen is supplied at a minimum pressure of 67 Bar at a fixed connection point.
- TR3: The system shall not have an electricity cable connection to the shore.
- TR4: The PEM electrolyser will be supplied with at least 2% of its nominal power at all times.
- TR5: The lifetime of the project is fixed at 25 years.
- TR6: The hydrogen temperature shall not exceed 100 °C.
- MR7: The model should output an LCOH of the total lifetime of the project in €/kg.
- MR8: The model should be computable for each selected variable over the full range from the lower bound to the upper bound of this variable.
- MR9: The model should be constructed such that it can compute the LCOH with only the input vector costing of the variables that will be optimized.

TR1 and TR3 follow from the research objective and scope discussed in the introduction. TR2 is a requirement based on the maximum pressure that Gasunie allows. TR4 is a direct constraint from the technology readiness at the moment. TR5 will be fixed in the current scope of the research. It is based on the lifetime of an offshore wind farm as in the future the hydrogen production facility and wind farm could be realised simultaneously. TR6 is a safety requirement.

The MR7 requirement is needed as the LCOH is the objective that will be optimized with MDO. The unit of €/kg is an industry-standard unit used to measure the competitiveness of the hydrogen energy source. In order for the model to not give an error during optimization MR8 is required. It ensures that, although the

model is discontinuous it will output a LCOH for each combination. Furthermore, MR9 follows from the fact that the model will have more input variables but these are fixed within the modules to give the optimizer the chance to only give the optimization design vector as an input to the model. Several software packages require this way of formatting and this requirement makes sure that these packages can be implemented.

4.2. SYSTEM OVERVIEW

The aim of the system modelling is to output the LCOH of offshore hydrogen production using offshore wind energy. Meanwhile, the system will not have a grid connection. The list of the different system components that will be part of the scope of this thesis is listed below.

- Electrolyser
- Compressor
- Hydrogen pipeline
- Fuel cell
- Desalination unit
- Offshore platform
- High voltage cable

The electrolyser system component is a strict requirement to produce hydrogen. It will be modelled to give an efficiency of the function of operating pressure and operating temperature. The type of electrolyser used is a PEM electrolyser. As stated in TR4, it will need to be supplied with 2% of its nominal power at all times. Furthermore, the electrolyser power will drive the hydrogen mass flow that is processed by the compressor and the pipeline. The desalination module will take care of this task. The electrolyser will have a limited range of pressure at which it can output the hydrogen. The hydrogen will need to be compressed by the hydrogen compressor in order to reach the minimum pressure of 67 bar as stated in TR2.

The seawater required for the electrolysis needs to be desalinated and treated before being used in the electrolyser. The desalination and deionization module is be modelled such that it outputs the power requirements. The desalination module will supply the water with a specific quality required for the electrolyser. The fuel cell module is required since the system will not have a grid connection to shore. The electrolyser needs power at all times. Since there is the availability of hydrogen in the pipeline a fuel cell is proposed in this thesis to supply the electrolyser with power. The fuel cell will use hydrogen and convert it to electrical power. This in turn will be delivered to the electrolyser. The four subsystems, electrolyser, compressor, desalination and fuel cell, are placed on an offshore platform. The platform will be modelled for cost. A detailed design of the offshore platform is outside the scope of this research. However, offshore platforms are widely used in the industry and accurate costs for the technology are available.

Lastly, the hydrogen pipeline is the only modelled subsystem not placed on the offshore platform. This subsystem transports the hydrogen to the fixed location. This location could be the location of the hydrogen network. Another option could be a fixed hydrogen offtaker located close to shore. The hydrogen pipeline module includes a calculation for the pressure drop and speed of hydrogen flow. The overview of the system as well as the system boundary guarded by the scope of the research is shown in Figure 4.1.

The subsystems for desalination, electrolysis and compression require considerate amounts of power. These systems are modelled to have a power output. Since finding a polynomial for each power curve at different power settings is complicated, the systems will output a list of power settings from 1% to 100% with increments of 1%. 100% is the maximum or nominal power of the electrolyser system. Each of the subsystems supplies a CAPEX and OPEX to the LCOH calculation module. This module calculates the overall hydrogen

production and computes the costs of the project over the whole lifetime. Once both the hydrogen production and cost are known the LCOH is calculated.

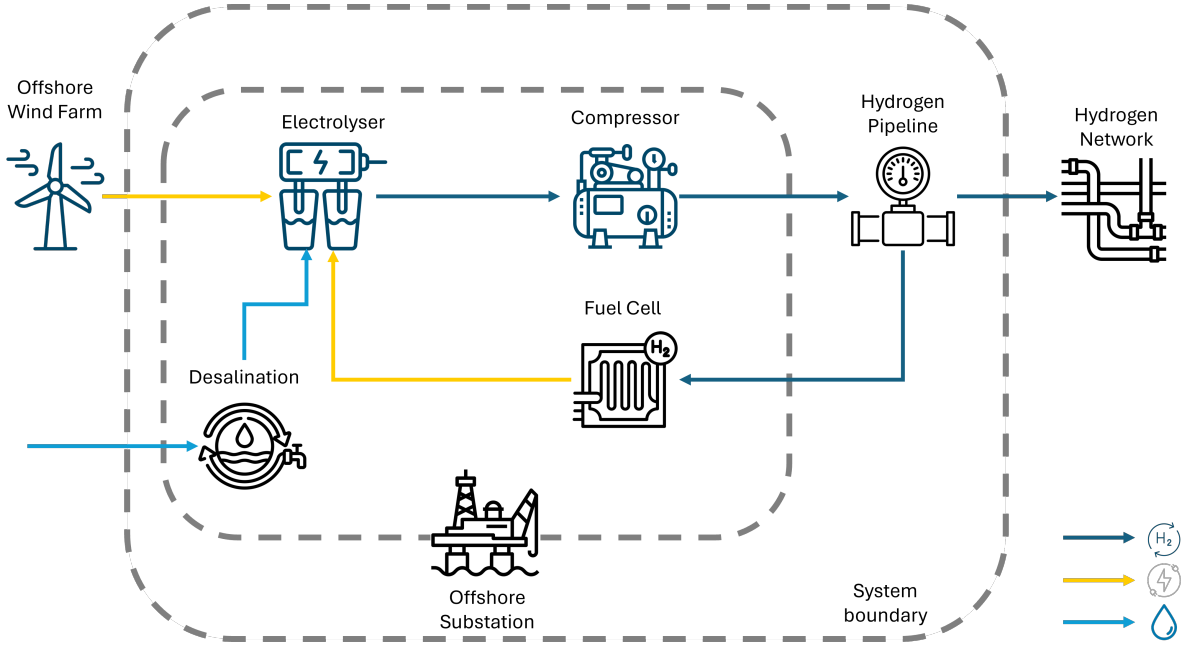

Figure 4.1: Overview of the modelled system

The system boundary is chosen to start at the electricity cable and end before the hydrogen network that was proposed by Gasunie. Since the electrolyser will be placed off-grid it will use all the electricity of the wind farm it is connected to. To simplify the calculation of energy allocation and the cost of energy it is assumed that the costs of the wind farm installation and maintenance is safeguarded by the LCOE of offshore wind. In this research, the LCOE of offshore wind was fixed at 80€/MWh. In the last few years, the LCOE of offshore wind has increased significantly due to inflation and increasing steel prices. Steel is one the main drivers of WTG costs [68].

4.3. ELECTROLYSER MODELLING

The selection of the electrolyser has been made in the previous section. The required inputs and outputs of the electrolyser module are shown in Table 4.1. Research has shown that the pressure and temperature of the electrolyser influence the operating voltage and efficiency of the electrolyser [69, 70]. The electrolyser module will output a list of hydrogen mass flows at each power setting. From the hydrogen mass flow the water requirement for the water desalination is calculated. The hydrogen mass flow will be a function of the power of the electrolyser, the operating temperature and the operating pressure of the electrolyser.

Table 4.1: Electrolyser module inputs and outputs

Inputs	Symbol	Outpouts	Symbol
Electrolyser power	W_{elec}	Hydrogen mass flow at 100 power settings	$\dot{m}_{h_2}$
Electrolyser operating pressure	p_{elec}	Water requirement at 100 power settings	$\dot{m}_{h_2o}$
Electrolyser operating pemperature	T_{elec}	CAPEX electrolyser	$CAPEX_{elec}$
		OPEX electrolyser	$OPEX_{elec}$

The efficiency of the electrolyser is governed by the efficiency of the stack and the efficiency of the other

equipment around the stack. The efficiency of the electrolyser stack is calculated using Equation 4.1 [71].

$$\eta_{stack} = \frac{\mathrm{V_{th}}}{\mathrm{V_{cell}}} = \frac{V_{th}}{V_{\mathrm{th}} + V_{\mathrm{act}} + V_{\mathrm{ohm}} + V_{\mathrm{conc}}} \tag{4.1}$$

The cell voltage can be calculated as shown in Equation 3.5. Therefore the overpotentials, V_{act}, V_{ohm} and V_{conc} will need to be defined as a function of the operating temperature and pressure of the electrolyser in order to calculate the hydrogen mass flow output. The thermoneutral voltage as earlier explained is a function of pressure and temperature. The lookup table for the thermoneutral voltage is shown in Table 4.2. It shows that the thermoneutral voltage increases with pressure. This would potentially increase the efficiency since the cell voltage does not linearly scale with the thermoneutral voltage. On the other hand, a higher temperature reduces the thermoneutral voltage, which has a negative effect on the stack efficiency

Table 4.2: Electolyser thermoneutral cell voltage [V] at various pressures and temperatures [4]

Temperature	Pressure								
	$1bar$	$25bar$	$50bar$	$75bar$	$100bar$	$200bar$	$300bar$	$400bar$	$500bar$
25°C	1.229	1.299	1.312	1.32	1.325	1.339	1.347	1.352	1.356
75°C	1.19	1.268	1.283	1.292	1.299	1.315	1.324	1.33	1.335
100°C	1.153	1.252	1.269	1.279	1.286	1.303	1.313	1.32	1.325

The activation overpotential is a function of the operating temperature and current density in the model and is calculated using Equation 4.2 [4]. Where R is the universal gas constant, T is the operating temperature of the cell, F is Faraday's constant, I is the current density, α_{anode} and $\alpha_{cathode}$ are the charge transfer coefficient of the anode and cathode respectively and lastly the $i_{0,cathode}$, $i_{0,anode}$ are the exchange current density for anode. The activation overpotential is not affected by the pressure of the cell. However, it is governed by the temperature and current density. The activation overpotential is the biggest of the three overpotentials. An increase in temperature linearly increases the activation potential and thus reduces the efficiency of the stack. An increase in the current density is a cause of higher power supplied to the same electrolyser. This will increase the activation overpotential. This means that at higher power settings the electrolyser is less efficient than at the lowest possible power of 10%.

$$V_{\mathrm{act}} = \frac{RT}{\alpha_{\mathrm{anode}} F} \ln\left(\frac{i}{i_{0,\,\mathrm{anode}}}\right) + \frac{RT}{\alpha_{\mathrm{cathode}} F} \ln\left(\frac{i}{i_{0,\,\mathrm{cathode}}}\right) \tag{4.2}$$

Up next, is the Ohmic overpotential. The Ohmic overpotential is related to the Ohmic losses in the cell. The Ohmic overpotential is calculated using Equation 4.3 [4]. It is governed by the current and the resistance in the cell. R_{initial} is the Ohmic resistance at a 0 °C. This includes the resistance of the anode and cathode material as well as the gas separators and membranes. The Ohmic resistance is decreased with temperature. Therefore, a higher temperature results in lower ohmic losses in the cell.

$$V_{ohm} = \left(R_{\mathrm{initial}} - \left[4 \times 10^{-6} \ln(T - 273.15) + 4 \times 10^{-6} \ln T^2\right]\right) \times i \tag{4.3}$$

Lastly, the electrolyser stack losses are finalized by finding the concentration losses. These are governed by bubbles forming close by the anode and cathode. These create changes in the concentration of the substances required in the reactions in the anode and cathode. These losses change depending on the length the electrolyser has been on. However, this model will not incorporate the time-dependent control in the electrolyser. Therefore the concentration losses are assumed to be constant and are taken from the steady state concentration losses from Roy *et al.*[4]. Furthermore, the concentration losses are increasing with the current density. Which means the concentration losses are higher at higher power settings. This follows from a higher hydrogen production around the electrodes.

$$V_{\text{con}} = 0.00001 \times i - 4 \times 10^{-9} \times i^2 + 10^{-9} \times i^3 \tag{4.4}$$

SYSTEM EFFICIENCY & TEMPERATURE CONTROL

The electrolyser stack has an efficiency following the pressure and temperature in the previous section. However, the operating temperature of the stack defines for a large part the cooling power required to keep the stack at the defined operating temperature. Pressure has a small effect on temperature control, this is therefore neglected since the temperature has a much greater influence on the cooling regime [5]. In [5] a model is presented which calculates the temperature control power requirement for three current densities (0.5, 1 and 1.5 A/cm^2) and three operating temperatures of 45, 65 and 75 $°C$ for a 100 kW electrolyser. These values have been used as reference values to calculate the temperature control power in the electrolyser module. On top of the stack efficiency, the other systems required in the electrolyser will require power as well. These systems require around 14% of the total power in the electrolyser system according to [4]. Therefore, the stack efficiency is multiplied by 0.86 to find the system efficiency.

ELECTROLYSER MODULE OUTPUTS

The electrolyser module is required to output the hydrogen mass flow at the 100 power settings ranging from 1 to 100% of maximum power. Therefore for each power setting it calculates the efficiency of the cell with the overvoltages explained earlier in the section. The power setting is linearly converted in a current density. A power setting of 1% is given a current density of 0.05 A/cm^2 and the maximum power setting of 100% is converted to a density of 0.5 A/cm^2. In the earlier sections, several articles referenced a maximum current density of 2% A/cm^2. After evaluating the efficiency in the module at 2% A/cm^2 it became clear that the cooling power required to operate at that current density would make the efficiency close to 0. Since [4] uses a maximum current density of 0.5 A/cm^2 this value was taken as the maximum current density in the module. From the efficiency, Equation 3.6 is used to calculate the hydrogen production rate at each current density. Lastly, the water mass flow required to produce the hydrogen is calculated using Equation 4.5

$$\dot{m}_{H_2O} = 10\dot{m}_{H_2} \tag{4.5}$$

The final outputs of the module also contain the $CAPEX_{elec}$ and $OPEX_{elec}$ of the electrolyser. These figures scale linearly with the electrolyser power. In Table 3.2 the cost of electrolysers was estimated to be 1400-2300€/kW. However, this does not include the extra costs associated with placing the electrolyser on an offshore platform. In this model, it is therefore important to include these supplementary costs. Private communication within Eneco estimates the electrolyser costs to be 2700€/kW. The $OPEX_{elec}$ is estimated by Eneco to be 4.5% of the electrolyser. Furthermore, the stacks of the electrolyser have a maximum operating lifetime of 60000 hours. Therefore these need to be replaced if the operating time of the electrolyser over the lifetime of the project is higher than 60000 hours. This will be calculated later on in the performance module and an extra CAPEX figure is added for each stack replacement.

Table 4.3: Look-up table temperature control power needed [kW] per 100 kW electrolyser [5]

Temperature °C	Current Density A/cm^2			
	0	0.5	1	1.5
50	8.6	12	16.8	23.1
65	0.4	6	12.8	20.8
75	-7	0	8	17
90	-21.2	-12.1	-1.7	9.4

4.4. FUEL CELL

For the electrolyser to be placed offshore one major hurdle needs to be taken. The electrolyser will require a minimum power when it is not producing hydrogen. Estimates for the percentage of the minimum power range from 5% [72, 73] to 0% [32]. Currently, no PEM electrolyser can be completely shut down over and over again without sever degradation. Experts at Eneco estimate it to be around 2%. Therefore the fuel cell is modelled to supply the electrolyser with 2% of P_{elec}. The inputs and outputs of the fuel cell module are shown in Table 4.4

Table 4.4: Fuel Cell Module inputs and outputs

Inputs	Symbol	Outpouts	Symbol
Electrolyser Power	W_{elec}	Hydrogen mass flow into fuel cell	$\dot{m}_{h_2}$
Electrolyser Operating Pressure	p_{h_2}	Fuel cell CAPEX	$CAPEX_{fc}$
Electrolyser Operating Temperature	T_{h_2}	Fuel cell OPEX	$OPEX_{fc}$

There are many types of hydrogen fuel cells. For this module, a Proton Exchange Membrane Fuel cell was chosen since this type of fuel cell has been used in thousands of applications in the USA [74]. Furthermore, the system will have similarities to a PEM fuel cell which could be a cost reduction in operating costs once placed on the offshore platform. In [75] a model has been proposed which incorporates the pressure and temperature and calculates the operating specifications for a PEM Fuel cell. This model will be used in the fuel cell module.

The efficiency of the fuel cell has to be calculated from the temperature and pressure input of the hydrogen. The efficiency of the fuel cell is calculated using Equation 4.6 [75]. Where V_{th} is the thermoneutral voltage. V_{act}, V_{ohm} and V_{conc} are the activation, ohmic and concentration overvoltage. These are essentially the losses in the fuel cell stack.

$$\eta_{fc} = \frac{V_{th}}{V_{th} - V_{act} - V_{ohm} - V_{conc}} \tag{4.6}$$

The activation overpotential is calculated using Equation 4.7 [76]. The constants ξ_1 until ξ_4 are given in Table 4.5.

$$\Delta V_{act} = \xi_1 + \xi_2 T_{fc} + \xi_3 T_{fc} \ln\left(C_{O_2}\right) + \xi_4 T_{fc} \ln(I) \tag{4.7}$$

The concentration of dissolved oxygen, C_{O_2}, is calculated using Henry's law shown in Equation 4.8 [77]. I is the current in the cell which is set at 30 A. An optimisation could be made on the optimal operating voltage, current and the number of cells placed in a series. This is however, outside of the scope of the research and would have limited effect on the outcome since the fuel cell is only operational for a small fraction of the time and is only 2% of the electrolyser size.

$$C_{O_2} = \frac{p_{O_2}}{5.08 \times 10^6 e^{\left(-\frac{498}{T_{fc}}\right)}} \tag{4.8}$$

Next to the activation overpotential, there is a second loss of the fuel cell due to ohmic losses. This overpotential is calculated using Equation 4.9. Where R_{ion} is the resistance the ions have to the flow and is a function of the membrane thickness, conductivity of the membrane and the cell area A_{cell}, R_{ele} is the electronic resistance, and R_{con} is the contact resistance of the electrodes [75].

$$\Delta V_{\text{ohm}} = R_{\text{ion}}\, I + (R_{\text{ele}} + R_{\text{con}})\, I_{\text{ext}} \tag{4.9}$$

Lastly, the concentration overpotential, V_{con}, is calculated using Equation 4.10. The concentration overpotential is caused by losses due to concentration reduction of the gasses close to the electrode surface. In Equation 4.10 R is the universal gas constant, I_L the limit current at which the partial pressures of the reactants fall to zero, I the operating current and n is the number of molecules involved in the reaction and F is the Faradays constant.

$$\Delta V_{\text{con}} = \left(1 + \frac{1}{\alpha}\right) \frac{RT}{nF} \ln \frac{I_L}{I_L - I} \tag{4.10}$$

Table 4.5: PEM fuel cell parameters

Parameter	Value	Parameter	Value	Parameter	Value
F(C)	96485	ξ_1	1.00	$\tau_m(\mu\text{m})$	25
p_{O_2}(atm)	$\simeq 0.21$	ξ_2	-3.4×10^{-3}	λ_m	7
p_{H_2O}(atm)	1	ξ_3	-7.80×10^{-5}	R$(kJ(kmolK)^{-1})$	8.314
$I_{L,C}$(A)	47	ξ_4	1.85×10^{-4}	η_{aux}	0.8

After calculating the overpotential and the efficiency of the stack using Equation 4.6 the hydrogen mass flow required to produce enough energy is calculated using Equation 4.11 [75]. The extra efficiency loss related to the system components of the fuel cell is taken to be 0.8.

$$\dot{m}_{h_2,fc} = \frac{0.02 W_{elec}}{\eta_{stack} \eta_{aux} LHV_{h_2}} \tag{4.11}$$

Fuel cells will run at only one power setting during the lifetime of the system. This is the 2% of the electrolyser maximum power. In the Bosch fuel cell system, the maximum efficiency of 55% is reached at 35% of maximum power [78]. The fuel cell in this system is run at maximum power since the CAPEX of the fuel cell is relatively high compared to the running time of the fuel cell over the 25-year lifetime of the project. Since an optimization of the fuel cell size is outside of the scope of this thesis it is hard to say if over-sizing the electrolyser is an improvement on the LCOH.

The fuel cell has an estimated $CAPEX_{elec}$ of 1500 €/kW [79]. Since fuel cells are already used in vehicles as well as marine environments compared to electrolysers the $OPEX_{elec}$ is estimated to be 2% of the $CAPEX_{elec}$ [80].

4.5. WATER TREATMENT SYSTEM

The electrolyser will require non-salty water to supply the necessary hydrogen atoms. This water requirement can be in the tens of kg per second. The purity of the water is important to keep the degradation of the electrolyser at a minimum. The PEM electrolyser is expected to require ASTM Type II water to operate properly without considerable loss of efficiency and degradation of the stack [81]. This type of water will require the desalination of salty seawater and further de-ionisation to comply with the ASTM Type II water content. Furthermore, the pressure of the water supplied will need to be higher than atmospheric pressure if the electrolyser operates at elevated pressures.

Table 4.6: Water Treatment Module inputs and outputs

Inputs	Symbol	Outpouts	Symbol
Electrolyser Power	$\dot{m}_{h_2o}$	Water treatment power at 100 power settings	$\dot{W}_{water}$
Electrolyser pressure	p_{elec}	CAPEX water treatment	$CAPEX_{water}$
Electrolyser temperature	T_{elec}	OPEX water treatment	$OPEX_{water}$

The specific energy required in kWh/m^3 to desalinate seawater using reverse osmosis (RO) is dependent on the salinity of the water and is calculated by Equation 4.12 [82] The average salinity of the North Sea water is 35000 mg/L [83].

$$SEC_{RO} = 3.708 + \frac{1.109}{20000}\left(salinity - 30000\right) \tag{4.12}$$

In the module, electrodeionization (EDI) is modelled to deionize the water. This method has been proven to work well in combination with RO to produce water with a low enough quantity of minerals [84]. The specific energy in kWh/m^3 is calculated using Equation 4.13. It is a function of the electric conductivity required of the water in the permeate.

$$SEC_{\text{edi}} = -0.395\sigma_{\text{per}}^2 - 1.404\sigma_{\text{per}} + 2.684 \tag{4.13}$$

Not only does the water need to be desalinated it also has to be pumped up to the electrolyser and compressed to the electrolyser operating pressure. Since the offshore platform has a height of 45 meters the pump power can be calculated using Equation 4.14. Where Δh is the height difference, g is the gravitational acceleration of 9.81 m/s and $\dot{m}_{H_2O}$ is the water mass flow in kg/s.

Not only does the water need to be desalinated, it also has to be pumped up to the electrolyser and compressed to the electrolyser operating pressure. Desalination ensures the removal of salts and other impurities, making the water suitable for the electrolysis process and preventing damage to the electrolyser components. The challenge does not end with desalination; the water must then be transported to the electrolyser situated on an offshore platform. Given the platform's height of 45 meters above sea level, this requires substantial pumping power. The pump power can be calculated using Equation 4.14, where Δh represents the height difference, g is the gravitational acceleration of 9.81 m/s^2, and $\dot{m}_{H_2O}$ is the water mass flow in kg/s. Additionally, the water must be compressed to match the operating pressure of the electrolyser, which typically operates at high pressures to ensure optimal hydrogen production efficiency. This compression step is crucial as it ensures the water enters the electrolyser at the correct pressure, thereby maintaining the integrity and performance of the electrolysis process. Each of these steps—desalination, elevation, and compression—adds to the overall energy requirements and operational complexity, emphasizing the importance of optimizing these processes to minimize energy consumption and maximize efficiency in offshore hydrogen production.

$$W_{pump} = \dot{m}_{H_2O}\Delta hg \tag{4.14}$$

The compressor power is modelled with the pressure that needs to be supplied p_{elec}, the water mass flow and the compressor efficiency η_{compr} in Equation 4.15. The compressor efficiency is estimated to be 75% [4]. In contrast to the ideal gas hydrogen, the water compression formula follows a more generic pattern and linearly scales with the pressure required and water mass flow required. The systems for pressurizing water have been used for a long time and the technology readiness can be assumed as high. Even a generic espresso machine is already capable of pressurizing water to 12 bar [85].

$$W_{compr,H_2O} = \frac{p_{elec} * \dot{m}_{H_2O}}{\eta_{compr}} \tag{4.15}$$

If we multiply the specific energy consumption from the Reverse Osmosis (RO) and Electrodeionization (EDI) processes with the water mass flow, and then add the power required for the pump and compressor, we can calculate the total power consumption of the water treatment system using Equation 4.16.

$$W_{water} = \left(SEC_{RO} + SEC_{EDI}\right)\dot{m}_{H_2O} + W_{pump} + W_{compr,H_2O} \tag{4.16}$$

The power of the water treatment is now known so the last parameters calculated by the module are the $CAPEX_{water}$ and $OPEX_{water}$. In Wenten *et al.* the costs of the RO and EDI were estimated and these were used to calculate the costs of the water treatment system. The specific CAPEX are 9400 €/(m^3/h) and since the EDI is a high-maintenance system it will require more OPEX than the other subsystems. The OPEX is estimated to be 16.5% of the $CAPEX_{water}$.

4.6. HYDROGEN COMPRESSION

The hydrogen produced in the electrolyser will leave at a certain pressure, temperature and purity. To comply with the standard hydrogen pressure in the hydrogen infrastructure especially the pressure and purity will need to be increased to reach the expected quality. In this model, the compression and purifying are performed in the module Hydrogen Compression and Treatment. This module includes the modelling of a hydrogen compressor.

Table 4.7: Hydrogen Compressor Module inputs and outputs

Inputs	Symbol	Outpouts	Symbol
Electrolyser Power	$\dot{m}_{h_2o}$	Water treatment power at 100 power settings	$\dot{W}_{water}$
Electrolyser pressure	p_{elec}	CAPEX water treatment	$CAPEX_{water}$
Electrolyser temperature	T_{elec}	OPEX water treatment	$OPEX_{water}$

There are different types of hydrogen compressors available for the compression of hydrogen. This includes reciprocating or piston compressors, diaphragm compressors and linear compressors. Of these three mechanical compressor types linear compressors are not yet available for the scale of hydrogen flow required in this project. [86] For higher flow rates diaphragm compressors have low power consumption and low cooling requirement. However, the maximum pressure that can be achieved with this type of compressor is below 30 Bar [87] Therefore in this project, a reciprocating compressor will be modelled for efficiency and costs. The reciprocating compressor can compress high pressure up to 1000 bar. The reciprocating compressor is visualised in Figure 4.2 [88]. The main limitation of this type of compressor is that it needs to work without lubricating oil. Lubrication oil can contaminate the hydrogen. Therefore maintenance work is higher on this compressor.

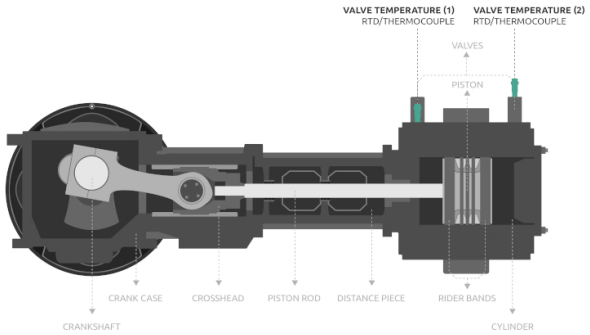

Figure 4.2: Reciprocating Compressor

The modelled reciprocating compressor can have a maximum compression ratio of 2 per compression stage. Therefore, if the compressor has a higher compression ratio than 2 more than one stage is required. The compressor power required for one stage is calculated using Equation 4.17. Where z is the compressibility factor, k is the ratio of specific heat and is 1.41 for hydrogen, T is the input temperature and R is the universal gas constant. The isentropic efficiency, η_{isen} is estimated to be 0.70.

$$P_{\text{single stage}} = \left(\frac{k}{k-1}\right)\left(\frac{Z}{\eta_{\text{isen}}}\right) TR \left[\left(\frac{P_{\text{out}}}{P_{\text{in}}}\right)^{\left(\frac{k-1}{k}\right)} - 1\right] \tag{4.17}$$

The losses compared to isentropic compression will increase the hydrogen temperature. The increase in hydrogen is calculated using Equation 4.18. Where Π is the compression ratio and n_{stage} is the number of stages.

$$T_{out} = T_{in}\left(\Pi^{\frac{k-1}{k}}\right)^{n_{stage}} \tag{4.18}$$

For safety reasons, the hydrogen may not exceed a temperature of 100°C. Therefore, with several compressor stages, the hydrogen will need to be intercooled in between stages to less than ° C. This inter-cooling power is not incorporated in the model since this will be much less power than the reciprocating compressor needs. The CAPEX of the compressor is estimated to be 2800 €/kW with the compressor needing about 6% of OPEX each year. This figure is slightly higher than the other systems since the compressor is lubricant-free and the materials inside the compressor will need more frequent replacement.

4.7. HYDROGEN PIPELINE

A hydrogen pipeline is required to transfer the hydrogen produced by the electrolyser to the hydrogen infrastructure. The pipeline could vary in length depending on the Offshore Platform's locations and the hydrogen network's connecting point. Furthermore, the pipeline design influences the hydrogen mass flow, velocity in the pipeline and the pressure drop due to friction losses. Especially the pressure drop is important to calculate at what pressure the hydrogen is delivered to the hydrogen grid. In this section, an explanation of the modelling and calculation of the hydrogen pipeline module is given.

Table 4.8: Hydrogen Pipeline Module inputs and outputs

Inputs	Symbol	Outpouts	Symbol
Input Pressure	p_{compr}	Minimum Hydrogen pressure pipeline output	$p_{pipe,out}$
Input Temperature	T_{compr}	Maximum hydrogen velocity	u_{limit}
Start Location	$Location_{OFS}$	Maximum allowable hydrogen velocity	$u_{erosional}$
End Location	$Location_{ONS}$	CAPEX electrolyser	$CAPEX_{pipe}$
Diameter pipeline	D_{pipe}	OPEX electrolyser	$OPEX_{pipe}$

Hydrogen pipelines are, in contrast to electrolysis widely used in the world for hydrogen transmission for the petroleum industry. There are currently over 1000 km of hydrogen pipelines operated by refinery facilities in Belgium and Germany alone [58]. Therefore, information about hydrogen pipeline's technical and financial parameters is more readily available compared to large-scale PEM electrolysers.

The hydrogen pipeline model will aid in transporting the pressurised hydrogen from the compressor on the offshore platform to the selected connection point on the hydrogen grid. The hydrogen from the compressor will have a certain mass flow ($\dot{m}_{h2}$), gas pressure (p_{compr}) and temperature (T_{compr}). On top of that the module will be given two sets of coordinates. One set for the location of the electrolyser offshore platform and another set for the location of the connection point. From this information, the module calculates the length of the hydrogen pipeline between the two sets of coordinates according to the Haversine formula shown in Equation 4.19.

$$L_{pipe} = 2r \arcsin\left(\sqrt{\sin^2\left(\frac{\varphi_2 - \varphi_1}{2}\right) + \cos(\varphi_1)\cos(\varphi_2)\sin^2\left(\frac{\lambda_2 - \lambda_1}{2}\right)}\right) \tag{4.19}$$

Where r is the radius of the earth taken as 6371 km, φ_1 and φ_2 are the lateral coordinates of the start and end point respectively and λ_1 and λ_2 are the longitudinal coordinates of the start and end point. The length of the pipeline is required to calculate the pressure drop in the pipeline. The pressure drop in the pipeline is an important factor to calculate to evaluate the output pressure at the connection point of the pipeline to the hydrogen network. The pressure drop is caused by the friction losses with the pipeline wall. Since there is a required minimum pressure at which the power is supplied to the hydrogen network from the pressure drop a minimum pressure will follow. The output pressure is calculated using equation Equation 4.20 [89].

$$P_2^2 = P_1^2 - GT_f LZ\left(\frac{P_b Q}{5.747 \times 10^{-4} f T_b D^{2.5}}\right)^2 \tag{4.20}$$

Where P_2 is the output pressure of the pipeline, P_1 is the input pressure; Q is the hydrogen mass flow rate; T_f is the average gas flowing temperature, L is the length of pipe in km and Z is the compressibility factor. P_b and T_b are the reference pressure and temperature respectively. G is the specific gas gravity which is around 0.07 as the density of hydrogen gas is around 7% that of air. D is the diameter of the pipeline and this is an input to the module.

The compressibility factor, Z, is a function of temperature and pressure and is calculated by linearly interpolating Table 4.9[90]

Table 4.9: Hydrogen compressibility factor look-up table

Temperature	Pressure (MPa)						
(°C)	**0,1**	**1**	**5**	**10**	**30**	**50**	**100**
0	1,0006	1,0062	1,0313	1,0637	1,2022	1,3462	1,7032
25	1,0006	1,0059	1,0297	1,0601	1,1879	1,3197	1,6454
50	1,0006	1,0056	1,0281	1,0567	1,1755	1,2969	1,5964
75	1,0005	1,0053	1,0266	1,0536	1,1644	1,2770	1,5542
100	1,0005	1,0050	1,0252	1,0507	1,1546	1,2596	1,5175

Lastly, f is the dimensionless friction factor of the pipeline. This factor is influenced by the pipeline material and diameter of the pipeline as well as the Reynolds number (Re) of the hydrogen flow. The Colebrook-White equation in Equation 4.21 [89] can be used to calculate the friction factor. It is challenging to get an exact solution to the equation. Therefore, the solution is numerically approximated in the model. Since the module will calculate the output pressure and velocities at all 100 mass flow rates given by the electrolyser module this numerical approximation is performed 100 times.

$$\frac{1}{\sqrt{f}} = -2\log_{10}\left(\frac{e}{3.7D} + \frac{2.51}{Re\sqrt{f}}\right) \tag{4.21}$$

The dimensionless Reynolds number is calculated using Equation 4.22[89]. Where V is the average velocity of the pipeline in m/s, D is the diameter of the pipe in m and ν is the kinematic viscosity of hydrogen. The kinematic viscosity is calculated using Equation 4.23[89]. This equation numerically approximates the kinematic viscosity given by the NIST table [91] with a maximum error of 0.1% within the model temperature and pressure boundaries.

$$Re = VD/\nu \tag{4.22}$$

$$\nu = \nu_{ref} + \left(0.0368(P-1) + 0.000047(P-1)^2 - 0.00011(T-248) + 0.96(P/1)\right) * 10^{-5} \tag{4.23}$$

The factor e, the roughness of the pipeline is required to calculate the relative roughness to the inner diameter of the pipeline. This requires a selection of the pipeline material in order to calculate the relative roughness. Hydrogen pipelines are mostly made of carbon steel and this material is widely used in pipelines [92] The main problem regarding this material is hydrogen embrittlement. This fatigue mechanism is the most important fatigue factor at higher hydrogen concentrations in the pipeline. This fatigue mechanism is further used in the model and it is assumed the pipeline will be able to function for the 25-year lifetime of the project. The roughness of the carbon steel pipeline is estimated at 0.1 mm [89] The hydrogen gas velocity in the pipeline is calculated usingEquation 4.24 [89]. With V and μ defined the Reynolds number can be calculated with Equation 4.22.

$$V = 14.7349\left(\frac{Q_\mathrm{b}}{D^2}\right)\left(\frac{P_\mathrm{b}}{T_\mathrm{b}}\right)\left(\frac{ZT}{P}\right) \tag{4.24}$$

With all prior calculations finished the friction factor is now known. Using the friction factor, the pressure drop is finally outputted so it can be analysed in the optimization if it follows the constraints set. Another constraint that should be considered regarding the pipeline, is the maximum allowable hydrogen velocity in the pipeline. The erosional velocity $u_{erosional}$, is calculated using Equation 4.25. Where Z is the compressibility factor. The maximum velocity may not exceed 50% of the erosional velocity. Therefore, the velocity in the pipeline will be bound by this velocity in the model. For the optimizer, this will add a necessary constraint regarding the velocity in the pipe.

$$u_{erosional} = 100\sqrt{\frac{ZRT}{29GP}} \tag{4.25}$$

Hydrogen pipelines have certain industry-standard inner diameters. These diameters are listed, with their costs per km, in Table 4.10. Since the diameter will probably be mass-produced, one of the selected diameters from Table 4.10 will have to be chosen. The model will therefore use the diameter that is given to the model and select the next bigger diameter from the list. The $CAPEX_{pipe}$ is then selected from Table 4.10. The $OPEX_{pipe}$ is then taken to be 5% of the $CAPEX_{pipe}$.

Table 4.10: Different industry standard inner pipeline diameters and specific cost

Pipeline Inner Diameter [inch]	2	4	6	8	10	12	16	20	24	28	30	32	34	36
Pipeline Cost [M€/km]	0.3	0.33	0.38	0.41	0.49	0.771	0.872	1.169	1.352	1.529	1.662	1.804	1.874	2.209

4.8. ELECTRICITY CABLE

Since the electricity cable is also part of the system it needs to be modelled for cost according to the wind farm rated power and length of the cable. The length of the cable is adjustable since the electrolyser location will be varied in the optimization. This makes the cost estimation of the electricity cable a critical component of the offshore hydrogen production system. The key factors that influence the cost of the cable are shown in Table 4.11.

Table 4.11: Electricity Cable Module inputs and outputs

Inputs	Symbol	Outpouts	Symbol
Wind Farm nominal Power	W_{wf}	Electricity cable length	L_{cable}
Start Location	$Location_{wf}$	Electricity Cable	$CAPEX_{cable}$
End Location	$Location_{ofs}$	OPEX Electricity Cable	$OPEX_{cable}$

This involves several key factors including the length of the cable, the type and capacity of the cable, installation complexities, and maintenance requirements. The length of the cable is determined by the distance

from the offshore wind farm to the electrolyser platform and further to the onshore grid connection point. There are typically two types of high-voltage cables, a high-voltage direct current (HVDC) or high-voltage alternating current (HVAC) cable. The selection is generally made with the total length the cable has to transfer. Below 100 km typically HVAC cables are utilized [16]. In this study, the electrolyser distance stays below 100 km and therefore the HVAC cable is used to assume the cost of the cable. The length of the cable is calculated using the same formula for the hydrogen pipeline length as shown in Equation 4.26

$$L_{cable} = 2r \arcsin\left(\sqrt{\sin^2\left(\frac{\varphi_2 - \varphi_1}{2}\right) + \cos(\varphi_1)\cos(\varphi_2)\sin^2\left(\frac{\lambda_2 - \lambda_1}{2}\right)}\right) \tag{4.26}$$

The cable's capacity is exactly the same as the wind farm's nominal power to ensure all wind farm power can be transported to the electrolyser. The CAPEX of the cable includes the installation of the cable. The installation involves trenching and the cable material is generally constructed using copper. Copper is expensive and this drives the cost of the electricity cable. Furthermore, the cable needs to be insulated well since seawater is particularly conductible. The cost of the electricity cable can be estimated from the wind farm power only. This assumes that the cost of placing the cable is constant. Normally the selection and length of cable will cause distinct selection of the size of the vessel. These nonlinearities are not incorporated in the model. The cable CAPEX per km is estimated using Equation 4.27[93].

$$CAPEX_{cable,km} = \left(1.36 * W_{wf} + 206.13\right) L_{cable} \tag{4.27}$$

Lastly, the $OPEX_{cable}$ is estimated to be 5% of the cable capex from Eneco's internal cost estimation.

4.9. OFFSHORE PLATFORM

For the electrolysers to function in an offshore location an offshore platform is required. A detailed design of this platform is outside the scope of this research. Therefore, this module requires only the maximum power of the electrolyser and calculates the CAPEX and the yearly OPEX of the platform The inputs and outputs are shown in Table 4.12.

Table 4.12: Offshore Platform Module inputs and outputs

Inputs	Symbol	Outpouts	Symbol
Electrolyser Power	W_{elec}	CAPEX Offshore Platform	$CAPEX_{ofs}$
		OPEX offshore platform	$OPEX_{ofs}$

The platform type chosen for the model is jacket foundation. This type of foundation is used in 90% cases and can be utilized in varying sea depths up to 500m [94, 95]. Since the North Sea is of relatively low depth and never exceeding 500 m close to the Dutch shore the jacket foundation can be used in almost any location. This module does not vary any parameters with sea depth. A sea depth of 45 meters has been chosen to estimate the cost figures. This depth is a good average of the plots in which offshore hydrogen is analyzed. The capital expenditure linearly scales with the electrolyser at 550000 € per kW electrolyser [35]. This figure includes a 10% increase, due to recent inflation and rise in material costs such as steel.

The jacket foundation platforms are only usable for up to 600 MW of electrolysers due to the weight of the electrolyser systems and the maximum platform size that sea vessels can carry to the location. Therefore the CAPEX costs will have extra installation costs per platform installed. The installation costs that are added are 20% of the CAPEX of a 600 MW platform. Lastly, the OPEX costs are estimated to be 3% of the CAPEX cost on a yearly basis.

4.10. PERFORMANCE CALCULATION

The performance calculation module finally calculates the LCOH of the system. This module requires all the CAPEX and OPEX of each subsystem, the different energy requirements at the 100 power settings, the hydrogen mass flow of the electrolyser at each power setting and lastly the hourly wind farm power output for 1 year. The different inputs and outputs of this module are shown in Table 4.13

Table 4.13: Performance Calculation Module inputs and outputs

Inputs	Symbol	Outpouts	Symbol
Electrolyser Power	W_{elec}	Levelized-Cost-of-Hydrogen	LCOH
Compressor power	W_{compr}	Total CAPEX	$CAPEX_{total}$
Water treatment power	W_{water}	Total OPEX	$OPEX_{total}$
Hydrogen mass flow	$\dot{m}_{h_2}$	Total Hydrogen production	$total_{H_2}$
Hydrogen mass flow fuel cell	$\dot{m}_{h_2,fc}$	Total runtime hours	runtime
Length HV cable	L_{cable}	Number of stack replacements	$n_{replace}$
CAPEX electrolyser	$CAPEX_{elec}$	Total LCOE expenditure	$total_{LCOH}$
OPEX electrolyser	$OPEX_{elec}$		
CAPEX compressor	$CAPEX_{compr}$		
OPEX compressor	$OPEX_{compr}$		
CAPEX pipeline	$CAPEX_{pipe}$		
OPEX pipeline	$OPEX_{pipe}$		
CAPEX water treatment	$CAPEX_{water}$		
OPEX water treatment	$OPEX_{water}$		
CAPEX fuel cell	$CAPEX_{fc}$		
OPEX fuel cell	$OPEX_{fc}$		
CAPEX offshore platform	$CAPEX_{off}$		
OPEX offshore platform	$OPEX_{off}$		
CAPEX offshore cable	$CAPEX_{cable}$		
OPEX offshore cable	$OPEX_{cable}$		

The general formula for LCOH used in this model is shown in Equation 4.28 [12]. Where $CAPEX_0$ is the total CAPEX at year 0. $OPEX_t$ is the OPEX in each year t. r is the discount rate to compensate for inflation. $H_{2,t}$ is the yearly hydrogen production. i is the yearly estimated inflation. This formula assumes all CAPEX cashflows are dated at the start of the project. Furthermore, most OPEX contributors will be constant over each year. However, the effect of the OPEX in the last year is much smaller than the first year. This is due to the discount rate applied to the project. The discount rate relates to the cost of capital. Investing money in a project requires lending it from a third party and paying interest or the company invests its own money which it could otherwise invest in other projects. The OPEX that is required to be paid in the last year of the project is discounted by several decades of interest rates. The discount rate will have a positive effect on the cost of OPEX. In contrast, will the production of hydrogen also be discounted by the discount rate. Hydrogen produced in the last year of the project will be of less value to the project at the start. The CAPEX that is invested in the first year will only see the profits of the last year's hydrogen production 25 years in the future in the 25-year lifetime of the project. The formula does not take into account any Development Expenditure. This expenditure relates to the development costs that are made to design the project. These costs are not known for offshore hydrogen projects as it has not been done before. Therefore these costs have not been included.

$$\text{LCOH} = \frac{\text{CAPEX}_0 + \sum_{t=1}^{T} \frac{\text{OPEX}_t (1+i)^t}{(1+r)^t}}{\sum_{t=1}^{T} \frac{H_{2,t}(1+i)^t}{(1+r)^t}} \tag{4.28}$$

The total CAPEX is calculated using Equation 4.29. Where each of the CAPEX from the different subsystems is added up. The CAPEX sum is only added in the first year of the system. In a project normally the CAPEX

is spread out over a few years before production starts and revenue can be made. It is hard to predict when these costs are incorporated. Since, the main cost will be the electrolyser which is one of the last subsystems to be placed. It is therefore assumed all CAPEX is spend at the start of the project.

$$\text{CAPEX}_{\text{sum}} = \text{CAPEX}_{\text{elec}} + \text{CAPEX}_{\text{pipe}} + \text{CAPEX}_{\text{cable}} + \text{CAPEX}_{\text{off}} + \text{CAPEX}_{\text{compr}} + \text{CAPEX}_{\text{water}} + \text{CAPEX}_{\text{fc}} \quad (4.29)$$

The OPEX of each system is outputted as a yearly figure from each of the subsystem modules. The total OPEX of the system is calculated using Equation 4.30. The OPEX of each subsystem was a percentage of the CAPEX that would be required on a yearly basis over the whole lifetime of the project. The lifetime of the project can be varied in the performance calculation. In the future, this variable can be used as an input variable to the optimization. As the lifetime of the project increases hydrogen production could be increased significantly. The lifetime variable is currently not used in the optimization design vector. However, since there is a discount rate applied to the hydrogen production and the OPEX the larger the lifetime the less effect on the LCOH this will have.

$$\text{OPEX}_{\text{sum}} = \text{OPEX}_{\text{elec}} + \text{OPEX}_{\text{pipe}} + \text{OPEX}_{\text{cable}} + \text{OPEX}_{\text{off}} + \text{OPEX}_{\text{compr}} + \text{OPEX}_{\text{water}} + \text{OPEX}_{\text{fc}} \quad (4.30)$$

The only OPEX that is varied is the replacement of electrolyser stacks after 80000 runtime hours. The performance module will calculate the total amount of hours that the electrolyser will be running. Every time the 80000-hour mark is passed the performance model adds a percentage of the CAPEX to the OPEX in that year. This should estimate the cost of replacing only the stacks in the electrolyser. The cost of replacing the stacks is estimated to be 166000 €/MW electrolyser [35]. This figure is higher than ENECO estimates on land. A higher figure is expected since replacing the stacks on the offshore platform is a lot more costly. It will involve the need for stable weather and the personnel will need to be trained to work offshore.

4.10.1. HYDROGEN PRODUCTION CALCULATION

The calculation of the CAPEX and OPEX in the prior section was kept relatively simple. The other side of the formula for LCOH involves the total hydrogen production each year. The total hydrogen production is generally calculated with the use of work required by the subsystems and the power available from a wind farm. The three subsystems that require power during the production of hydrogen are the electrolyser, water treatment and compressor. Each of the modules for those subsystems outputs their required work as a list of the 100 power settings from 1% to 100%. The total work required at each power setting k is calculated using Equation 4.31

$$W^k_{total} = W^k_{elec} + W^k_{compr} + W^k_{water} \quad (4.31)$$

The list of total work at each power setting k is now used to select the highest power setting that can be used to produce hydrogen at each moment with the given wind energy power outputted. Eneco has given access to the hourly production data of an offshore wind farm with a rated power of 760 MW. This data runs from the year 1980, based on older wind data to the year 2023. The data gives the power that is available at the end of the cable when it reaches shore in average MW at each hour. The wind energy data is variable since the weather changes. At higher wind speeds the wind farm creates more power. The data spans more than 40 years and is plenty to use for the analysis of a 25-year lifetime hydrogen production project. An option was to use the full 25-year span to calculate the LCOH. However, to decrease computation time the model only calculates the hydrogen production for one year. Subsequently, it uses this reference hydrogen production for each year in the calculation. This will reduce the access of a list from 25*24*365=219000 computations to just 8760 computations.

Before using the wind farm power data the data is slightly increased to account for the fact that there are normally cable losses over large distances which are now reduced as the hydrogen production facility is situated

offshore and reduces the length of the cable. Therefore, the performance calculation module increases the power that is produced from the wind farm and metered at the shore slightly. In Apostolaki-Iosifidou *et al.* the losses in HVAC and HVDC cables are estimated. The losses for the transmission, substation and conversion are mentioned. The losses in the cable were fitted with an exponential function. The losses in the cable range from 0.4% at 1 km cable length to 4.57% at 117 km. In order to estimate the decrease in cable losses the retrofitted curve is used to remove the losses. After that, the losses related to the reduced cable length to the electrolyser offshore platform are added. The formulas for calculation is shown in Equation 4.32 [16]

$$P_{wf,nom} = \frac{P_{wf}}{1 - 0.8088\left(e^{0.0144L_{total}} + e^{*0.0144L_{cable}}\right)} \tag{4.32}$$

The power of the wind energy farm will fall into three categories with off-grid electrolysis. It is lower than the work required to run the electrolyser at 10%, higher than what the electrolyser will require at 100% rated power or in between those two figures. If the first option applies the highest power setting is chosen. If the wind farm power falls into the third category the wind farm will choose the highest W^k_{total} that is still lower than the wind farm power for that hour. The model will then select the appropriate hydrogen production from the hydrogen production list provided by the electrolyser module calculate the amount of hydrogen produced in an hour and add that to the yearly hydrogen production rate.

If the wind farm power falls below the 10% power setting the electrolyser will not produce any hydrogen and nothing is added to the power production. Contrarily, if the power falls below the 2% power setting the electrolyser will need to be supplied with the extra energy. Earlier in this report it was established that this will be supplied by a fuel cell using the remaining hydrogen in the pipeline to produce electric power. The hydrogen required by the fuel cell is then subtracted from the yearly total hydrogen production. The algorithm will then continue with the next hour and start again by selecting the power setting. The general flow chart of the hydrogen production decision matrix is shown in Figure 4.3

After this entire loop, the hydrogen production that can be generated in a single year is deducted from the hydrogen that the fuel cell will require for a constant power supply. The hydrogen is then added to the total hydrogen production of the year, discounted by the discount rate to the power of the year of production, in order to trace it back to the first year of production. With the discounted hydrogen production known the LCOH can be calculated with the OPEX and CAPEX calculated earlier using Equation 4.28. This figure will then be used as the objective of the optimization to minimize.

The CAPEX and OPEX of each system related to electrolyser power are summarized in table Table 4.14. Some figures are not directly related to the electrolyser power. In this case, a baseline scenario is chosen and the CAPEX of the subsystem is normalised to 100 MW electrolyser to visualise the amount of investments required per 100 MW of electrolyser. The 100 MW electrolyser mark is an interesting marker as the first demonstration tender for offshore hydrogen in the Dutch North Sea will be 100 MW.

Table 4.14: List of CAPEX and relative OPEX per year of the different subsystems that are used in the performance calculation

Subsystem	CAPEX	OPEX [% CAPEX]
Electrolyser		4.5%
Compressor		3.0%
Pipeline		5.0%
Desalination		16.6%
Offshore Platform		3.0%
HV Cable		5.0%
Fuel Cell		2.0%

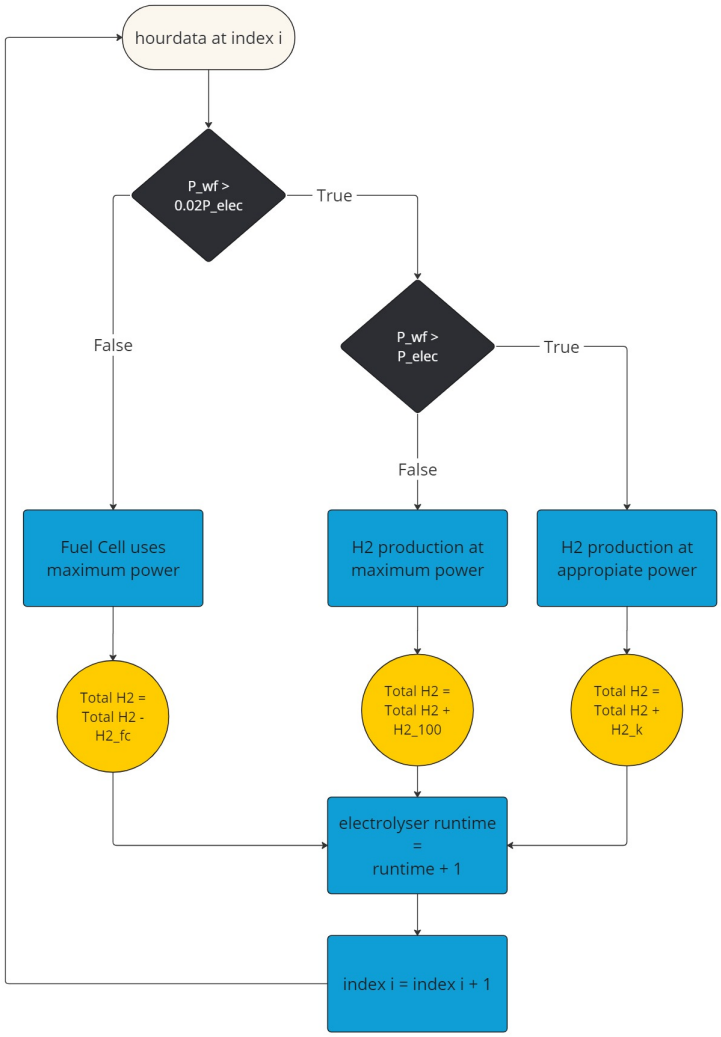

Figure 4.3: Flow chart hydrogen production calculation

4.11. OPTIMIZATION

The optimization problem that is dealt with in this report is summarized in Equation 4.33. The optimization aims to minimize the objective function of LCOH of offshore hydrogen production utilizing offshore wind energy. Where the constraints that arose from the modelling include a minimum output pressure of 67 Bar at the end of the pipeline. The end of the pipeline is located at a fixed connection point to a hydrogen network. Furthermore, the output pressure of the hydrogen compressor should be higher than the operating pressure of the electrolyser. The optimizer is given this constraint to keep it from producing negative values in the hydrogen compressor module. Lastly, the third constraint governs the maximum speed in the pipeline such that it will not exceed the erosional velocity in the pipeline.

$$\begin{aligned} &\min LCOH(x) \\ &\text{s.t.} \begin{cases} \min \quad p_{\text{pipe,out}} \geq 67Bar \\ p_{compr} \succ p_{elec} \\ u_{limit} \succ u_{pipe} \end{cases} \end{aligned} \tag{4.33}$$

The design vector required to compute the LCOH includes 7 variables. These variables are shown in Table 4.15. The table includes the upper and lower bounds of the model. The electrolyser power, W_{elec}, could possibly be lower than 600 MW and higher than 800 MW. However, this variable is not expected to deviate too far from the wind farm power of 760 MW. If the optimizer is restricted by these bounds, the bounds can be adjusted accordingly. T_{elec} is restricted by the cooling or heating requirements of the electrolyser. It is not expected that the optimizer will exceed these values. If the temperature is below 323.15K, or 50 °C, the cooling power required is substantial. On the upper bound the heating required to be added is considerable. The x and y locations were given 1° of freedom on both sides. It is expected that these will not be exceeded as all the locations directly between the start and end locations are within these bounds. The compressor output pressure is on the lower end bounded by the minimum pressure of 67 bar required by the hydrogen network. The upper bound is decided by the module not being able to calculate the compression factor above 100 Bar. Lastly, the pipeline minimum diameter is constrained by the industry standard pipeline sizes.

Table 4.15: Starting value, upper and lower bounds of the design vector

Run #	Unit	lower bounrd	initial design vector	upper bound
W_{elec}	MW	600	700	800
T_{elec}	K	323.15	333.15	363.15
p_{elec}	Bar	1	30	50
x_{loc}	°	51.2	52.2	53.2
y_{loc}	°	3.5	4.5	5.5
D_{pipe}	mm	50.8	609.6	914.4
P_{compr}	Bar	40	100	100

Combining all the previously explained modules inputs and outputs with the LCOH function and the constraints an eXtended Design Structure Matrix (XDSM) can be constructed. The XDSM of the design problem is shown in Figure 4.4 . The XDSM summarized the inputs and outputs of the different subsystems in one flow governed by the optimizer. The optimizer module is shown with a blue circular block in the top left corner. The starting design vector is annotated with ^{0} and inputted from the top in the optimizer module. The different variables of the design vector are then used when calling the different subsystem modules. For example, the electrolyser module is called first by the optimizer. It requires the power of the electrolyser, W_{elec}, the pressure of the electrolyser, p_{elec}, and temperature, T_{elec} as inputs. The module then outputs the electrolyser hydrogen mass flow at each power setting k to the LCOH calculation, compressor and desalination unit and gives a required water mass flow to the desalination unit.

4.11.1. OPTIMIZATION ALGORITHM

The model to be optimised is subject to a number of complications, the most significant of which is the presence of several discontinuous calculations. The most prominent of these is the selection of pipeline diameter. Other discontinuities include the number of compressor stages, the power setting of the electrolysers and the potential for electrolyser stack replacements. Additionally, it is challenging to decide whether the design space is convex or non-convex. Furthermore, if the design space is non-convex, it is unclear how this non-convexity takes shape. Will there be a multitude of local optima? Are these optima shallow and are there saddle points? Given the discontinuity of the design space, it is challenging to predict. For the optimization, however, it is crucial to identify a global optimum. The discontinuities will create smaller local optima.

The primary objective of this research is to identify an algorithm that is well-suited to the optimization problem and can efficiently identify the global optimum without undue computational expense. Developing a bespoke optimization algorithm would necessitate a significant investment of time and is therefore beyond the scope of this research. There are numerous open-source Python packages available for the optimization of complex problems, as referenced in [96]. The selected algorithm must be capable of identifying the global optimum in order to identify the optimal design. Furthermore, the algorithm must be able to cope with the complex constraints. Most open-source optimization packages in Python require the constraints to be lin-

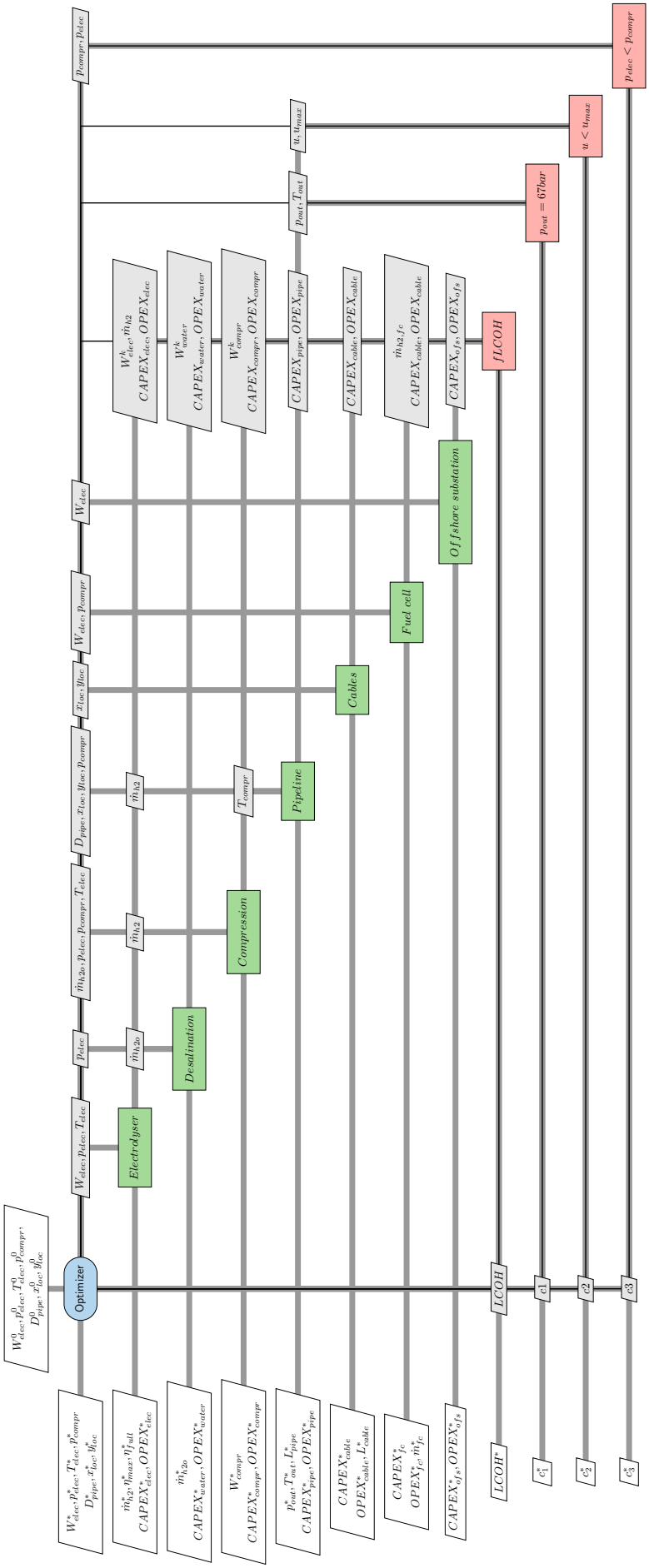

Figure 4.4: XDSM diagram

ear and computable from the design vector alone. In this model, the constraint for pipeline velocity and the constraint for the 67 bar minimum output pressure are outputs of the LCOH calculation. Therefore, the Mystic Python package was chosen to optimize the system [97]. The package has the ability to define constraints that are calculated with the use of more variables than the design vector. For example, the pressure at the output of the pipeline will not only be varied with the design vector but also be related to the length of the cable, input pressure and temperature. Therefore, it is crucial that the constraints can be selected and adjusted customarily. Additionally, it contains a selection of peer-reviewed optimisation algorithms which include gradient-based search methods, differentiable gradient-based methods and a genetic algorithm

From the Mystic package, a differential evolution algorithm is chosen to have a good probability to be a good fit to the optimization problem. This algorithm was published by Storn and Price in 1997 [98]. The algorithm is a population-based, stochastic optimization method that can solve complex optimization problems. It can in theory cope with nonlinear design spaces but requires a continuous design space. For the off-grid offshore hydrogen production model this could be problematic due to the discontinuous nature of the optimization problem. However, there is not a simple one-method-fits-all solution to a discontinuous optimization problem. The reason the differential evolution algorithm might be able to cope with the discontinuous design space is that is a stochastic algorithm. The algorithm uses an iterative process of choosing the best candidate solutions while decreasing it stepsize as the number of iterations increases. The algorithm performs its iteration in four phases: initialization, mutation, crossover and selection.

The **initialization** phase consists of the following two steps:

- A population of candidate solutions is chosen at random. This population consists of an n-by-d matrix. Where n is the size of the population and d is the number of parameters in the design vector that is optimized.
- The size of the population will not vary over the optimization.

The **mutation** phase will mutate the population as follows:

- A mutant vector is generated for each vector in the population. Three distinct individuals are randomly are chosen from the population
- The mutant vector is then chosen using Equation 4.34. where X_{r1}, X_{r2} and X_{r3} are chosen from the population and F is the mutation factor.

$$V_i = X_{r1} + F \cdot (X_{r2} - X_{r3}) \tag{4.34}$$

The **crossover** phase follows the following pattern:

- In order to see if the mutant vector will have any result. A trial vector U_i is constructed by mixing the mutant vector V_i with the target vector X_i. The amount of influence that the mutant vector has can be adjusted with the crossover probability variable. This variable is an input to the differential evolution algorithm.
- For each variable d in the vector a random number is generated. If it is higher than the crossover probability it replaces the target vector in the population. If not, the value takes the target vector.

The **selection** phase follows the following pattern:

- The trial vector U_i is used to compute the LCOH. It is compared to the LCOH reached by the target vector X_i.

- If the trial vector U_i has a better or equal LCOH it will replace the target vector. The population is then after this iteration and the algorithm starts again with the mutation phase until the algorithm runs into a termination due to for example a maximum number of iterations or the improvement on the objective function falling below the predefined tolerance.

The main advantages of this algorithm are that it does not require a differentiable objective function and it uses a heuristic approach to solve nonlinear design problems. The algorithm is genetic and is stated to find a global optimum. The main drawback could be that it requires continuous design spaces. In short, the algorithm mutates a target vector with randomly generated mutations. In the first round, the target vector is the initial design vector shown in Table 4.15. The best results from computing the objective function with the mutated vector are crossed over such that a new target vector is found for the next round.

This differential evolution algorithm may prove to be a promising solution to the optimization algorithm. In order to test its effectiveness, a Monte-Carlo simulation could be a suitable approach. However, a Monte Carlo simulation is associated with a significant computational cost. For instance, varying each of the seven variables over a range of 10 different increments would necessitate the evaluation of approximately 10 million functions. This would necessitate a significant investment of time, and the evidence thus far suggests that this method is not a viable option for finding the optimal solution at a reduced cost.

To best compare the algorithm in convergence speed and overall minimum LCOH a gradient-based optimization algorithm was selected from the Mystic Python software. In this case, the Powell-Conjugate or simply Powell's method was chosen. This method is derivative-free. The whole model is not differentiable and that mitigates the number of gradient-based algorithms that can be used.

The algorithm starts with an initial design vector for the solution and a list of directions. In each iteration, the algorithm performs a series of line searches along each of the directions, with the aim of identifying the minimum value of the function in those directions. Once the line searches have been completed for all directions, the algorithm updates the directions based on the results of the line searches. The direction update process involves the adjustment of one of the previous directions with a new direction that is a linear combination of the preceding directions. The new direction is selected to be conjugate to the remaining directions, thereby ensuring efficient progress towards the minimum. The algorithm iterates through the set of directions, optimising each direction in turn. Periodically, the set of directions is reset in order to ensure that they remain conjugate and effective in reducing the function value.

The algorithm terminates when the change in the function value between iterations falls below a certain threshold, indicating that the algorithm has converged to a local or global optimum. Alternatively, the algorithm will terminate if a certain number of function evaluations or iterations is reached. These numbers can be adjusted within the Mystic package.

5

RESULTS

In this chapter, the results of the model and optimization are visualized and discussed. Firstly, the electrolyser is analysed for performance regarding the pressure and temperature. This will be followed by a summary of the baseline scenario result. This included a financial and technical view of the baseline scenario and the expected outcome of the optimizer. In the latter section the optimizer design space is analysed and the optimizer results are shown. The optimized design is compared to the baseline design and a sensitivity analysis is performed.

5.1. ELECTROLYSER PERFORMANCE

The electrolyser module accurately modelled the performance of the electrolyser as a function of the operating pressure and temperature. Figure 5.1 shows the effect of pressure on the efficiency of the electrolyser module. The effect of pressure is minimal. Therefore, a close-up of Figure 5.1 is shown in Figure 5.2. The pressure effect on the electrolyser between 18 and 80 bar is less than 1

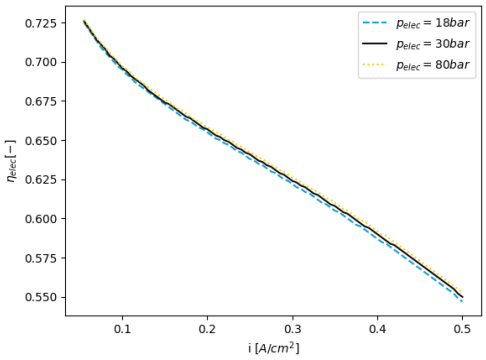

Figure 5.1: Electrolyser efficiency at current density range with different operating pressures and T=60°C

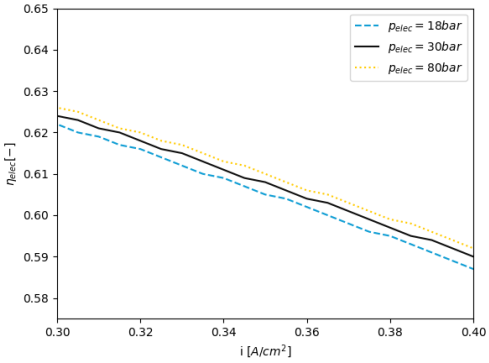

Figure 5.2: Close-up of Figure 5.1

As we have seen in the modelling of the system the operating temperature of the electrolyser has an effect on all three over-voltages as well as the temperature control power required. In Figure 5.3 the efficiency of the electrolyser module at various stack operating temperatures is shown for the range of current densities applied. The temperature effect on the efficiency is larger than the pressure effect. Furthermore, the highest efficiency is reached by running at 65°C and low power setting. At a higher power setting and thus higher current density the highest efficiency is reached when the temperature is 75°C. There is therefore not a clear optimal temperature. If the electrolyser is run at a high load the optimal temperature is a little higher.

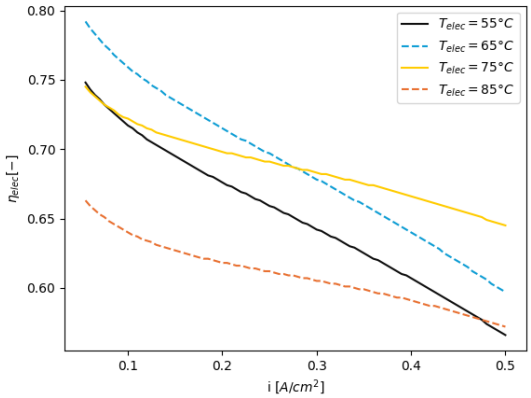

Figure 5.3: Temperature effect on the electrolyser efficiency curve over the whole range of the electrolyser current density

5.2. PRESSURE ANALYSIS

In the previous section, it was shown, that the operating pressure of the electrolyser has a limited effect on the efficiency of the electrolyser stack. However, the pressure has a more profound effect on the power required for the water desalination and pump as well. Since the model gives the required compressor output pressure to the compressor module a lower input pressure also has an effect on the pressure ratio in the compressor. Therefore, a better way of viewing the effect of electrolyser pressure is by analysing how the water pump power relates to the post-compression of hydrogen. To compare the two, the pressure of the electrolyser can be varied while keeping the pressure of the compressor output stable. In Figure 5.4 the power requirements for the water treatment and hydrogen compressor are plotted as a function of the electrolyser operating pressure while the output pressure of the compressor is kept constant at 70 bar. Furthermore, the electrolyser has a maximum power of 740 MW and is running at 30% maximum power for all data points.

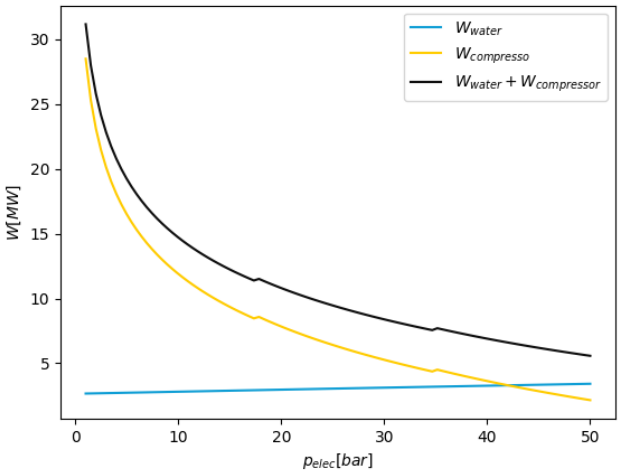

Figure 5.4: Water Treatment and Compressor power at varying electrolyser pressure with a 700 MW electrolyser and p_{compr} = 70 bar at 30% power setting

From Figure 5.4, it is clear that the total work of the water treatment, shown with the blue line for the full range of electrolyser pressure, is lower than the work of the hydrogen compressor. Furthermore, the work of the water treatment varies linearly with the electrolyser pressure. It must also be noted that the power of the water treatment is less than 5 MW. Compared to the electrolyser using 220 MW this is a small fraction. This was to be expected from the earlier calculations showing the relatively low power needed for desalination.

On the other hand, the compressor power required shows a more exponential growth as the pressure of the electrolyser decreases. Especially, when running the electrolyser at 1 bar of pressure, the pressure ratio will reach 70. This requires more than 8 compressor stages with a maximum compression ratio of 2. The compressor stage jump is clearly visible in the yellow line at around 18 bar and 35 bar. Decreasing the compressor stages slightly increases the power required for compression. This shows the need for more compression stages at higher compression ratios in order to reduce the power.

If we add both the water treatment work and compressor work together, shown with the black line, there is a steep decline at higher electrolyser pressure. This means that it is more efficient to operate the electrolyser at higher pressure. The electrolyser pressure has a limited effect on the efficiency of the electrolyser itself as we have seen in the previous sections. On the other hand, is compressing hydrogen much more energy-intensive than compressing the water prior to the hydrogen production. If we are to optimize the system it should be expected that the optimizer prefers higher electrolyser pressures.

From the above analysis, it can be expected that a higher electrolyser pressure is favourable for a lower LCOH outputted by a full computation of the model including the performance module. In order to visualise the effect of electrolyser pressure a heatmap is shown in Figure 5.5 for the LCOH in €/kg. On the x-axis, the power of the electrolyser is varied from 600 MW to 800 MW. Keep in mind the wind farm will produce a maximum of 760 MW. On the y-axis, the pressure of the electrolyser is varied from a minimum of 1 Bar to the maximum allowable pressure of 50 bar. Especially, at lower pressures the LCOH increases steeply to more than 17 Euro/Kg. The optimal W_{elec} changes with the pressure.

As the pressure of the electrolyser increases the work required by the hydrogen compressor and water treatment systems decreases. This allows for more power usage by the electrolyser. Therefore at an electrolyser pressure of 10 bar the optimal LCOH is achieved at 725 MW since the hydrogen compressor and water treatment require around 35 MW of work at maximum power of the electrolyser. At 50 bar the optimal W_{elec} is close to 750 MW. If you keep the electrolyser at the same pressure and increase the electrolyser's maximum power, the total CAPEX and OPEX increase. However, there is not enough power from the wind farm to run

the electrolyser at full power and have enough power for the compressor and water treatment. Therefore, the maximum power setting of 100% is not possible and there is a jump increase in LCOH shown by a lighter blue colour in Figure 5.5. On the other hand, if you increase the pressure there is more power available for the electrolyser and therefore the optimal W_{elec} increases if you keep the other values constant.

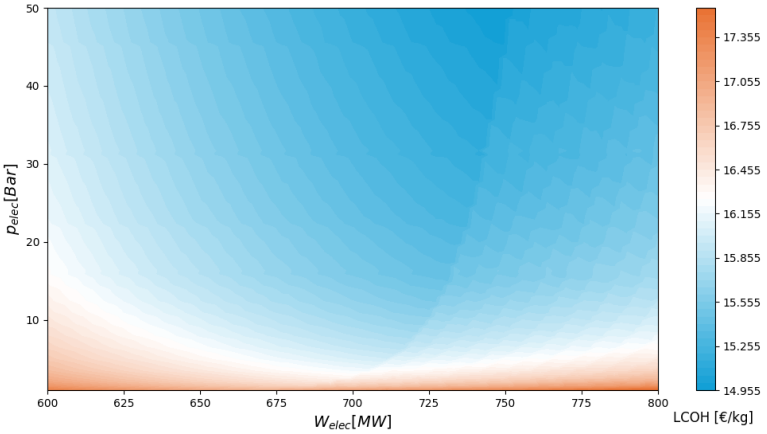

Figure 5.5: LCOH heatmap with varying electrolyser power and operating pressure around the baseline scenario

5.3. BASELINE SCENARIO

For a better interpretation of the optimization results a baseline scenario or design is chosen to compare the optimisation results. This baseline scenario is also the initial design vector in the optimization results discussed later in this chapter. It will be used to analyse the effectiveness of optimizing the system for LCOH. The baseline design is constructed with the use of the initial design vector shown in Table 4.15. The wind farm used in the baseline scenario is a 760 MW wind farm with a location that is 56 km away from the proposed connection point. Furthermore, the project is assumed to be producing hydrogen for 25 years.

5.3.1. WIND FARM POWER AVAILABILITY

To understand the results of the model, it is first necessary to analyse the wind power data to understand the process of how the LCOH is calculated. The distribution of the available power of the wind farm is shown in Figure 5.6. The positive powers are shown in the blue shades. The bar which shows the availability of power below 0 MW is shown in red. The distribution follows a fairly constant flow, almost always below 5%, except for the maximum or nominal power of 760 MW. The availability of the wind farm at maximum power is almost 35 %. The reason for this increase in availability is that all wind turbines have the maximum power that they can produce. This maximum power is called the rated power and is reached at lower wind speeds than the maximum wind speeds at which the wind turbine generator can produce power. Therefore, the availability of 760 MW represents all the times when the wind speed exceeds the speed required to make the rated power in the wind turbine generator.

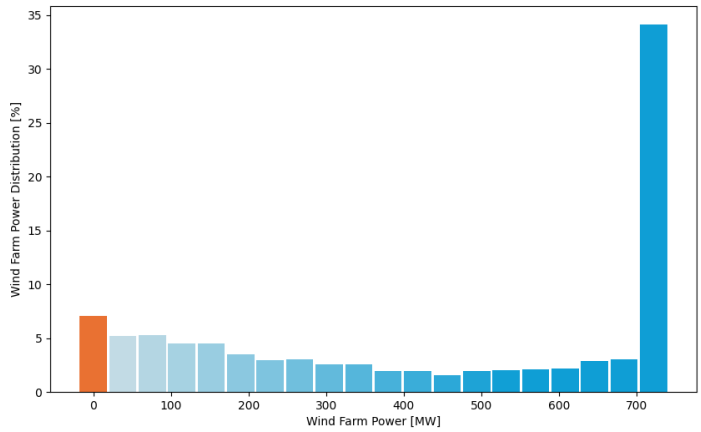

Figure 5.6: Wind Farm power data distribution in 5% intervals for a 760 MW wind farm in the North Sea (Hollandse Kust West)

At first, it might look like the size of the electrolyser would be a trade-off between extra cost for the electrolyser and producing more hydrogen. However, since the nominal wind power is available at almost 35% it can be expected that the optimization will try to optimize for the maximum use of the energy that is available.

On the other side of the graph, there is also a relatively large amount of time that the wind farm will not produce any power. In fact, if the wind farm is not producing any power it requires 3.6 MW for the balance of the plant. This power would then have to be supplied by the fuel cell. In the performance calculation, it was assumed that this power was not supplied by the fuel cell. To check whether this would be a good assumption a zoom-in of the distribution graph is shown in Figure 5.7. Again the positive availability is shown in blue and negative power needed for balance of plant is shown in red. Clearly visible is the 4% availability at the -3.6 MW mark corresponding to the percentage of time that there is no wind energy being produced. If we compare this with the 2% mark of 14 MW in the baseline scenario this is actually quite considerable. This would add around 25% to the power that the fuel cell would have to produce in an off-grid setting.

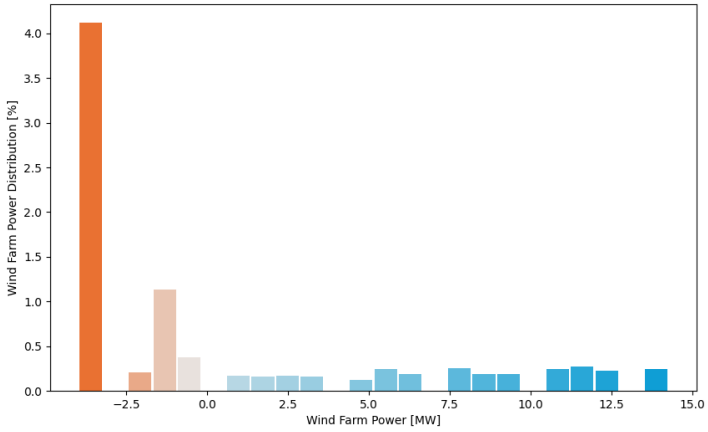

Figure 5.7: Wind farm power data distribution around the 0 MW mark for a 760 MW wind farm in the North Sea (Hollandse Kust West)

5.3.2. TECHNICAL ANALYSIS

The baseline scenario was chosen such that it would give a feasible design to start the optimization with. The baseline input vector and resulting LCOH are shown in Table 5.1. The baseline input vector was chosen such that the model would be in a feasible design space regarding the constraints in the pipeline. The resulting LCOH of hydrogen is 15.50 €/kg. However, this figure can be decreased considerably if the power of the electrolyser is better optimised.

Table 5.1: Baseline input vector and LCOH

Run #	W_{elec}	T_{elec}	p_{elec}	y_{loc}	x_{loc}	D_{pipe}	P_{compr}	LCOH
	MW	K	Bar	°	°	mm	Bar	€/kg
Baseline	700	333.15	30	52.2	4.5	609.8	100	15.50

To better understand the reason for the high LCOH compared to earlier research presented in chapter 2, it is useful to look into the production of hydrogen and the energy usage of the different systems. The baseline electrolyser has a maximum power of 700 MW. In the electrolyser module the hydrogen production rate is calculated. For the 700 MW baseline electrolyser, the hydrogen production rate is shown from 0 to 700 MW power in Figure 5.8. The hydrogen production is 0 until 70 MW, which is the 10% mark that the electrolyser will require to produce hydrogen. Furthermore, the graph is slightly exponentially decreasing due to the lower efficiency of the electrolyser at higher power and thus higher current density.

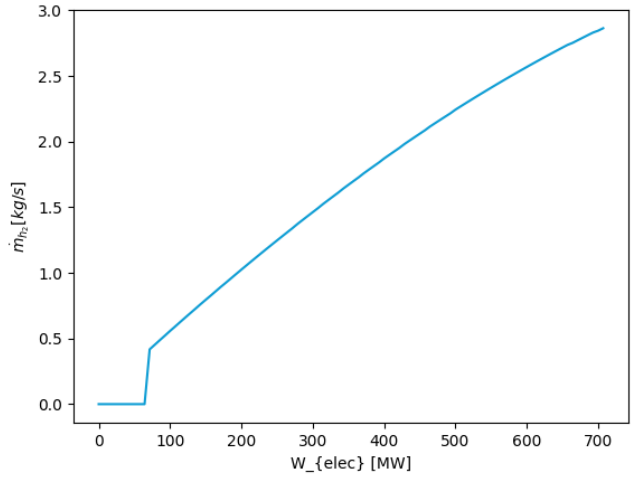

Figure 5.8: Electrolyser hydrogen production rate for a 700 MW electrolyser with p_{elec} = 30 bar and T_{elec} = 60$C°$

The amount of hydrogen produced in one year is dependent on the hydrogen production rate and how often the electrolyser can be turned on. By combining the wind farm availability distribution and the electrolyser relative operating power the distribution of power settings of the electrolyser over one year can be constructed and is shown in Figure 5.9. It must be noted that the total work required at 100 % power setting is 727 MW. There is therefore more power available in a large part of the time than can be used by the system. Visible in Figure 5.9 is the large amount of time that the electrolyser is running at maximum power. The electrolyser availability largely follows the wind farm power availability in Figure 5.6. The only difference is that the electrolyser is turned of more often since the electrolyser is not producing any hydrogen at lower power settings.

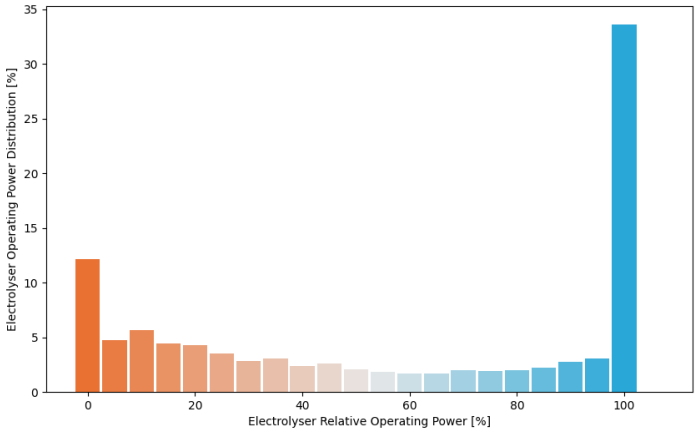

Figure 5.9: Electrolyser availability distribution in 5% Intervals for a 760 MW wind farm in the North Sea (Hollandse Kust West), with a 700 MW electrolyser and accompanied compressor and water desalination power

The total work required over the whole range of the 700 MW electrolyser is shown in Figure 5.10. This shows that most power is distributed to the electrolyser, and only a small portion is required for the water treatment and hydrogen compressor.

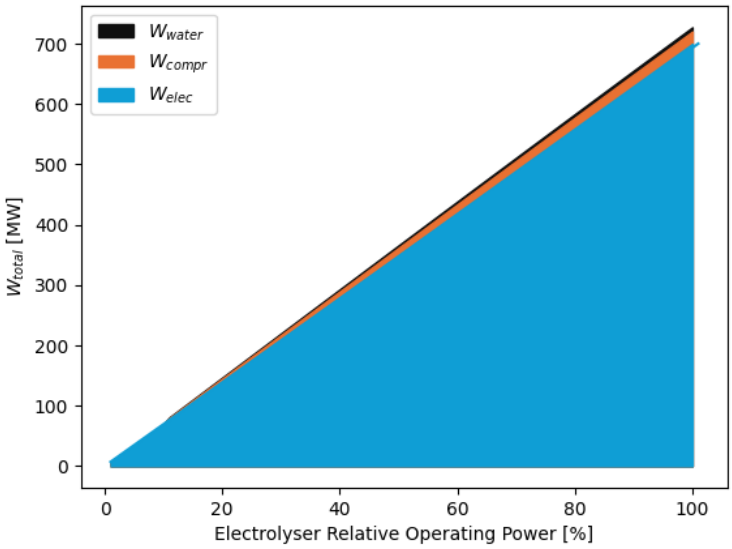

Figure 5.10: Work required for the whole system at each power setting for a 700 MW electrolyser

The total hydrogen production in one year, the hydrogen requirement for the fuel cell and the resulting hydrogen that can be delivered to the grid in one year are shown in Table 5.2. Over 55 million kg of hydrogen is produced each year. On the other hand, is around 1% of this hydrogen subtracted from the delivered hydrogen to power the fuel cell. Earlier this section it was established that assuming the power for the wind farm in standby mode would not be significant but turned out to be about 25% of the electrolyser standby power. This, on the other hand, would subtract only 0.25% of the total hydrogen produced. Adding the balance of plant requirements to the model could be a minor improvement on the accuracy of the model. It would in

turn reduce the net amount of hydrogen produced and increase the LCOH.

Table 5.2: Hydrogen production totals per year

Results	Quantity kg/year
Total hydrogen production	55,039,242
Fuel Cell hydrogen consumption	540,721
Netto Hydrogen production	54,498,521

With the total hydrogen production the total LHV energy efficiency of the whole system is calculated and shown in Table 5.11. The efficiency of the whole system is 48% at the baseline scenario. Later in this chapter, an analysis will be made of the efficiency after the optimization. This figure is comparable to the estimation made by other studies discussed in chapter 2 of 58% and 41% for a system 100 km from shore.

Table 5.3: Off-grid wind-based hydrogen production system efficiency per year for 760 MW wind farm and 700 MW electrolyser

Variable	Quantity
Netto Hydrogen production	54,498,521 kg
Total wind energy	3,780,227 MWh
Lower heating Value hydrogen	33.3 kWh/kg
Total system efficiency	48.0 %

Lastly, it is useful to look at the transmission and pipeline results from the baseline to get a better understanding of the drivers later in the optimization. The pipeline length, HVAC cable length, pressure drop and efficiency loss in the cable are shown in Table 5.12. Transmission losses are higher at 1.78% for just 32 km of electricity cable. This was one of the reasons why offshore hydrogen was proposed as a good option to produce hydrogen. With the large pipeline diameter chosen in the baseline, the pressure drop in the pipeline is minimal. This shows that less energy is lost in the transportation of hydrogen than what would be lost in the transmission of electricity to shore.

Table 5.4: Off-grid wind-based hydrogen production electricity transmission and hydrogen pipeline results for the baseline scenario

Variable	Quantity
HVAC cable length	32.9 km
HVAC transmission loss	1.78 %
Hydrogen pipeline length	24.2 km
Pressure loss pipeline	0.07 Bar

5.3.3. FINANCIAL ANALYSIS

To understand what drives the LCOH in the model it is necessary to analyse the financial results of the baseline scenario. There are three major factors contributing to the total cost of the project. These are the CAPEX, OPEX and LCOE from the offshore wind farm. The LCOE and the power available are not adjusted in the model. The wind farm is fixed at 760 MW and since the choice was made to model a fuel cell for backup power there is no cable to land available.

The CAPEX and yearly OPEX of the modelled subsystems are listed in Table 5.5. As expected is the electrolyser cost the major cost factor for the whole system. The second biggest cost factor is the offshore platform. Since the offshore platform cost would not be needed if the electrolyser is placed on land these CAPEX and OPEX figures are considerably high with almost 20% of the total CAPEX. The fuel cell on the other hand does not contribute significantly to the total CAPEX and OPEX. With 21 million Euros of CAPEX, this is in the order of 1% of the CAPEX of the electrolyser.

Table 5.5: CAPEX and OPEX of different subsystems in baseline design for a 700 MW off-grid electrolyser placed on an offshore platform

Substystem	CAPEX [M€]	CAPEX [%]	OPEX [M€]	OPEX [%]
Electrolyser	1733	74.0%	78	80.1%
Pipeline	37	1.8%	2	2.1%
Platform	454	19.4%	11	11.3%
Compressor	57	2.4%	2	2.1%
Fuel Cell	21	0.9%	0.4	0.4%
Electric Cable	41	1.7%	2	2.2%
Water Treatment	10	0.4%	2	1.9%
Total	2343	100%	97.4	100%

After calculating the hydrogen production and the CAPEX and OPEX the cost of the three main categories contributing to the LCOH can be calculated per kilogram of hydrogen produced. The highest contributor to the LCOH is the LCOE of 80 €/MWh. This contributes to about 60% of the total cost of the system. On the other hand, the CAPEX and OPEX together are close to 40% of the cost. This means that a 5% increase in electrolyser CAPEX to produce more hydrogen if power is available will result in a 2.1% increase in hydrogen production. Since the CAPEX and OPEX only contribute to about 40% of capex this will improve the LCOH significantly.

Table 5.6: LCOH breakdown for the baseline scenario

Total LCOH	CAPEX/kg H_2 [€/kg]	OPEX/kg H_2 [€/kg]	LCOE/kg H_2 [€/kg]
15.50	3.38	2.56	9.49

5.4. PIPELINE VS COMPRESSION

There is a trade-off between the hydrogen pipeline diameter and the input pressure of the pipeline. To reach a minimum hydrogen pressure of 67 bar at the connection point with the hydrogen network, the hydrogen compressor should supply the pipeline with hydrogen at a significantly large pressure above 67 bar. On the other hand, the pipeline diameter will influence the pressure losses due to friction.

In Figure 5.11 the LCOH is visualised for the full range of pipe diameter on the x-axis and compressor output pressure on the y-axis. Clearly visible are the jumps in LCOH, although small, at the different industry standard pipeline diameters. The lowest LCOH of hydrogen is achieved when the pipeline diameter is the smallest and the compressor output power is the lowest. Another jump in LCOH is seen around 79 bar of compressor output pressure. This jump is caused by the compressor using so much power that the electrolyser cannot run at full power without overshooting the total of 760 MW of power that is available from the wind farm. The maximum power setting is therefore reduced to 99%.

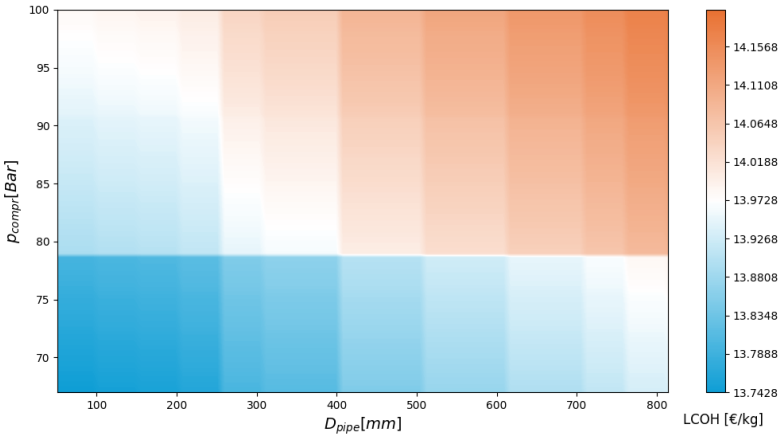

Figure 5.11: LCOH heatmap with varying pipeline diameter and compressor output power, the electrolyser output pressure is 30 Bar

5.5. LOCATION

In this section an analysis of the effect of x_{loc} and y_{loc} is made. In Figure 5.12 the lateral and longitudinal locations of the electrolyser are varied. A heatmap of the computed LCOH in that location is shown. Furthermore, a blue dot shows the location of where the network is to be connected to land. A red dot shows the location where the wind farm is. The distance between these two points is 65 km. The lowest LCOH is reached directly between the line of these two points. Furthermore, the closer the electrolyser is to the red-dotted wind farm connection point the lower the LCOH becomes. The reason for this is the lower cost of the pipeline per km than the electricity cable. Furthermore, the cable loses more energy due to transmission losses than the energy lost in the hydrogen pipeline as shown in Table 5.12.

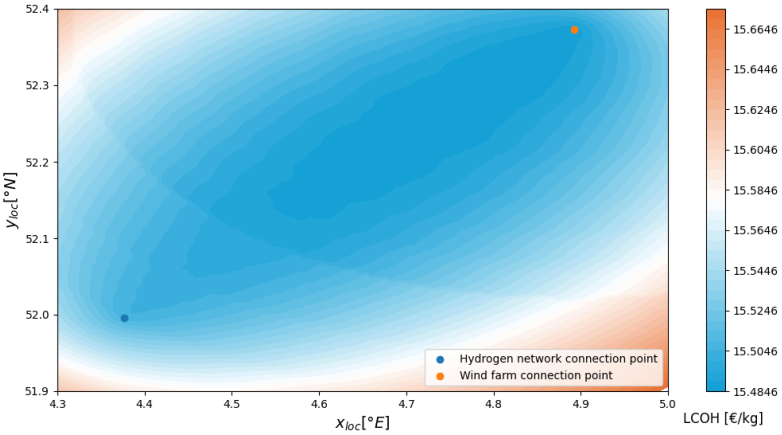

Figure 5.12: LCOH heatmap with varying longitudinal and lateral location of the offshore platform

5.6. OPTIMIZATION

Earlier in this chapter it has been shown that the design space is posing several possible problems for optimizing the system. Firstly, there are several aspects in the model which do not follow a continuous calculation. The discontinuous design space is most prominent in the selection of pipeline diameter. Furthermore, it was also visible in the selection of power settings for each hour and the number of stages in the compressor. The

design space is in large parts convex, but the discontinuous pipeline diameter and the power setting create local minima.

In chapter 4, a differential evolution algorithm was chosen using the Mythic python package to find an optimal design for LCOH using 7 variables. Furthermore, the constraints that were used had no tolerance and could not be exceeded for the optimal result. The results of using this optimization algorithm are shown in Table 5.7. The algorithm selected seems to find different optimum each time. For run number 3 it took 260 iterations with a total number of 2610 function evaluations. It took the algorithm 175 seconds to come to this local optimum. The termination reason was that the objective function did not improve more than 0.005 €/kg after the last iteration.

Table 5.7: Results of first 3 runs with differential evolution optimization

Run #	W_{elec}	T_{elec}	p_{elec}	y_{loc}	x_{loc}	D_{pipe}	P_{compr}	LCOH
	MW	K	Bar	°	°	mm	Bar	€/kg
Baseline	700	333.15	30	52.2	4.5	609.8	100	15.50
1	750.32	348.03	50.00	52.28	4.75	594.32	67.56	13.88
2	751.30	347.84	50.00	52.35	4.85	405.78	71.72	13.83
3	749.89	346.86	50	52.37	4.88	508.00	68.77	13.93

In order to analyse what causes the algorithm to find different results in each three runs, it is useful to visualise the largest differences in the optimized design vectors. From Table 5.7 the largest difference occurs in the diameter of the pipe and the compressor power. Therefore, the heatmap in Figure 5.11 is adjusted such that the three runs are visible in Figure 5.13. Furthermore, the two constraints regarding the minimum pressure and erosional velocity are shown. The feasible design space is shown on the right side of the dotted line. All three runs have closed in on the dotted line. This means that the minimum pressure constraint is active. This is as expected since having an extra high-pressure output would require more power without increasing the hydrogen production.

From Figure 5.13 there is a clear point that should yield a lower LCOH when the pipeline diameter is between 300 and 400 and a compressor output pressure of 75 bar. This point would still comply with the constraints. The optimizer algorithm selects random points to mutate the design vector. Therefore, the optimizer is not reaching the same point while running the exact code. Furthermore, the figure only shows two design variables. The code will have to vary all seven variables at the start. On top of that, in order to find a lower LCOH it has to find a vary both the pipeline diameter and the compressor output pressure simultaneously. As the iterations start to accumulate, the algorithm decreases the size of the mutations and it will run into the local optima. In this case, three different local optima are reached in the three runs.

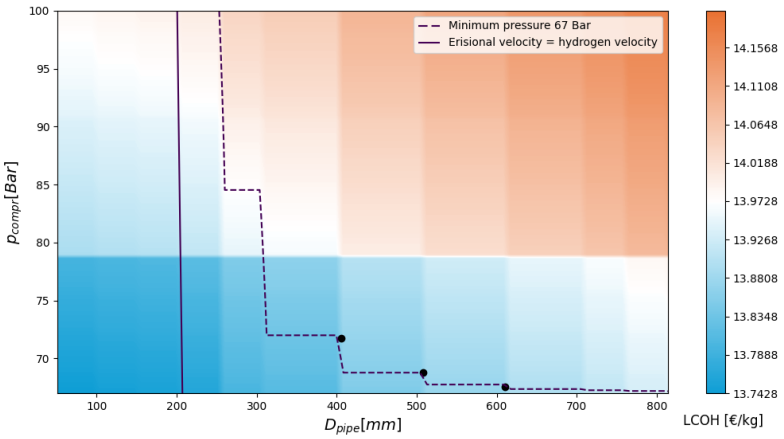

Figure 5.13: LCOH heatmap with varying pipeline diameter and compressor output power

A good option to look at is to rerun the optimization algorithm and change the initial design vector to the optimal design vector found in the previous run. This will give it the freedom to have bigger mutations again while already being really close to the optimal value. The results for rerunning the algorithm two more times are shown in Table 5.8. Including the first run the total time to run the optimizer was 475 seconds with 9060 function evaluations. The LCOH has been reduced by a further 0.06 €/kg. The diameter of the pipeline is decreased further and the hydrogen compressor compresses the hydrogen to a higher pressure compared to the earlier local optimum. The LCOH reduced by 1.68 €/kg.

Table 5.8: Design vector and resulting LCOH after rerunning the differential evolution algorithm three times for a 760 MW offshore wind farm

Run #	W_{elec}	T_{elec}	p_{elec}	y_{loc}	x_{loc}	D_{pipe}	P_{compr}	LCOH
	MW	K	Bar	°	°	mm	Bar	€/kg
Baseline	700	333.15	30	52.2	4.5	609.8	100	15.50
1	750.32	348.03	50.00	52.28	4.75	594.32	67.56	13.88
Final	751.9	347.824	50.00	52.37	4.89	360.6	72.06	13.82

To analyse the effectiveness of the differential evolution algorithm a gradient-based algorithm was chosen to optimize the system. The results of several runs are shown in the Table 5.9. The function evaluations required to produce the following outputs are 8310, 8730 and 8220, respectively. This means Powell's conjugate gradient-based algorithm was slightly faster in converging. However, the results are comparable to the differential evolution algorithm. The LCOH of the three runs is between 13.93 and 13.83. This is comparable to the differential evolution results in Table 5.7. The main difference between the local optima found in the Powell's conjugate algorithm is the slight change in pipeline diameter and the compressor outlet pressure. Compared to the sequential differential evolution algorithm it performs slightly worse. On the other hand, it needs fewer computations of the model while the LCOH is only slightly higher. This could therefore be a good option to use as a starting point. Especially, if in earlier stages of a similar project several design options need to be analysed after optimisation. In later stages of the design it could be more useful to utilize the more computation expensive sequential differential evolution algorithm.

Table 5.9: Design vector and LCOH after running the Powells conjugate algorithm three times for a 760 MW offshore wind farm

Run #	W_{elec}	T_{elec}	p_{elec}	y_{loc}	x_{loc}	D_{pipe}	P_{compr}	LCOH
	MW	K	Bar	°	°	mm	Bar	€/kg
Baseline	700	333.15	30	52.2	4.5	609.8	100	15.50
1	744.26	347.82	50.00	52.34	4.84	247.44	100	13.92
2	752.92	347.62	50.00	52.37	4.89	495.16	68.79	13.85
3	748.325	347.62	50.00	52.37	4.89	255.83	84.55	13.88

5.7. FINANCIAL ANALYSIS OPTIMIZED DESIGN

In Table 5.10 the optimized results for the hydrogen production are shown. The hydrogen needed for the fuel cell stays more or less the same. On the other hand, hydrogen production is increased by 5000 tonnes or almost 10%. This could be explained by the fact that the electrolyser power is increased and all the energy is used more optimally.

Table 5.10: Hydrogen production totals per year for optimized design

Results	Quantity kg/year	Quantity kg/year Baseline
Total hydrogen production	60,095,683	55,039,242
Fuel Cell hydrogen consumption	549,922	540,721
Netto Hydrogen production	59,545,760	54,498,521

Table 5.11: Off-grid wind-based hydrogen production system efficiency per year for 760 MW wind farm and 751 MW electrolyser in the optimized design

Variable	Optimized	Baseline
Netto hydrogen production	60,095,683 kg	54,498,521 kg
Total wind energy	3,780,227 MWh	3,780,227 MWh
Lower heating value hydrogen	33.3 kWh/kg	33.3 kWh/kg
Total system efficiency	52.9%	48.0 %

Lastly, it is useful to look at the transmission and pipeline results from the baseline to get a better understanding of the drivers in the optimisation. The pipeline length, HVAC cable length, pressure drop and efficiency loss in the cable are shown in Table 5.12 for the optimized and baseline results. The cable length decreased due to the high cost of the HVAC cable, and the relatively lower cable losses for a shorter cable. On the other hand, the pipeline got longer and the pressure loss increased. The main reason is that a decrease in pipeline diameter is cheaper than an increase in compressor work required over the whole LCOH calculation. It does however not reduce the HV cable length to 0. One reason for this is that the gradient of LCOH for the location becomes very shallow and there is no real benefit for the optimizer to move even closer to the wind farm.

Table 5.12: Off-grid wind-based hydrogen production transmission and transportation losses per year for 760 MW wind farm and 751 MW electrolyser after optimization

Variable	Optimized	Baseline	Change
HVAC cable length	6.2 km	32.9 km	-81.0%
HVAC transmission loss	0.4%	1.78 %	-77.5%
Hydrogen pipeline length	48.8 km	24.2 km	+101.7%
Pressure loss pipeline	4.48 Bar	0.07 Bar	-

The breakdown of the LCOH and the three contributors is shown in Table 5.13. The largest contributor to the costs is the LCOE of offshore wind electricity. This contributes 8.69 €/kg at an LCOE price of 80 €/kWh. The CAPEX and OPEX of the system are contributing much smaller amounts. The LCOH has decreased by 1.68 compared to the baseline scenario. The most important decrease comes with the fact that hydrogen production has increased by almost 10%. The CAPEX and OPEX have slightly increased compared to the baseline. But the hydrogen production has increased even more. This creates a lower LCOH due to the CAPEX, OPEX and stable LCOE being divided over more hydrogen mass.

Table 5.13: LCOH breakdown of optimized design

Design	Total LCOH	CAPEX/kg H_2 [€/kg]	OPEX/kg H_2 [€/kg]	LCOE/kg H_2 [€/kg]
Baseline	15.50	3.38 (21.8%)	2.56 (16.5%)	9.49 (61.2%)
Optimized	13.82	2.92 (21.1%)	2.22 (16.1%)	8.69 (62.9%)
Relative Change	-10.8 %	-13.6 %	-13.3 %	-8.4 %

5.8. SENSITIVITY ANALYSIS

Lastly, this chapter concludes with the results from varying several inputs to the model. From the cost electrolyser to the efficiency of the electrolyser as well as the Internal Rate of Return (IRR) . The different measures all have one thing in common. The LCOH is prone to large increases in all categories. Especially, the IRR rate is high since the electrolyser will only earn back the investment over a 25-year lifespan. As we have seen in chapter 2 the PEM electrolyser technology is not fully developed yet. CAPEX is assumed to be decreasing until 2030. However, a 10% decrease in CAPEX will only decrease the LCOH by 0.38 €/kg. This will never reduce the whole system's LCOH to a point where it can be competitive with grey hydrogen. On the other hand, can bigger improvements be made when the system is 10% efficient. This leads to an decreas of 1.25 €/kg in LCOH. This is an almost 10% decrease. Another important factor is the LCOE. The biggest improvements

could be made when the IRR will decrease by 2%. This is however, never a possibility since companies can not suddenly reduce their internal IRR ratings. It shows that with a long lifetime of the project, the IRR has a big effect on the LCOH.

Table 5.14: LCOH breakdown

Parameter	Offset	LCOH
Optimized Design	-	13.82
$CAPEX_{elec}$	+10%	14.20
	-10%	13.44
$OPEX_{elec}$	+10%	13.99
	-10%	13.64
η_{elec}	+10%	12.57
	-10%	15.29
$LCOE$	+10%	14.69
	-10%	12.95
IRR	+2%	16.05
	-2%	11.79

With all the possible sensitivities that are shown above the LCOH is affected at different levels. However, it can not be concluded that with different financial and technical improvements, the LCOH is suddenly competitive. Even returning to the lower LCOE from a few years ago will not make up the gap between offshore wind-based hydrogen production and grey hydrogen.

6

CONCLUSIONS

In this chapter, the results from modelling and optimizing an off-grid offshore hydrogen production plant using wind energy are discussed. The model used in this research contained an electrolyser, water desalination, pump and compressor, hydrogen compressor, offshore platform, a fuel cell and hydrogen pipeline. The main research question to be answered in this thesis was the following:

To what extent can Multidisciplinary Design Analysis & Optimization reduce the Levelized-Cost-Of-Hydrogen of off-grid offshore hydrogen production using wind energy?

The three sub-questions that aided in answering this research question were the following:

- How is the off-grid offshore electrolyser system modelled?
- What system parameters drive the LCOH optimum?
- What MDAO method is best suitable for optimizing off-grid offshore hydrogen production?

SUMMARY

Firstly, this chapter will start with the conclusions gathered from the research. It will follow up on the limitations of the model and the research. Lastly recommendations for further research are listed.

6.1. DISCUSSION

In this report, the electrolyser system was modelled with the use of water treatment, an offshore platform, a PEM electrolyser, hydrogen compression and a hydrogen pipeline. In particular, modelling the electrolyser efficiency according to the pressure and temperature at which it operates proves to be effective in finding an optimal design. Almost all the systems modelled around the electrolyser depend heavily on the pressure and temperature of the hydrogen. As seen in chapter 2, the water treatment system is important to model. It is a hard requirement for the electrolyser to have desalinated and highly purified water to prevent degradation. This system uses low amounts of energy compared to the electrolyser. The water treatment system is linearly dependent on the electrolyser operating pressure. On the other hand, the hydrogen compressor requires more work than the water treatment system. The work required for the compressor scales exponentially with the pressure difference between the electrolyser pressure and the compressor output pressure. The hydrogen pipeline is governed by the length of the pipeline, the diameter chosen and the output of the compressor. This relationship between pipeline diameter, length and compressor output pressure is hard to optimize since they have to be varied simultaneously to see their effect.

In the model, the design vector contains seven design variables. The design variables have a huge variation in their effect on the LCOH. The most important variable is the W_{elec}. This variable has a large effect on both the hydrogen production and the costs on the other hand. The effect of pressure on the electrolyser efficiency was shown to be limited. In contrast, the auxiliary systems used less power at higher pressures. This shows that varying the electrolyser operating pressure is having an effect on the LCOH. The temperature of the electrolyser mainly has an effect on the electrolyser's efficiency. This effect is considerable as it can gain or lose more than 10% of efficiency in the electrolyser module. Outside the electrolyser, the temperature effects are not modelled as well. They are considered to be quite low and heat exchangers are more efficient

than the cooling of electrolyser stacks. The longitudinal and lateral location of the electrolyser could be coupled together in a factor of how far the electrolyser is between the wind farm and the connection point. The coordinates were modelled such that the model could incorporate sea depth overlays in the cost of the offshore substation. Furthermore, the pipeline and electricity cable might not be able to be laid in a straight line between the two points. The selection of compressor output pressure and diameter of the pipeline have a large effect on each other. If chosen together they can make sure constraints are met along the pipeline, and a reduction of LCOH is possible.

The question that was to be answered in this research was if the modelled problem could be optimized by using an MDO setup. The model can go through several thousand function evaluations within a minute. There is always a payoff between the computation time and the detail of the model. Modelling the system with clearly separated modules which can be called separately to validate proved to be an efficient method. Having a low computation time aided in visualising the design space. The visualisation aided in finding the problem with the optimization problem. The model contains several discontinuities that are a result of the different hydrogen pipeline diameters, the power settings, the compression stages required and the number of offshore platforms. These discontinuities proved to cause problems in the optimization. The power setting of the electrolyser was used to reduce the computation time of the system. Also, any linear model on offshore electrolysis with water desalination and compression is not yet available. This would have been a good addition to the model. The conclusions drawn from the pressure analysis are however very useful for future selection of the electrolysers in the future.

A differential evolution algorithm is a good option for non-differentiable, continuous design spaces. Although the design space is not completely continuous and contains smaller non-convex regions the algorithm was chosen since it was open-source and readily available. Furthermore, it was interesting to see how far the optimizer could come. The optimizer was considerably effective in finding local optima close to the global optimum. In fact, only the combination of compressor output pressure and pipeline diameter proved to be problematic. The solution to this problem was to rerun the differential evolution algorithm a few times starting each new run with the optimal vector from the last run. This gave the algorithm more freedom to find global optimum which it got cut off from because the step sizes were decreasing as the number of iterations increased. The final LCOH of hydrogen was decreased by about 1.6 €/kg from the baseline design vector. The largest contribution to this decrease was the increase in maximum electrolyser power as the pressure of the electrolyser increased. On the other hand, does the location of the electrolyser have a small effect on the LCOH as the hydrogen pipeline is cheaper than the high voltage electricity cable. Furthermore, it seems to be preferable to decrease the pipeline diameter and increase the hydrogen compressor work and output pressure. This effect is small but a few cents decrease in LCOH is still preferred with the total amounts of hydrogen produced.

The LCOH of the baseline design was 15.50 €/kg. This is much higher than the reported possible LCOH of 5 €/kg in several reports. The main reason for this is that the LCOE of offshore wind has increased drastically in the last few years. Therefore only the cost of the electricity already drives the LCOH significantly above 5 €/kg. Another factor in this much higher figure is the price of the electrolysers and the added cost of placing the electrolyser offshore. The 13-15 €/kg estimate from the model and optimization is not far off from the expectations within ENECO. Hydrogen produced on land will probably be cheaper. The cost reduction in the electricity cable does not add up to the extra costs related to the offshore substation, placing the electrolyser offshore and the operational expenditure at sea. The Dutch government will have to subsidise the gap between offshore green LCOH to make offshore electrolysis compatible with the LCOH of grey or blue hydrogen and a feasible investment option for Eneco. Most assumptions and limitations in the model had a decreasing effect on the costs. On the production side leakage and hydrogen quality control in the pipeline could reduce the possible reduction even more. Both these facts only strengthen the conclusion that offshore hydrogen production is far from economically feasible.

In conclusion, can Multidisciplinary Design Analysis & Optimization reduce the Levelized-Cost-Of-Hydrogen of off-grid offshore hydrogen production using wind energy? The simple answer is, that it is possible to reduce the LCOH considerably by optimizing the size of the electrolyser in parallel with the operating pressure and temperature. Smaller improvements can be made by simultaneously choosing the hydrogen compressor

output pressure and diameter of the hydrogen pipeline. Lastly, the design space is discontinuous. This leads to the fact that the genetic sequential differential evolution algorithm showed the best results in optimizing for LCOH.

6.2. LIMITATIONS

The model is effective in exposing some major drivers in the LCOH of offshore hydrogen production utilizing wind energy. However, the model has some limitations which are listed below.

- The electrolyser is mainly modelled for the thermodynamic and electrical performance of the cell and the following temperature control. In practice, the membrane of the PEM fuel cell has limitations on the thickness and the pressure that can be applied. The model has not made an attempt to model the physics of the membrane and the added cost of possible thicker membranes.
- The suppliers of electrolysers will supply electrolysers at fixed pressure outputs. It is not possible to simply run the electrolyser supplied at a different pressure. However, the model is currently set up to be more freely in adjusting the pressure to see the overall effect on the system cost and hydrogen production.
- The intercooler in the hydrogen compression is not accounted for in the power division. Although this is a smaller contributor to the power requirement it will reduce the hydrogen production in the future.
- The offshore platform that is modelled only uses the electrolyser power to estimate the costs. Furthermore, the offshore substation will require power to run. Also, personnel is needed to run and service the equipment. All these costs are not incorporated in the model and would increase the LCOH. Furthermore, the offshore platform will have different costs depending on the sea depth. The model does have the ability to adjust the longitudinal and lateral location separately. This would give it the ability to incorporate sea depth in the cost calculation in the future.
- The model assumes one year of wind energy and uses this year to calculate the hydrogen output for each year of the lifetime of the system. This method was chosen to reduce the computation time considerably. The model calculates the hydrogen production for each hour. This also means that the effects of climate change over the years are not incorporated into the calculation. If the availability of the wind farm is higher or lower, the hydrogen production could be affected directly.
- In real life electrolysers have a start-up time from standby. This could take several minutes. Furthermore, the temperature will take time to settle into a constant. Both these effects are not incorporated in the model.
- There is currently not a lot of information available on the degradation of PEM electrolysers. Values of overvoltage increase have been mentioned but PEM electrolysers of this size are not operational yet. The model does replace the stacks after a certain amount of hours but does not incorporate losses related to degradation during this time.

6.3. RECOMMENDATIONS

For future research, there is a lot of improvement to be made on the details of the modelling. This model has mainly focused on the thermodynamic effects on the LCOH. Within the electrolyser, the temperature effects on efficiency are high. However, all the different effects have been taken from research that was done in isolated testing facilities [4, 5]. Using data from larger operational electrolysers on land to predict the efficiency will increase the accuracy of the model. Furthermore, the electrolyser module will have more than just the temperature and pressure as input parameters. The membrane materials, as well as the cathode and anode materials, are the major contributors to the electrolyser price. By varying the electrolyser pressure these materials are also changing, or the volume of raw material changes. These factors can be added for better

representation. On the other hand, can the model also be adjusted to take pre-calculated electrolyser system outputs. Then several industry suppliers can submit their data and the model runs through all electrolyser options and finds the best match.

The modelling of the substation is currently limited to a simple cost calculation. However, the substation is prone to a few factors that influence the cost. The weight and area of the electrolyser system have an effect on the amount of steel used, and therefore the cost [99]. The biggest contribution that can be made is adding the factor of sea depth to the module. The cost of the offshore substation is related to the depth of the seabed. In the case of the North Sea, the sea depth varies only small amounts at shorter distances. Incorporating sea depth will also significantly increase the location effect on the LCOH.

In the model, the location of the electrolyser can be altered longitudinally and laterally. However, from the results, it was concluded that moving the electrolyser is only effective along a straight line between the end and the start point. This was a result of not including any geological locations in the model. In the future, it would be a good addition to add specified pipeline corridors as well as sea depth and seabed material in the model. This would improve the cost estimation and could lengthen the hydrogen pipeline even further to better estimate the cost of placing the platform. This would also justify the use of two variables instead of just one variable for the location of the subsystem.

The model also does not take into account when the electrolyser is on land. It is for now too complicated to include costs of land area, and even finding a plot to build the electrolyser on land. However, comparing the LCOH of electrolysis when placing the electrolyser on the coastline would improve the understanding of the costs related to the project. Furthermore, optimizing the layout of the wind farm simultaneously with this hydrogen model would also be a great addition in the future. Maybe the electrolyser could be placed in the middle of the wind farm.

For the optimization, the sequential differential evolution algorithm proved to be successful in improving the LCOH compared to a gradient-based Powell's conjugate method. However, the differential evolution algorithm can also be adjusted by the amount of cross-variation and mutations that are computed each round. This could be fruitful in finding a more optimal LCOH while decreasing the number of computations. Another option could be, to combine the more efficient gradient-based algorithm with genetic algorithms. By starting with the genetic algorithm and when it converges to a local optimum, start with the differential evolution algorithms. Lastly in this research, the model was optimized for the seven variables. For future research, can the x and y location variables be joined together in a factor of how far the electrolyser is on the line from the connection point to the wind farm. The electrolyser maximum power has the most significant effect on the LCOH but this effect is influenced by the operating temperature and pressure. For future optimization, it is useful to better understand the cross-variable sensitivity. This is a challenge since the design space is discontinuous and most methods for sensitivity analysis, such as Sobol, require a continuous design space.

In order to successfully install an offshore hydrogen production facility, a number of factors must be solved first. The government will have to start with a tender on a smaller scale. The uncertainties regarding large-scale electrolysis are high. Mainly since there are no operating facilities on land of the 500 MW scale. It is a huge step to think it is possible to install 500 MW offshore electrolysers by 2030. This pathway will have to be adjusted and a start should be made on technology demonstrations as soon as possible. Otherwise, the path to more offshore hydrogen production will take a lot more time and might eventually never happen. The gap between LCOH of offshore electrolysis en grey hydrogen is 200%. This will not simply be reduced by better and cheaper technologies. Therefore, subsidies will always be needed in the near future.

Lastly in order to quantitatively assess the difference between offshore hydrogen production and producing the hydrogen at the connection point of the wind farm on shore, it would be a good addition to also build a similar model for the second option. Comparing both models and their resulting LCOH will give a better view on the advantages and disadvantages of both systems.

BIBLIOGRAPHY

[1] Gasunie, *Waterstofnetwerk Nederland,* (2023).

[2] *Dolphyn Hydrogen - phase 1 final report,* Final Report (2019).

[3] *Global Hydrogen Review 2023*, Tech. Rep. (2023).

[4] A. Roy, S. Watson, and D. Infield, *Comparison of electrical energy efficiency of atmospheric and high-pressure electrolysers,* International Journal of Hydrogen Energy **31**, 1964 (2006).

[5] R. Keller, E. Rauls, M. Hehemann, M. Müller, and M. Carmo, *An adaptive model-based feedforward temperature control of a 100 kW PEM electrolyzer,* Control Engineering Practice **120**, 104992 (2022).

[6] *The Paris Agreement | UNFCCC,* (2015).

[7] *Global hydrogen trade to meet the 1.5°C climate goal*, Tech. Rep. (International Renewable Energy Agency, Abu Dhabi, 2022).

[8] J. S. Hill, *Sealhyfe produces first green hydrogen at sea from offshore wind farm,* (2023).

[9] A. Rogeau, J. Vieubled, M. de Coatpont, P. Affonso Nobrega, G. Erbs, and R. Girard, *Techno-economic evaluation and resource assessment of hydrogen production through offshore wind farms: A European perspective,* Renewable and Sustainable Energy Reviews **187** (2023), 10.1016/j.rser.2023.113699.

[10] A. Singlitico, J. Østergaard, and S. Chatzivasileiadis, *Onshore, offshore or in-turbine electrolysis? Techno-economic overview of alternative integration designs for green hydrogen production into Offshore Wind Power Hubs,* Renewable and Sustainable Energy Transition **1**, 100005 (2021).

[11] T. Runser, S. Arend, and R. W. De Doncker, *Stand-Alone Offshore Wind Energy and Water Electrolysis: A Study on Optimal Electrolyzer Sizing,* in *2023 25th European Conference on Power Electronics and Applications (EPE'23 ECCE Europe)* (IEEE, Aalborg, Denmark, 2023) pp. 1–9.

[12] M. Scolaro and N. Kittner, *Optimizing hybrid offshore wind farms for cost-competitive hydrogen production in Germany,* International Journal of Hydrogen Energy **47**, 6478 (2022).

[13] C. Ríos, P. Molina, C. Martínez de León, and J. J. Brey, *Simulation of the optimal plant size to produce renewable hydrogen based on the available electricity,* Stand-Alone Offshore Wind Energy and Water Electrolysis: A Study on Optimal Electrolyzer Sizing (2023), 10.1016/j.ijhydene.2023.08.306.

[14] José G. García Clúa, R. J. Mantz, and H. De Battista, *Optimal sizing of a grid-assisted wind-hydrogen system,* Energy Conversion and Management **166**, 402 (2018).

[15] O. S. Ibrahim, A. Singlitico, R. Proskovics, S. McDonagh, C. Desmond, and J. D. Murphy, *Dedicated large-scale floating offshore wind to hydrogen: Assessing design variables in proposed typologies,* Renewable and Sustainable Energy Reviews **160**, 112310 (2022).

[16] E. Apostolaki-Iosifidou, R. Mccormack, W. Kempton, P. Mccoy, and D. Ozkan, *Transmission Design and Analysis for Large-Scale Offshore Wind Energy Development,* IEEE Power and Energy Technology Systems Journal **6**, 22 (2019).

[17] *Plug EX-4250D Electrolyzer (English),* (2023).

[18] A. Alkaisi, R. Mossad, and A. Sharifian-Barforoush, *A Review of the Water Desalination Systems Integrated with Renewable Energy,* Energy Procedia 1st International Conference on Energy and Power, ICEP2016, 14-16 December 2016, RMIT University, Melbourne, Australia, **110**, 268 (2017).

[19] Q. Ma and H. Lu, *Wind energy technologies integrated with desalination systems: Review and state-of-the-art,* Desalination **277**, 274 (2011).

[20] M. A. Abdelkareem, M. El Haj Assad, E. T. Sayed, and B. Soudan, *Recent progress in the use of renewable energy sources to power water desalination plants,* Desalination Desalination using Renewable Energy, **435**, 97 (2018).

[21] D. Colombo, M. De Gerloni, and M. Reali, *An energy-efficient submarine desalination plant,* Desalination **122**, 171 (1999).

[22] Z. M. Ghazi, S. W. F. Rizvi, W. M. Shahid, A. M. Abdulhameed, H. Saleem, and S. J. Zaidi, *An overview of water desalination systems integrated with renewable energy sources,* Desalination **542**, 116063 (2022).

[23] T. Egeland-Eriksen, J. F. Jensen, Ulleberg, and S. Sartori, *Simulating offshore hydrogen production via PEM electrolysis using real power production data from a 2.3 MW floating offshore wind turbine,* International Journal of Hydrogen Energy **48**, 28712 (2023).

[24] Y. Morales, P. Samanta, F. Tantish, H. Horn, and F. Saravia, *Water management for Power-to-X offshore platforms: an underestimated item,* Scientific Reports **13**, 12286 (2023).

[25] N. S. Hasan, M. Y. Hassan, M. S. Majid, and H. A. Rahman, *Review of storage schemes for wind energy systems,* Renewable and Sustainable Energy Reviews **21**, 237 (2013).

[26] A. Ozarslan, *Large-scale hydrogen energy storage in salt caverns,* International Journal of Hydrogen Energy HYFUSEN, **37**, 14265 (2012).

[27] I. Sorrenti, T. B. H. Rasmussen, G. Xydis, P. Enevoldsen, and S. You, *Correlations between component size green hydrogen demand and breakeven price for energy islands,* Renewable and Sustainable Energy Reviews **183**, 113439 (2023).

[28] Y. Jiang, W. Huang, and G. Yang, *Electrolysis plant size optimization and benefit analysis of a far offshore wind-hydrogen system based on information gap decision theory and chance constraints programming,* International Journal of Hydrogen Energy **47**, 5720 (2022).

[29] G. Lei, H. Song, and D. Rodriguez, *Power generation cost minimization of the grid-connected hybrid renewable energy system through optimal sizing using the modified seagull optimization technique,* Energy Reports **6**, 3365 (2020).

[30] F. Fan, S. Skellern, D. Campos-Gaona, and J. Nwobu, *Wind-farm and hydrogen-storage co-location system optimization for dynamic frequency response in the UK,* Clean Energy **7**, 157 (2023).

[31] A. Buttler and H. Spliethoff, *Current status of water electrolysis for energy storage, grid balancing and sector coupling via power-to-gas and power-to-liquids: A review,* Renewable and Sustainable Energy Reviews **82**, 2440 (2018).

[32] M. Carmo, D. L. Fritz, J. Mergel, and D. Stolten, *A comprehensive review on PEM water electrolysis,* International Journal of Hydrogen Energy **38**, 4901 (2013).

[33] Tom Smolinka and Martin Günther, *Stand und Entwicklungspotenzial der Wasserelektrolyse zur Herstellung von Wasserstoff aus regenerativen Energien*, Tech. Rep. (2011).

[34] *Kamerbrief voorkeurslocaties demonstratieprojecten waterstof op zee - Kamerstuk - Rijksoverheid.nl,* (2023), last Modified: 2023-06-28T13:50 Publisher: Ministerie van Algemene Zaken.

[35] *NORTH2 OFFSHORE HYDROGEN Feasibility Study*, Tech. Rep. (Ramboll, 2023).

[36] *Front Matter,* in *Pipeline Planning and Construction Field Manual*, edited by E. S. Menon (Gulf Professional Publishing, Boston, 2011) pp. i–ii.

[37] R. Carapellucci and L. Giordano, *Modeling and optimization of an energy generation island based on renewable technologies and hydrogen storage systems,* International Journal of Hydrogen Energy **37**, 2081 (2012).

[38] Lhyfe, *Sealhyfe produces its first kilos of green hydrogen in the Atlantic,* (2023), url: https://www.lhyfe.com/press/lhyfe-announces-that-sealhyfe-the-worlds-first-offshore-hydrogen-production-pilot-produces-its-first-kilos-of-green-hydrogen-in-the-atlantic-ocean/, accessed: 18-10-2023.

[39] *ERM Dolphyn Hydrogen Phase 2 final report,* Final Report (2021).

[40] RWE, *AquaVentus – Hydrogen production in the North Sea | RWE,* (2021), url: https://www.rwe.com/en/research-and-development/hydrogen-projects/aquaventus/, accessed: 23-7-2021.

[41] OYSTER, *Project - Oyster Project,* (2023), url: https://oysterh2.eu/about/project/, accessed: 13-10-2023.

[42] D. Snieckus (d_snieckus), *Salamander floating wind project off Scotland gets gassed up with new-look hydrogen kit,* (2021), section: energy_transition.

[43] Crosswind, *Crosswind Innovations,* (2023), url: https://www.crosswindhkn.nl/innovations, accessed: 13-10-2023.

[44] Thomas Schiestel, *H2Wind – Self-sufficient offshore H2 electrolysis,* (2023).

[45] Poshydon, *Poshydon | Proces,* (2023), url: https://poshydon.com/nl/home/proces-2/, accessed: 13-10-2023.

[46] H2RES, *H2RES Sustainable hydrogen production,* (2023), url: https://h2res.dk/?lang=en, accessed: 13-10-2023.

[47] *Vergleich von Systemvarianten zur Wasserstoffbereitstellung aus Offshore-Windkraft*, Tech. Rep. (AFRY, 2022).

[48] Ton van Wingerden, Daan Geerdink, Corin Taylor, Claas F. Hülsen, *Specification of a European Offshore Hydrogen Backbone*, Tech. Rep. (2023).

[49] H. Noh, K. Kang, and Y. Seo, *Environmental and energy efficiency assessments of offshore hydrogen supply chains utilizing compressed gaseous hydrogen, liquefied hydrogen, liquid organic hydrogen carriers and ammonia,* International Journal of Hydrogen Energy **48**, 7515 (2023).

[50] L. Collins (l_collins), *Offshore hydrogen | Germany plans 1GW of wind-powered green H2 production at sea, with pipeline to shore,* (2023), section: policy.

[51] A. Buljan, *Denmark Launches World's First Power-to-X Tender,* (2023).

[52] *The first PtX tender in Denmark has been determined: Six projects will establish electrolysis capacity on more than 280 MW,* (2023).

[53] Renewables, *Denmark backs 280 MW of electrolysers in first PtX tender,* (2023).

[54] M. Lehner, R. Tichler, H. Steinmüller, and M. Koppe, *Water Electrolysis,* in *Power-to-Gas: Technology and Business Models*, SpringerBriefs in Energy (Springer International Publishing, Cham, 2014) pp. 19–39.

[55] J. Proost, *State-of-the art CAPEX data for water electrolysers, and their impact on renewable hydrogen price settings,* International Journal of Hydrogen Energy **44**, 4406 (2019).

[56] M. J. Ginsberg, M. Venkatraman, D. V. Esposito, and V. M. Fthenakis, *Minimizing the cost of hydrogen production through dynamic polymer electrolyte membrane electrolyzer operation,* Cell Reports Physical Science **3**, 100935 (2022).

[57] I. Vincent, E.-C. Lee, and H.-M. Kim, *Comprehensive impedance investigation of low-cost anion exchange membrane electrolysis for large-scale hydrogen production,* Scientific Reports **11**, 293 (2021).

[58] O. Schmidt, A. Gambhir, I. Staffell, A. Hawkes, J. Nelson, and S. Few, *Future cost and performance of water electrolysis: An expert elicitation study,* International Journal of Hydrogen Energy **42**, 30470 (2017).

[59] S. Abedi, A. Alimardani, G. B. Gharehpetian, G. H. Riahy, and S. H. Hosseinian, *A comprehensive method for optimal power management and design of hybrid RES-based autonomous energy systems,* Renewable and Sustainable Energy Reviews **16**, 1577 (2012).

[60] TOPSOE, *Green Hydrogen | Efficient green hydrogen electrolysis,* Url: https://info.topsoe.com/green-hydrogen, accessed: 6-9-2023.

[61] Bloomenergy, *Affordable Clean Hydrogen Starts Here,* (2023), url: https://www.bloomenergy.com/bloomelectrolyzer/, accessed: 7-9-2023.

[62] Sunfire, *Sunfire - Renewable hydrogen (HyLink),* (2023), url: https://www.sunfire.de/en/hydrogen, accessed: 7-9-2023.

[63] J. B. Hansen, *Solid oxide electrolysis – a key enabling technology for sustainable energy scenarios,* Faraday Discussions **182**, 9 (2015).

[64] A. A. AlZahrani and I. Dincer, *Thermodynamic and electrochemical analyses of a solid oxide electrolyzer for hydrogen production,* International Journal of Hydrogen Energy **42**, 21404 (2017).

[65] S. Grigoriev, V. Fateev, D. Bessarabov, and P. Millet, *Current status, research trends, and challenges in water electrolysis science and technology,* International Journal of Hydrogen Energy **45**, 26036 (2020).

[66] M. Ozturk and I. Dincer, *A comprehensive review on power-to-gas with hydrogen options for cleaner applications,* International Journal of Hydrogen Energy **46**, 31511 (2021).

[67] M. Nasser, T. F. Megahed, S. Ookawara, and H. Hassan, *A review of water electrolysis–based systems for hydrogen production using hybrid/solar/wind energy systems,* Environmental Science and Pollution Research **29**, 86994 (2022).

[68] A. Elia, M. Taylor, B. Ó Gallachóir, and F. Rogan, *Wind turbine cost reduction: A detailed bottom-up analysis of innovation drivers,* Energy Policy **147**, 111912 (2020).

[69] M. N. I. Salehmin, T. Husaini, J. Goh, and A. B. Sulong, *High-pressure PEM water electrolyser: A review on challenges and mitigation strategies towards green and low-cost hydrogen production,* Energy Conversion and Management **268**, 115985 (2022).

[70] T. Zhou and B. Francois, *Modeling and control design of hydrogen production process for an active hydrogen/wind hybrid power system,* International Journal of Hydrogen Energy **34**, 21 (2009).

[71] S. Shiva Kumar and V. Himabindu, *Hydrogen production by PEM water electrolysis – A review,* Materials Science for Energy Technologies **2**, 442 (2019).

[72] G. Matute, J. M. Yusta, J. Beyza, and L. C. Correas, *Multi-state techno-economic model for optimal dispatch of grid connected hydrogen electrolysis systems operating under dynamic conditions,* International Journal of Hydrogen Energy **46**, 1449 (2021).

[73] V. A. Martinez Lopez, H. Ziar, J. W. Haverkort, M. Zeman, and O. Isabella, *Dynamic operation of water electrolyzers: A review for applications in photovoltaic systems integration,* Renewable and Sustainable Energy Reviews **182**, 113407 (2023).

[74] E. Ogungbemi, T. Wilberforce, O. Ijaodola, J. Thompson, and A. G. Olabi, *Review of operating condition, design parameters and material properties for proton exchange membrane fuel cells,* International Journal of Energy Research **45**, 1227 (2021), _eprint: https://onlinelibrary.wiley.com/doi/pdf/10.1002/er.5810.

[75] A. Omran, A. Lucchesi, D. Smith, A. Alaswad, A. Amiri, T. Wilberforce, J. R. Sodré, and A. G. Olabi, *Mathematical model of a proton-exchange membrane (PEM) fuel cell,* International Journal of Thermofluids **11**, 100110 (2021).

[76] R. F. Mann, J. C. Amphlett, M. A. I. Hooper, H. M. Jensen, B. A. Peppley, and P. R. Roberge, *Development and application of a generalised steady-state electrochemical model for a PEM fuel cell,* Journal of Power Sources **86**, 173 (2000).

[77] P. R. Pathapati, X. Xue, and J. Tang, *A new dynamic model for predicting transient phenomena in a PEM fuel cell system,* Renewable Energy **30**, 1 (2005).

[78] Bosch, *The fuel cell electric drive,* (2020), url: https://www.bosch-engineering.com/media/downloads/beg_digitalbrochure_the-fuel-cell-electric-drive_en_rgb_300dpi_20200907.pdf, Accessed: 25-5-2024.

[79] *Clean Hydrogen JU - SRIA Key Performance Indicators (KPIs) - European Commission,* (2022).

[80] K. Maleki Bagherabadi, S. Skjong, and E. Pedersen, *Dynamic modelling of PEM fuel cell system for simulation and sizing of marine power systems,* International Journal of Hydrogen Energy **47**, 17699 (2022).

[81] H. Becker, J. Murawski, D. V. Shinde, I. E. L. Stephens, G. Hinds, and G. Smith, *Impact of impurities on water electrolysis: a review,* Sustainable Energy & Fuels **7**, 1565 (2023).

[82] J. Kim, K. Park, D. R. Yang, and S. Hong, *A comprehensive review of energy consumption of seawater reverse osmosis desalination plants,* Applied Energy **254**, 113652 (2019).

[83] W. Dormann, *The Surface Salinity of the North Sea and Baltic Sea Area,* in *Terrestrial Coastal Ecosystems in Germany and Climate Change*, edited by D. Mossakowski and U. Irmler (Springer International Publishing, Cham, 2023) pp. 67–73.

[84] I. G. Wenten, Khoiruddin, F. Arfianto, and Zudiharto, *Bench scale electrodeionization for high pressure boiler feed water,* Desalination **314**, 109 (2013).

[85] M. Kuhn, S. Lang, F. Bezold, M. Minceva, and H. Briesen, *Time-resolved extraction of caffeine and trigonelline from finely-ground espresso coffee with varying particle sizes and tamping pressures,* Journal of Food Engineering **206**, 37 (2017).

[86] G. Sdanghi, G. Maranzana, A. Celzard, and V. Fierro, *Review of the current technologies and performances of hydrogen compression for stationary and automotive applications,* Renewable and Sustainable Energy Reviews **102**, 150 (2019).

[87] M.-R. Tahan, *Recent advances in hydrogen compressors for use in large-scale renewable energy integration,* International Journal of Hydrogen Energy **47**, 35275 (2022).

[88] istecadmin, *Temperature measurements for reciprocating compressors,* (2020).

[89] E. S. Menon, *Chapter 8 - Pipeline Hydraulic Analysis,* in *Pipeline Planning and Construction Field Manual*, edited by E. S. Menon (Gulf Professional Publishing, Boston, 2011) pp. 123–175.

[90] N. O. o. D. a. , *NIST Office of Data and Informatics,* Publisher: National Institute of Standards and Technology, url: https://webbook.nist.gov/cgi/cbook.cgi?Name=hydrogen&Units=SI, accessed: 22-5-2024.

[91] E. Lemmon, M. L. Huber, and M. O. McLinden, *NIST Standard Reference Database 23: Reference Fluid Thermodynamic and Transport Properties-REFPROP, Version 8.0,* NIST (2007), last Modified: 2021-10-12T11:10-04:00 Publisher: Eric Lemmon, Marcia L. Huber, Mark O. McLinden.

[92] H. W. Lee, M. B. Djukic, and C. Basaran, *Modeling fatigue life and hydrogen embrittlement of bcc steel with unified mechanics theory,* International Journal of Hydrogen Energy European Fuel Cells and Hydrogen Piero Lunghi Conference 2021, **48**, 20773 (2023).

[93] P. Djapic and G. Strbac, *Cost benefit methodology for optimal design of offshore transmission systems* (Department for Business, Enterprise & Regulatory Reform, London?, 2008) oCLC: 520517336.

[94] F. Fu, *Chapter Eight - Design of Offshore Structures,* in *Design and Analysis of Tall and Complex Structures*, edited by F. Fu (Butterworth-Heinemann, 2018) pp. 251–293.

[95] X. Tian, Q. Wang, G. Liu, Y. Liu, Y. Xie, and W. Deng, *Topology optimization design for offshore platform jacket structure,* Applied Ocean Research **84**, 38 (2019).

[96] *SciPy API — SciPy v1.13.1 Manual,* Url: https://docs.scipy.org/doc/scipy/reference/index.html, accessed: 24-6-2024.

[97] *mystic package documentation 0.4.3.dev0,* (2024), url: https://mystic.readthedocs.io/en/latest/index.html, accessed: 5-6-2024.

[98] R. Storn and K. Price, *Differential Evolution – A Simple and Efficient Heuristic for global Optimization over Continuous Spaces,* Journal of Global Optimization **11**, 341 (1997).

[99] S. Sánchez, J.-S. López-Gutiérrez, V. Negro, and M. D. Esteban, *Foundations in Offshore Wind Farms: Evolution, Characteristics and Range of Use. Analysis of Main Dimensional Parameters in Monopile Foundations,* Journal of Marine Science and Engineering **7**, 441 (2019), number: 12 Publisher: Multidisciplinary Digital Publishing Institute.